# Supersymmetry
# A study of the supersymmetric opposite sign di-lepton channel

MAIKEN PEDERSEN
DEPARTEMENT OF PHYSICS
UNIVERSITY OF OSLO
NORWAY


June 2008

## Acknowledgements

With thanks to my supervisor Prof. Farid Ould-Saada for his patient help and support throughout.

A special thanks also to Dr. Borge K. Gjelsten for a great contribution close to the final delivery date and the whole Oslo group of Experimental Particle Physics. Thank you for a very good and inspiring work enviroment.

# Introduction

Supersymmetry (SUSY) has become a very popular, so far unconfirmed theory that attempts to solve some of the problems encountered with the Standard Model (SM) of fundamental particles and their interactions. Although the SM has been extremely successful and no experimental contradiction has been found, it has some important shortcomings, and alternative models such as SUSY must be considered. SUSY is in short a supersymmetric extension of the SM, and relates matter with force through a symmetry of spin states. SUSY introduces new heavy particles, so called sparticles which are superpartners of a SM particle and gauginos which are superpartners of the gauge bosons.

The so far largest high energy physics experiment is about to be started at CERN, the European Organization for Nuclear Research close to Geneva in Switzerland. The Large Hadron Collider (LHC) will produce proton-proton collisions at a center of mass energy of 14 TeV. At these high energies possibilities for discovering physics beyond the SM are present. A large community of physicists have prepared for possible discovery of new physics, studying ways to extract deviations from the already confirmed SM background.

This thesis will investigate one possible manifestation of new physics, through the supersymmetric decay resulting in a final-state of opposite sign di-leptons, large missing transverse energy and a large multiplicity of jets. Our challenge will be to pick out the events that could possibly either be our signal or mimic it, and be able to differentiate between the two.

In this quest we will first give a brief historical overview of particle physics and its theoretical framework in Chapter 1. In Chapter 2 we will look closer at the particle content of the Supersymmetric model, and identify our final-states to study. We will then, in Chapter 3, turn our focus on to the experiment by giving an overview of the ATLAS (A ToroidaL ApparatuS) at CERN, and describe some of the work done in order to finalize commissioning of the detector. Since the experiment has yet to start, simulated data corresponding to some months of running at the LHC has been used, these simulated data will be briefly introduced in chapter 4. In Chapter 5 we will study particle identification, in particular lepton identification and isolation. Selection methods (so called cuts) will be studied in Chapter 6, and a set of criteria will be chosen in order to make our final analysis in Chapter 7. We will on this basis evaluate if discovery is possible, and have a brief look at possible mass measurements.

# Contents

**Contents** iii

**List of Figures** v

**List of Tables** viii

**1 The Standard Model and Supersymmetry - brief introduction to particle physics and its theoretical framework** 1
- 1.1 Introduction to particle physics . . . 1
  - 1.1.1 The particle adventure . . . 2
- 1.2 The SM . . . 2
- 1.3 Some important shortcomings of the SM . . . 4
- 1.4 Supersymmetry . . . 5
  - 1.4.1 The minimal supersymmetric model and the minimal supergravity model . . . 6
  - 1.4.2 mSUGRA . . . 8

**2 SUSY in mSUGRA** 9
- 2.1 Mass evolution . . . 9
- 2.2 General sparticle evolution . . . 10
  - 2.2.1 Gauginos . . . 10
  - 2.2.2 Squarks and sleptons . . . 11
- 2.3 SUSY mass spectra from IsaJet . . . 11
- 2.4 Branching ratios for mSUGRA processes leading to leptons and jets . . . 14
  - 2.4.1 Coannihilation point - SU1 . . . 14
  - 2.4.2 Focus point SU2 . . . 15
  - 2.4.3 Bulk region - SU3 . . . 16
  - 2.4.4 Low Mass - SU4 . . . 17
  - 2.4.5 Funnel region - SU6 . . . 17
- 2.5 General feature of SUSY . . . 18
- 2.6 Conclusion . . . 18

**3 The Atlas Detector and commissioning** 19
- 3.1 Proton collisions . . . 20
- 3.2 Coordinate system . . . 20
- 3.3 Magnet system . . . 20
- 3.4 The inner detector - the tracker . . . 20
  - 3.4.1 Pixel detector . . . 22
  - 3.4.2 Silicon Strip Tracker . . . 23
  - 3.4.3 Transition Radiation Tracker . . . 23
- 3.5 The Calorimetry . . . 23
  - 3.5.1 The Electromagnetic Calorimeter . . . 23
  - 3.5.2 The Hadronic Calorimeter . . . 24
- 3.6 Muon system . . . 24
- 3.7 Trigger and Data Acquisition . . . 24
- 3.8 Commisioning of the ATLAS detector systems . . . 25
- 3.9 The Online Global Inner Detector Monitoring . . . 25
  - 3.9.1 Preparing the monitoring for online implementation . . . 25

**4 Analysis Tools and Monte Carlo data** **29**
4.1 Using simulated data . . . 29
4.2 Background and signal data samples . . . 29

**5 Selecting and defining signal leptons, jets and $\not{E}_{\mathrm{T}}$** **33**
5.1 Generated leptons . . . 34
5.2 Reconstructed leptons and jets . . . 37
5.2.1 Leptons . . . 37
5.2.2 Jets . . . 42
5.3 Missing Transverse Energy . . . 42
5.4 Looking closer at lepton isolation criteria . . . 43
5.4.1 Calorimeter based lepton isolation . . . 43
5.4.2 Investigating the isolation cut . . . 44
5.4.3 Lepton-jet veto . . . 48
5.5 Conclusions . . . 49

**6 Selecting the SuperSymmetric event** **51**
6.1 Two leptons with opposite sign . . . 52
6.2 Lepton pt . . . 52
6.3 MissET . . . 53
6.4 Number of jets and $p_T$ of hardest jet . . . 56
6.5 Optimizing $\not{E}_{\mathrm{T}}$ and jet cut . . . 59
6.6 $\not{E}_{\mathrm{T}}$ / MEFF . . . 63
6.7 Conclusion . . . 65

**7 Final analysis using effective mass and invariant mass** **67**
7.1 Effective Mass and significances . . . 68
7.2 Invariant mass of the two opposite sign, same flavour leptons . . . 77
7.3 Conclusions . . . 81

**A CERN Summer School 2007 - CMS experience** **82**
A.0.1 Analysis Tools . . . 82
A.0.2 Level 1 Trigger System of CMS . . . 82
A.0.3 Global Runs . . . 83
A.0.4 Conclusion . . . 86

**B End point formulas** **89**

**C Single Background Sample CutFlow Tables** **91**
C.1 Standard etcone20 isolation . . . 91
C.2 Normalized etcone isolation . . . 92

**References** **93**

# List of Figures


1.1 Particle Discoveries 1898-1964 . . . 2
1.2 Illustration of the radiative corrections to a Higgs boson. a) is the fermion loop, b) is the scalar loop. . . . 5
1.3 Running of the coupling constants . . . 6

2.1 Running of masses from the GUT scale to the Weak Scale [15] . . . 10
2.2 Decay of gluino through chargino, leading to a finalstate with a lepton and jets. . . . 15

3.1 The ATLAS detector . . . 19
3.2 The ATLAS coordinate system [10] . . . 21
3.3 Magnet system . . . 21
3.4 Inner detector . . . 22
3.5 Inner detector . . . 22
3.6 Data flow . . . 25
3.7 Scetch of the online monitoring setup. . . . 27
3.8 The Trigger and Data Acquisition Tool and the Online Histogram Presenter . . . 27
3.9 Number of hits per track and track through SCT and TRT . . . 27

5.1 Lepton $\eta$ and $p_T$ distributions for generated leptons. Primary (Prim M) and secondary (Sec M) leptons shown in these plots have a match (M) to a reconstructed lepton, while the leptons that are not matched (Not M) contain all not-reconstructed leptons. Signal sample SU3. . . . 34
5.2 Pt vs Eta distribution for Bulk Region SU3 MC generated electrons. . . . 35
5.3 Pt vs Eta distribution for Bulk Region SU3 MC generated muons. . . . 36
5.4 Number of leptons reconstructed as function of eta for electrons and muons respectively for the signal point SU3. Prim M and Sec M are respectively primary and secondary leptons that have a match to a generator-level lepton, while Not M are all leptons that do not have a generator level match. . . . 39
5.5 Transverse momentum $p_T$ for various categories of leptons as described in text. . . . 39
5.6 Transverse momentum $p_T$ for various categories of leptons for the leptonic $t\bar{t}$ sample T1 . . . 39
5.7 $p_T$ of reconstructed primary, secondary or not matched leptons for the low mass point SU4. $p_T$ cut on 10GeV is applied . . . 40
5.8 Reconstruction efficiency, reconstructed electrons/ generated electrons . . . 41
5.9 Reconstruction efficiency, reconstructed muons/ generated muon . . . 41
5.10 Angular distance $\Delta$R between the electron and the closest jet after electron-jet overlap removal but before lepton isolation. . . . 42
5.11 Transverse energy in a cone of 0.2 around the lepton, the leptons energy has been subtracted. 43
5.12 Distributions for the normalized transverse energy in a cone of 0.3 from electrons and muons respectively. Normalization is done by dividing the transverse energy in a cone around the lepton with the transverse momentum of the lepton itself. Signal sample SU3. . . . 44
5.13 First two rows show the pure etcone disttributions, while the next two rows show the normalized values. Efficiency $\epsilon_P$ of selecting primary leptons and the rejection $r_E$ of extra leptons, both as function of the cut in etcone value are shown. Lepton pt>10GeV, $|\eta|$<2.5. . . . 45
5.14 $(\epsilon_P) \times (r_E)$ as function of the cut in etcone value. . . . 46

5.15 Number of prompt (Prim) and secondary and not matched (Sec) leptons that pass or fail isolation requirements. The Standard isolation cut is etcone20<10GeV, while the Normalized isolation is etcone20/$p_T(lep)$<0.05. The two bottom plots have required 2 isolated leptons of opposite sign, while the first takes into account all events. The bottom left plot have a lepton $p_T$ requirement $lep^{hardest}, lep^{second}$ > (10,10), while the bottom right plot uses (20,10). . . . . 47
5.16 Angular distance $\Delta R$ between the lepton and the closest jet without any calorimeter isolation requirements. . . . . 48
5.17 Angular distance $\Delta R$ between lepton and jet after electron jet overlap removal, and after all particle definition cuts have been applied. SU3 signal sample. . . . . 49

6.1 Multiplicity of dilepton types in event according to sign and flavour. SU3 signal sample and the most important background sample, the T1 sample. . . . . 52
6.2 $p_T$ of reconstructed primary, secondary or not matched leptons for the bulk region signal point SU3. Event has 2 leptons of opposite sign. $P_T$ cut on the leptons of 10 or 20GeV is applied. 53
6.3 Missing transverse energy for a) the $t\bar{t}$ (semi) leptonic background and various signal samples. 2 isolated opposite sign leptons required, no generator level cuts, b) and c) have the generator based cuts applied $\not{E}_{\mathrm{T}}$ > 100 GeV, $p_T^{jet1,jet2}$> 100, 50GeV in addition to 2 isolated opposite sign leptons, b) shows various signal samples and the total background and c) signal sample SU3 and the various classes of backgrounds. . . . . 54
6.4 Effective mass when cutting on 3 values of $\not{E}_{\mathrm{T}}$ . 2 isolated leptons with opposite sign and extra generator-level cuts, a preselection of $\not{E}_{\mathrm{T}}$ > 100 GeV, $p_T^{jet1,jet2}$ > 100, 50 GeV have been applied. . . . . 55
6.5 Number of jets with $p_T$> 50 GeV. 2 isolated leptons of opposite sign have been required for all plots. Plot a) shows the $t\bar{t}$ (semi) leptonic SM background sample T1 together with various SUSY signal samples. Event has no other requirements than 2 isolated leptons of opposite sign, in particular no generator based cuts. Plot b) shows the sum of backgrounds and various signal samples, plot c) shows the sum of backgrounds, all background samples and the signal sample SU3. Plot b) and c) have applied the generator based cuts: $\not{E}_{\mathrm{T}}$ > 100GeV, $p_T^{jet1,jet2}$> 100, 50 GeV. . . . . 57
6.6 Transverse momentum $p_T$ of the hardest jet in the event. Plot a) show SM (semi) leptonic $tt\bar{t}$ sample "T1" and for the various SUSY signal samples. Only requirement on event is at least 2 opposite signed well-defined leptons required. Plot b) shows various signal samples versus the sum of all backgrounds, plot b) shows the signal sample SU3 together with the sum of all backgrounds, and also each class of backgrounds seperately. Event requirements for all 3 plots are at least 2 isolated opposite sign leptons, and for plot (b,c) additional generator-based cuts $\not{E}_{\mathrm{T}}$ > 100 GeV, $p_T^{jet1,jet2}$ > 100, 50 GeV. SU1 and SU6 have similar distribtutions as SU3 and are therefore not shown. . . . . 58
6.7 Effective mass when requiring event to contain 2 leptons of opposite sign, $\not{E}_{\mathrm{T}}$ > 100 GeV and 2, 3 or 4 jets with $p_T^{All}$ > 50 GeV, $p_T^1$ > 100 GeV . . . . . 60
6.8 Effective mass distributions after 2 leptons of opposite sign have been required, and in addition 3 jets satisfying $p_T^{JetAll}$ > 50 GeV, $p_T^{Jet1}$ > 100 GeV. Plots show effect of $\not{E}_{\mathrm{T}}$ cut for $\not{E}_{\mathrm{T}}$ > (100,150,200) GeV . . . . . 61
6.9 $\not{E}_{\mathrm{T}}$ / (MEFF), both plots require 2 leptons of opposite sign, and (b) requires in addition 2, 3 or 4 jets with $p_T^{JetAll}$ > 50 GeV$p_T^{Jet1}$ > 100GeV and $\not{E}_{\mathrm{T}}$ >100 GeV . . . . . 63

7.1 Signal decay chain for mass measurement of $\widetilde{\chi}_2^0$ . . . . . 67
7.2 Effective mass after consequetive cuts. Etcone20<10GeV lepton isolation . . . . . 69
7.3 Effective mass Meff for all SUSY signal points discussed and SM background after all cuts have been applied. . . . . 70
7.4 Significances as function of cut in effective mass Meff. The first row show results using the etcone20 isolation algorithm, while the second row uses the normalized netcone20. All other cuts are identical: $\not{E}_{\mathrm{T}}$ > 150 GeV, 3 jets $p_T^1$>100 GeV, $p_T^{2,3}$> 50 GeV, lepton $p_T^{1,2}$> 20,10 GeV 71
7.5 Leptonic W-boson decay . . . . . 77
7.6 Invariant mass of two opposite sign same flavour leptons after consecutive cuts for the SUSY signal sample SU3, and the SM background. Lepton isolation etcone20<10GeV . . . . . 78
7.7 Invariant mass of two leptons of opposite sign and opposite flavour after all cuts and flavour subtraction. Plots to the left have applied the standard etcone20 < 10 GeV isolation requirement, while the plots to the right have used the normalized lepton isolation etcone20 <0.05 . 80

A.1 Level 1 Trigger . . . . . 83

A.2 Bunch encoding . . . . . 84
A.3 No muon Segments . . . . . 85
A.4 DT hits . . . . . 87
A.5 $\Delta$ bunch July . . . . . 88
A.6 $\Delta$ bunch August . . . . . 88

# List of Tables


1.1 The matter particles of the SM. The neutrino, considered massless has no right handed component. Recent neutrino oscillations experiments have however proven that neutrino do have a tiny mass. . . . 3
1.2 The chiral supermultiplet fields of MSSM [15]. . . . 6
1.3 The gauge supermultiplet fields of MSSM, the gauginos. The winos and binos mix with the higgsinos giving charginos and neutralinos that are mass-eigenstates. The mixing of the $B^0$ and $W^0$ follows the SM-case giving the photon and Z-boson . . . 7
1.4 A total overview of the sparticles of Supersymmetry, their gauge- and mass-eigenstates. . . . 7

2.1 Ordered mass spectra (a) SU1, (b) SU2 and (c) SU3 . . . 12
2.2 Ordered mass spectra (a) SU4, (b) SU6, (c) SU8 . . . 13
2.3 Heaviest sparticles from each category . . . 13
2.4 Squark and gluino production cross sections as calculated by prospino 2.0.6 Numbers do not exactly correspond to the SUSY LO cross sections that I use, but will be used as a reference. 14

4.1 Background samples . . . 30
4.2 SUSY points . . . 31

5.1 Number of leptons generated, Bulk region SU3 . . . 35
5.2 Lepton definition and isolation requirements . . . 37
5.3 Alternative lepton definition . . . 38

6.1 Common cuts in a dilepton SUSY search . . . 51
6.2 Relative efficiency and rejection factors and significances when running over the $\not{E}_{\mathrm{T}}$ requirement. All events are required to have 2 isolated leptons of opposite sign, and extra generator-based requirements, but no additional requirement. First row, $\epsilon_S$ column states total number of signal events, first row $r_B$ column states total number of background events. . . . 56
6.3 Relative efficiency and rejection factors, and significances when requiring 2, 3 or 4 jets in the event. All events are required to have 2 leptons of opposite sign, and generator level preselection cuts: $\not{E}_{\mathrm{T}}$ >100GeV, $p_T^{jet1,jet2}$>100,50 GeV. First row, $\epsilon_S$ column states total number of signal events, first row $r_B$ column states total number of background events. . . . 59
6.4 Relative efficiencies and rejection factors, and significances when running over the $\not{E}_{\mathrm{T}}$ cut. All events have 2 isolated leptons of opposite sign, and 3 jets with $p_T^{JET1} \geq 100$, $p_T^{all} \geq 50$. First row, $\epsilon_S$ column states total number of signal events, first row $r_B$ column states total number of background events. . . . 62
6.5 Relative efficiencies and rejection factors, and significances when running over the $\not{E}_{\mathrm{T}}$ cut. All events have 2 isolated leptons of opposite sign, and 4 jets with $p_T^{JET1} \geq 100$, $p_T^{all} \geq 50$. First row, $\epsilon_S$ column states total number of signal events, first row $r_B$ column states total number of background events. . . . 62
6.6 Relative efficiency and rejection factors, and significances when running over the $\not{E}_{\mathrm{T}}$/Meff cut. All events have 2 isolated leptons of opposite sign, and 3 jets with $p_T^{JET1} \geq 100$, $p_T^{all} \geq 50$ and $\not{E}_{\mathrm{T}}$ >100GeV. First row, $\epsilon_S$ column states total number of signal events, first row $r_B$ column states total number of background events. . . . 64
6.7 Final choice of event cuts . . . 65

7.1 Significances as function of cut in Meff. Top table use lepton isolation etcone20 < 10 GeV, while bottom table uses the normalize netcone20 < 0.05. Significances are: $S1$ $S/\sqrt{B}$, $S2 : S/\sqrt{(B + (0.5B)^2)}$, $S3 : (SF - 0F)/\sqrt{(SF + OF)}$ and $S4 : (SF - 0F)/\sqrt{(2 \cdot OF)}$. Second column of the table reports number of background events (B), while first column of each SUSY sample is number of Signal (S) events. . . . . 72
7.2 Significances as function of cut in Meff. Top table use lepton isolation etcone20 < 10 GeV, while bottom table uses the normalize netcone20 < 0.05. Significances are: $S1$ $S/\sqrt{B}$, $S2 : S/\sqrt{(B + (0.5B)^2)}$, $S3 : (SF - 0F)/\sqrt{(SF + OF)}$ and $S4 : (SF - 0F)/\sqrt{(2 \cdot OF)}$ . Second column of the table reports number of background events (B), while first column of each SUSY sample is number of Signal (S) events. . . . . 73
7.3 Significances as function of cut in Meff. Top table use lepton isolation etcone20 < 10 GeV, while bottom table uses the normalize netcone20 < 0.05. Significances are: $S1$ $S/\sqrt{B}$, $S2 : S/\sqrt{(B + (0.5B)^2)}$, $S3 : (SF - 0F)/\sqrt{(SF + OF)}$ and $S4 : (SF - 0F)/\sqrt{(2 \cdot OF)}$. Second column of the table reports number of background events (B), while first column of each SUSY sample is number of Signal (S) events. . . . . 74
7.4 Number of signal events after consequetive cuts. Lepton isolation etcone20<10GeV, $p_T^{lep1,lep2}$> 20,10 GeV. Generator level cuts (Gen Cuts) $\not{E}_{\mathrm{T}}$ >100 GeV, 2 jets $p_T^{1,2}$ >100,50 GeV. . . . . 75
7.5 Number of SM background events grouped into categories. Cuts are made consequetive cuts. Lepton isolation etcone20<10GeV, $p_T^{lep1,lep2}$> 20,10 GeV. Generator level cuts (Gen Cuts) $\not{E}_{\mathrm{T}}$ >100 GeV, 2 jets $p_T^{1,2}$ >100,50 GeV. . . . . 76

C.1 Number of SM background events after consequetive cuts for each individual background sample. Lepton isolation etcone20<10GeV, $p_T^{lep1,lep2}$> 20,10 GeV. Generator level cuts (Gen Cuts) $\not{E}_{\mathrm{T}}$ >100 GeV, 2 jets $p_T^{1,2}$ >100,50 GeV. . . . . 91
C.2 Number of SM background events after consequetive cuts for each individual background sample. Lepton isolation etcone20<10GeV, $p_T^{lep1,lep2}$> 20,10 GeV. Generator level cuts (Gen Cuts) $\not{E}_{\mathrm{T}}$ >100 GeV, 2 jets $p_T^{1,2}$ >100,50 GeV. . . . . 92
C.3 Number of SM background events after consequetive cuts for each individual background sample. Normalized lepton isolation netcone20<0.05, $p_T^{lep1,lep2}$> 20,10 GeV. Generator level cuts (Gen Cuts) $\not{E}_{\mathrm{T}}$ >100 GeV, 2 jets $p_T^{1,2}$ >100,50 GeV. . . . . 92
C.4 Number of SM background events after consequetive cuts for each individual background sample. Normalized lepton isolation netcone20<0.05, $p_T^{lep1,lep2}$> 20,10 GeV. Generator level cuts (Gen Cuts) $\not{E}_{\mathrm{T}}$ >100 GeV, 2 jets $p_T^{1,2}$ >100,50 GeV. . . . . 92

# Chapter 1

# The Standard Model and Supersymmetry - brief introduction to particle physics and its theoretical framework

Particle physics deals with the believed smallest constituents of matter, and tries to explain their properties and interactions. Today's applied theories and models of particle physics were developed in the 1900s and put together in the 1970s to a coherent model called the Standard Model (SM).

We will start by a brief historical overview of particle physics, before going through the basic theoretical concepts of the SM. We will mention some of the Standard Model's important shortcomings, and introduce Supersymmetry as a possible solution, together with its basic theoretical framework.

## 1.1 Introduction to particle physics

The idea that matter must consist of elementary building blocks dates back to ancient times. One formulation of this in the western world was done by the Early Greek philosophers stating that the 4 elements: water, air, earth and fire constructed the world. Around 440 B.C Democritus launched the concept of the atomus being the smallest building block of all matter, and the search for this smallest constituent has been ongoing since. In the early 1800's the chemist John Dalton found evidence of particles believed to be in-divisible. Later, when the electron was discovered in 1897 by John Joseph Thomson, one had to conclude that the atom was not one indivisible particle, but made up of a positively charged sphere embedded with negatively charged electrons. This model was kept until 1909 when Hans Geiger and Ernest Marsden under the direction of Ernest Rutherford measured the scattering of alpha-particles off sheets of thin gold foil. They observed that the alpha-particles mainly went right through the foil as expected but that a few were actually back-scattered. Measurements of this scattering resulted in Ernest Rutherford's orbital theory of the atom. The theory postulates the atom as a dense central positive charge surrounded by a cloud of negatively charged electrons, and mostly empty space. Since then particle physics has

been through a revolution. Max Planck postulated quantized radiation, which lead to Albert Einstein proposing a quanta of light, the photon, which was to behave as a particle. Albert Einsteins famous relation between matter and energy $E = mc^2$ and the formulation of the special theory of relativity came the same year, in 1905. During the early and mid 1900's Einstein, together with important physicists like Paul Dirac, Werneer Heisenberg and Erwin Schroedinger amongst others, laid the foundation of modern physics as we know it, based on quantum mechanics and special relativity.

### 1.1.1 The particle adventure

From the 1930's and onward physicists discovered totally new particles, see figure 1.1, first from cosmic rays, and later in accelerators. The electron, proton and neutron were not any more the exclusive matter-particles, and a theory describing all these new particles and their interactions was necessary. In 1964 the first proposal was put forth of quarks as elementary particles making up the proton and neutron. This developed into a model of matter and interactions that has been called the Standard Model (SM). The SM has had great success in describing properties of matter

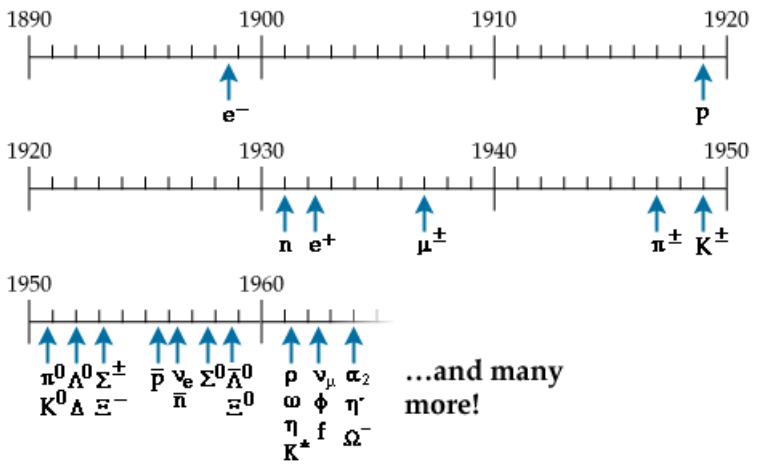


Figure 1.1: Particle Discoveries 1898-1964

and interactions and even predicting new particles that later have been found by experiment. Despite all the success in describing the microscopic world we are facing the fact that there are several questions that the SM cannot answer. In the next sections we will give a brief introduction to the SM, mention some important shortcomings and introduce Supersymmetry (SUSY) as a possible solution. The most important aspects of the SM and SUSY theory will also be given.

## 1.2 The SM

The SM is based on quantum field theory with gauge symmetries describing the dynamics of the systems. The gauge symmetries are conveyed through the groups $SU(3)_C \otimes SU(2)_L \otimes U(1)_Y$ [1] which describes quantum chromodynamics ($SU(3)_C$), weak interaction ($SU(2)_L$) and electromagnetic interactions ($U(1)_Y$) respectively. The subscript $Y$ denotes hypercharge, $L$ stand for left

[1] S stands for special, meaning that the matrices of a $SU(N)$ group have a determinant 1, while $U$ stands for unitary

- handed [2] and $C$ colour [3]. The fields are divided into matter fields and gauge fields, where the gauge fields describe the interactions allowed in the model. In a $SU(N)$ group there are $N^2-1$ independent elements of the $N \times N$ matrix which are then, from $SU(3)_C$ the 8 gluons, for $SU(2)_L$ 3 spin one particles $W_\mu^\alpha$ and from $U(1)$ one $B_\mu$. Abdus Salam, Sheldon Lee Glashow and Steven Weinberg showed that electromagnetism and weak interaction could be described by a common framework owing to relation 1.1. The group $SU_L(2) \otimes SU_Y(1)$ undergoes spontaneous symmetry breaking which mixes the $W_\mu^\alpha$ and $B_\mu$ resulting in the physical bosons, the $W^\pm$, $Z^0$, mediators of weak interaction and of finite range, and the photon $\gamma$ which is the messenger of electromagnetic interactions and has infinite range.

The fields of the SM are either spin half fermion fields, spin 1 boson fields or spin 0 scalar fields. The fermions are the matter particles of the SM, while the bosons[4], are the interaction particles. The SM scalar part has only 1 physical manifestation in form of the not yet confirmed Higgs boson, the only missing ingredient of the SM, if we forget the graviton transmitting gravity.

The matter fields, the fermions, are grouped into weak isospin states of left-handed doublets and right-handed singlets. Only left handed particles interact weakly, reflecting the subscript $L$ of the gauge group responsible for weak interaction $SU(2)_L$. This is due to the fact that parity is maximally violated in weak interactions. Precise experimental measurement on the Z-boson width points to exactly 3 light neutrinos, and hence 3 generations of particles giving us the the matter particle content of the Standard Model shown in table 1.1.

| Names | Spin 1/2 | SU(3),SU(2),U(1) |
|---|---|---|
| quarks | $(u_L \;\; d_L)$, $(c_L \;\; s_L)$, $(t_L \;\; b_L)$ | $(\mathbf{3}, \mathbf{2}, \frac{1}{3})$ |
| | $u_R^\dagger$, $c_R^\dagger$, $t_R^\dagger$ | $(\bar{\mathbf{3}}, \mathbf{1}, -\frac{4}{3})$ |
| | $d_R^\dagger$, $s_R^\dagger$, $b_R^\dagger$ | $(\bar{\mathbf{3}}, \mathbf{1}, \frac{2}{3})$ |
| leptons | $(\nu_e \;\; e_L)$, $(\nu_\mu \;\; \mu_L)$, $(\nu_\tau \;\; \tau_L)$ | $(\mathbf{1}, \mathbf{2}, -1)$ |
| | $e_R^\dagger$, $\mu_R^\dagger$,$\tau_R^\dagger$ | $(\mathbf{1}, \mathbf{1}, 2)$ |

Table 1.1: The matter particles of the SM. The neutrino, considered massless has no right handed component. Recent neutrino oscillations experiments have however proven that neutrino do have a tiny mass.

Electric charge, hypercharge and weak isospin are related through the formula

$$Q = I_3^W + \frac{1}{2} Y^W \tag{1.1}$$

where Q is the electric charge, $I_3^W$ the 3rd component of weak isospin, and $Y^W$ the hypercharge. $I_3^W$ have values $\pm\frac{1}{2}, 0$. As an example the up quark will then have an electric charge $u_Q = \frac{1}{2} + \frac{1}{2} \cdot \frac{1}{3} = \frac{2}{3}$, while the electric charge of the down quark will be $d_Q = -\frac{1}{2} + \frac{1}{2} \cdot \frac{1}{3} = -\frac{1}{3}$. Quarks come in 3 colours, and 2 up quarks and a down quark make up a colour neutral configuration as found in the proton.

All particle constituents and interactions are described through the Lagrangian density $\mathcal{L}$ which in a schematic form can be written as

$$\mathcal{L} = \mathcal{L}_0 + \mathcal{L}_{int} \tag{1.2}$$

where $\mathcal{L}_0$ describes the free field part, and $\mathcal{L}_{int}$ describes the interaction part. The interaction can be considered a perturbation of the free field [4]. The principle of gauge-invariance of the Lagrangian density $\mathcal{L}$ under *local* phase transformations puts strong constraints on the theory

[2] Right handed particles don't interact weakly

[3] Quarks come in 3 colours and make up colour - neutral configurations

[4] called gauge - bosons since their existence comes from the gauge- invariance principle of the interaction part of the Lagrangian which describes all properties of the particles and possible interactions

and as a consequence forces us to introduce new fields resulting in the physical photon, the W and Z bosons and the gluons.

The SM Lagrangian (1.2) is only able to describe massless particles. We need a mechanism in order to introduce masses for the gauge bosons and the fermions. By introducing an additional doublet Higgs scalar field

$$\Phi = \begin{pmatrix} \phi^+ \\ \phi^0 \end{pmatrix}$$

we acquire new terms in the Lagrangian, the free Higgs field terms and the interaction between fermions and bosons respectively. When the neutral component $\phi^0$ acquires a vacuum expectation value $vev \neq 0$ the $SU(2)_L \times U(1)_Y$ symmetry [5] of the Lagrangian is spontaneously broken through the Higgs mechanism[6] allowing masses of fermions and bosons. The photon still remains massless as required by the Special Theory of Relativity and $U(1)$ gauge invariance.

With the Higgs mechanism and the spontaneous symmetry breaking of $SU(2)_L \times U(1)_Y$ we now have a model that describes matter and interaction particles with masses as required. Together with QCD based on $SU(3)_C$, this makes up the SM.

## 1.3 Some important shortcomings of the SM

The SM has had a an enormous success as all theoretical implications have been confirmed except the Higgs mechanism. Despite this, several important questions cannot be answered by the SM, and physicists have proposed various solutions. One is the supersymmetric extension of the SM, so called Supersymmetry (SUSY). In this and the following section we will go through some shortcomings of the SM, and suggest solutions as proposed by SUSY.

One problem of the SM is the too high number of free parameters. The masses of the particles in the SM, although induced by the Higgs mechanism have to be set by hand since these are free parameters in the SM. The same goes for mixing angles, for instance the Weinberg angle $\theta_W$ parametrizes the mixing in the electroweak theory and the CKM (Cabbibo, Kobayashi, Maskawa) quark mass mixing parameters. Now that neutrino have mass, there are also the corresponding lepton mixing parameters. Another issue is that experiments strongly suggest 3 generation of particles which does not contradict the SM, but for which the SM does not have any explanation. Additional arguments pointing to physics beyond the SM is the fact that gravity indeed exists. The SM does not incorporate gravity, and any unification of all forces at ultra high energies would necessitate a quantum description of gravity. In addition the Universe seems to be filled with cold dark matter which we have not been able to measure, but see due to its gravitational impact. The SM does not have a candidate particle to explain this now that neutrinos are confirmed not to contribute substantially to the relic density. A further complication for the SM arises due to the introduction of the Higgs scalar field. Radiative corrections allow fermion loops, and in particular heavy top quarks loops, see figure 1.2 (a). These loops corrections to the mass of the Higgs boson are quadratically dependent on cut-off scale $\Lambda$ and go as

$$\Delta m_H^2|_f = \frac{\lambda_f^2}{8\pi^2}\left[-\Lambda^2 + 6m_f^2 \ln\frac{\Lambda}{m_f}\right] \tag{1.3}$$

where $\lambda_f$ is the fermion Yukawa coupling to the Higgs field and $m_f$ is the mass of the fermion in the loop. If the cut off scale $\Lambda$ is at the Planck scale[7] the corrections that 1.3 give to the Higgs mass far exceeds the theoretical limit of the Higgs mass which is $m_H \sim$ 100-1000 GeV. The Higgs field has this particularity since it is a scalar field. Vector fields (spin 1) or fermion fields (spin 1/2) do not encounter this problem as they are only logarithmically dependent on the cut-off scale $\Lambda$.

[5] The Glashow-Weinberg-Salam model of Electroweak theory

[6] Gerardus t'Hooft 1971

[7] Around $10^{19}$ GeV where gravity becomes important and a possible unification of all forces could take place

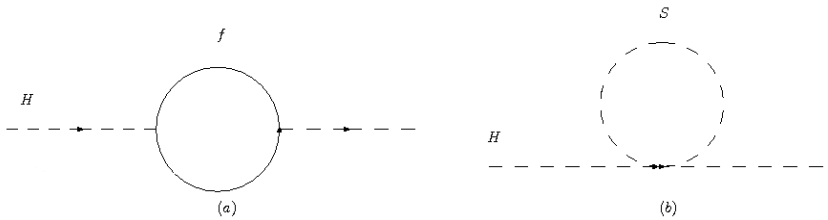


Figure 1.2: Illustration of the radiative corrections to a Higgs boson. a) is the fermion loop, b) is the scalar loop.

## 1.4 Supersymmetry

Supersymmetry conveys a symmetry between spin half fermions and integer spin bosons. This implies that each SM fermion has a supersymmetric partner which is a boson, and each SM boson has a supersymmetric fermion partner. Mathematically this can be described as

$$Q|\text{Boson} >= |\text{Fermion} >, \qquad Q|\text{Fermion} >= |\text{Boson} > \tag{1.4}$$

where $Q$ is some operator generating the transformation. The partners of the SM particles are called *superpartners* and in the *unbroken* description of Supersymmetry they have exactly the same properties as their SM partner except spin which differs by 1/2. This in particular means that they have the same mass and charge. The superpartners are arranged in supermultiplets with the same degree of freedom as their SM partners. This implies that for each SM fermion there must be 2 scalar superpartners, one for each of the fermion helicity states [8]. These chiral [9] superpartners are denoted with subscript R for right, or L for left, reflecting the two helicity states of their SM partner. Introducing this set of new particles has important consequences for instance for the loop corrections of the Higgs boson mass mentioned in the previous section. This is because the scalar partner of the fermion will enter the mass correction with opposite sign of that of the fermion as follows:

$$\Delta m_H^2|_S = \frac{\lambda_S^2}{16\pi^2}\left[\Lambda^2 - 2m_S^2 \ln\frac{\Lambda}{m_S}\right] \tag{1.5}$$

We can see by comparing equation (1.5) with (1.3) that by requiring each SM fermion to have 2 scalar superpartners, the quadratic dependency on the cut off scale $\Lambda$ cancels out since $\lambda_S = 2\lambda_f^2$, and we are left with only a logarithmic dependency which is acceptable in the frameworks of the theory, provided the scale $\Lambda$ is not too high.

Another motivation for studying supersymmetry is the effect it has on the running of the coupling constants from the weak scale to the Grand Unification Scale (GUT) where the electromagnetic, weak and strong coupling constants $\alpha_1, \alpha_2, \alpha_3$ meet, see figure 1.3. A unification including the strong force is desirable since it would convey an additional symmetry, and there should be no reason for needing 3 separate forces. Current measurements at the weak scale hint at a possible unification, but not completely. By introducing additional particles the slope of the extrapolation is altered in such a way that all three coupling constants $\alpha_1, \alpha_2$ and $\alpha_3$ meet at an energy scale 1 order of magnitude higher than expected before, at $10^{16}$. This higher value of unification is an additional benefit as it extends the theoretical lifetime of the proton making it consistent with experimental proton decay results [16].

[8] Helicity is the projection of the particles spin onto its momentum vector. The helicity is positive if the projection of the spin points in the same direction as the momentum, and negative if it points in the opposite direction.

[9] Chirality reflects an intrinsic handedness of the particle, either right-handed or left-handed. Only left-handed particles interact through the weak interaction.

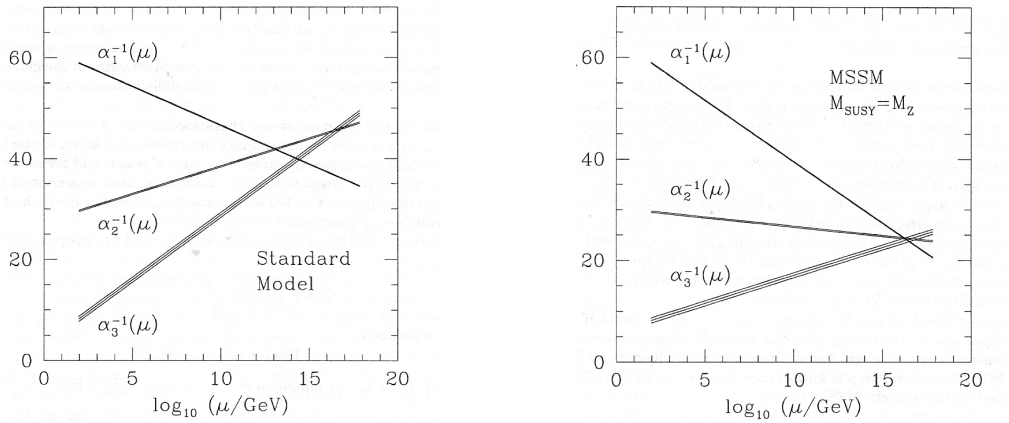


(a) (b)

Figure 1.3: Running of the coupling constants

### 1.4.1 The minimal supersymmetric model and the minimal supergravity model

A supersymmetric extension of the SM is not straightforward, and there is no single way to proceed. The new model should at least address the important shortcomings of the SM and not introduce a large amount of new weaknesses. A minimal extension of the SM, the MSSM is such an attempt. It is minimal in sense of particle content adding the minimal number of extra particles needed for the symmetry considerations. One superpartner is introduced for each SM particle, and these are arranged as earlier mentioned in supermultiplets. Tables 1.2 and 1.3 lists the chiral or matter supermultiplets and gauge supermultiplets respectively as suggested by [15]. Each supermultiplet contains the SM particle and its superpartner so that the internal quantum numbers are the same. Supersymmetric particles are denoted with a tilde $(\widetilde{\ })$ in order to distinguish them from their SM partner. One usually calls the supersymmetric particles, *sparticles*, so that the supersymmetric partner of a quarks is called a squarks and so on. The gauge bosons get the appendix -ino, gauge-boson partners are gauginos, the supersymmetric partner of the photon, photino and so on as summarized in figure 1.4.

| Names | Symbol | Spin 0 | Spin 1/2 | SU(3),SU(2),U(1) |
|---|---|---|---|---|
| squarks, quarks | Q | $(\widetilde{u}_L \ \ \widetilde{d}_L)$ | $(u_L \ \ d_L)$ | $(\mathbf{3},\mathbf{2},\frac{1}{6})$ |
| ($\times$ 3 families) | $\bar{u}$ | $\widetilde{u}_R^\star$ | $u_R^\dagger$ | $(\bar{\mathbf{3}},\mathbf{1},-\frac{2}{3})$ |
| | $\bar{d}$ | $\widetilde{d}_R^\star$ | $d_R^\dagger$ | $(\bar{\mathbf{3}},\mathbf{1},\frac{1}{3})$ |
| sleptons, leptons | L | $(\tilde{\nu} \ \ \widetilde{e}_L)$ | $(\nu \ \ e_L)$ | $(\mathbf{1},\mathbf{2},-\frac{1}{2})$ |
| ($\times$ 3 families) | $\bar{e}$ | $\widetilde{e}_R^\star$ | $e_R^\dagger$ | $(\mathbf{1},\mathbf{1},1)$ |
| Higgs, higgsinos | $H_u$ | $(H_u^+ \ \ H_u^0)$ | $(\widetilde{H}_u^+ \ \ \widetilde{H}_u^0)$ | $(\mathbf{1},\mathbf{2},\frac{1}{2})$ |
| | $H_d$ | $(H_d^0 \ \ H_d^-)$ | $(\widetilde{H}_d^0 \ \ \widetilde{H}_d^-)$ | $(\mathbf{1},\mathbf{2},-\frac{1}{2})$ |

Table 1.2: The chiral supermultiplet fields of MSSM [15].

In SUSY one need two Higgs multiplets in order to give masses to both the up-type and down-type quarks. The Higgs multiplets are listed together with the other matter-particles in table 1.2.

The Higgsino, bino and wino mix after electroweak symmetry breaking resulting in 4 neutral mass eigenstates the neutralinos: $\widetilde{\chi}_1^0, \widetilde{\chi}_2^0, \widetilde{\chi}_3^0$ and $\widetilde{\chi}_4^0$, and two charged mass eigenstates, the

| Names | Spin 1/2 | Spin 1 | $SU(3)_C, SU(2)_L, U(1)_Y$ |
|---|---|---|---|
| gluino, gluon | $\widetilde{g}$ | $g$ | $(\mathbf{8}, \mathbf{1}, 0)$ |
| winos, W bosons | $\widetilde{W}^{\pm}\ \widetilde{W}^{0}$ | $W^{\pm}\ W^{0}$ | $(\mathbf{1}, \mathbf{3}, 0)$ |
| bino, B boson | $\widetilde{B}^{0}$ | $B^{0}$ | $(\mathbf{1}, \mathbf{1}, 0)$ |

Table 1.3: The gauge supermultiplet fields of MSSM, the gauginos. The winos and binos mix with the higgsinos giving charginos and neutralinos that are mass-eigenstates. The mixing of the $B^0$ and $W^0$ follows the SM-case giving the photon and Z-boson

charginos: $\widetilde{\chi}_1^{\pm}, \widetilde{\chi}_2^{\pm}$. The third generation squarks and sleptons also mix resulting in a light sparticle with subscript $_1$ and a heavier with subscript $_2$. The gauge and mass eigenstates are listed in table 1.4.

| Names | Spin | $P_R$ | Gauge Eigenstates | Mass Eigenstates |
|---|---|---|---|---|
| Higgs boson | 0 | +1 | $H_u^0\ H_d^0\ H_u^+\ H_d^-$ | $h^0\ H^0\ A^0\ H^{\pm}$ |
| squarks | 0 | $-1$ | $\widetilde{u}_L\ \widetilde{u}_R\ \widetilde{d}_L\ \widetilde{d}_R$ | ($\sim$ not mixed) |
| | | | $\widetilde{s}_L\ \widetilde{s}_R\ \widetilde{c}_L\ \widetilde{c}_R$ | ($\sim$ not mixed) |
| | | | $\widetilde{t}_L\ \widetilde{t}_R\ \widetilde{b}_L\ \widetilde{b}_R$ | $\widetilde{t}_1\ \widetilde{t}_2\ \widetilde{b}_1\ \widetilde{b}_2$ |
| sleptons | 0 | $-1$ | $\widetilde{e}_L\ \widetilde{e}_R\ \widetilde{\nu_e}$ | ($\sim$ not mixed) |
| | | | $\widetilde{\mu}_L\ \widetilde{\mu}_R\ \widetilde{\nu_\mu}$ | ($\sim$ not mixed) |
| | | | $\tilde{\tau}_L\ \tilde{\tau}_R\ \widetilde{\nu_\tau}$ | $\tilde{\tau}_1\ \tilde{\tau}_2\ \widetilde{\nu_\tau}$ |
| neutralinos | 1/2 | $-1$ | $\widetilde{B}^0\ \widetilde{W}^0\ \widetilde{H}_u^0\ \widetilde{H}_d^0$ | $\widetilde{\chi}_1^0\ \widetilde{\chi}_2^0\ \widetilde{\chi}_3^0\ \widetilde{\chi}_4^0$ |
| charginos | 1/2 | $-1$ | $\widetilde{W}^{\pm}\ \widetilde{H}_u^+\ \widetilde{H}_d^-$ | $\widetilde{\chi}_1^{\pm}\ \widetilde{\chi}_2^{\pm}$ |
| gluino | 1/2 | $-1$ | $\widetilde{g}$ | ($\sim$ not mixed) |
| goldstino | 1/2 | -1 | $\widetilde{G}$ | ($\sim$ not mixed) |
| (gravitino) | (3/2) | | | |

Table 1.4: A total overview of the sparticles of Supersymmetry, their gauge- and mass-eigenstates.

### R-parity

R-parity is a quantum number that relates particles and sparticles through $R = (-1)^{2j+3B+L.}$ where j stands for spin, B for baryon number and L for lepton number. All supersymmetric particles have parity -1 while all SM particles have parity 1. MSSM does not necessarily conserve R-parity, but by choosing R-parity conservation the supersymmetric model acquires a tempting feature, namely a lightest supersymmetric particle, the LSP, which is stable and weakly interacting [10]. This is because by requiring R-parity conservation all supersymmetric particles are created in pairs, and all decays must contain an odd pair of supersymmetric particles. Each supersymmetric process will then contain two LSPs leaving a particular signature in form of large missing transverse energy $\not{E}_{\mathrm{T}}$ .

[10] The LSP is a candidate for dark matter, which interacts very weakly, it is a so called WIMP, Weakly Interacting Massive Particle.

### 1.4.2 mSUGRA

Since the supersymmetric particles have not been discovered, assuming they exist, the symmetry of the model must be broken, meaning not exact. This must lead to the SUSY particle getting a larger mass than their SM partner, otherwise they would already have been discovered. The masses must at least be heavier than the experimental limits put by SUSY searches at previous particle experiments.

When breaking the symmetry one allows for new mass terms in the Lagrangian density $\mathcal{L}$ which then are responsible for the large masses that we expect for the supersymmetric particles[11]. There are several models for breaking supersymmetry and one of these is the minimal Super Gravity model mSUGRA. mSUGRA breaks the symmetry in a "hidden" sector and mediates the breaking through gravity. At the GUT scale, the parameters of MSSM are assumed to be unified which leads to the following relation of the free parameters of mSUGRA [2]

$$\begin{aligned} g_1 = g_2 = g_3 &\equiv \boldsymbol{g_{GUT}} \\ M_1 = M_2 = M_3 &\equiv \boldsymbol{m_{1/2}} \\ m_Q^2 = m_U^2 = m_D^2 = m_L^2 = m_E^2 = m_{H_u}^2 = m_{H_d}^2 &\equiv \boldsymbol{m_0^2} \\ A_t = A_b = A_\tau &\equiv \boldsymbol{A_0} \end{aligned} \tag{1.6}$$

where $g_i$ are the coupling constants, $M_i$ are the SUSY fermion masses, $m_X^2$ the SUSY scalar masses and $A_0$ is related to the Higgs-sfermion-sfermion Yukawa couplings. We then end up with only 5 parameters which completely defines the supersymmetric mass hierarchy and these are

$$m_0, \quad m_{1/2}, \quad A_0, \quad \tan\beta, \quad \text{sign}\mu$$

where $\tan\beta$ is the relation between the two vacuum expectation values of the Higgs fields in SUSY $\tan\beta = \frac{v_u}{v_d}$ and $\mu$ is the Higgs mass parameter.

[11] The particle accelerator soon to be started at CERN has been built in order to investigate possibilities of new physics, and possibly discover the Higgs. The collider energy at 14TeV could allow supersymmetric processes.

# Chapter 2

# SUSY in mSUGRA

In the previous chapter we explained that the features of the SUSY model are dependent on the breaking mechanism we choose and the values we give the resulting free parameters, which in mSUGRA are 5, assuming GUT-scale unification of the gauge-couplings. The values we choose for these will completely determine the mass-hierarchy of the supersymmetric particles, and thereby the allowed decay-chains and the branching-ratios. This will furthermore affect the experimental signature and it is therefore important to understand and study the different points in the model. In addition to these model-specific features, mSUGRA also exhibits some general characteristics. These are large missing transverse energy $\not{E}_{\mathrm{T}}$ , due to the lightest supersymmetric, weakly interacting massive particle (WIMP) escaping the detector, large effective mass defined as $M_{eff} = \not{E}_{\mathrm{T}} + \sum_{i=1}^{4} p_T^{jet_i}$, which serves as a SUSY mass-scale, and in general many and hard jets and leptons from the squark and slepton decays. A subset of this are events that contain 2 final-state leptons of opposite sign. We will see that because the $\widetilde{\chi}_2^0$ can give us this we expect an excess of these types of events compared to the SM. There will also be correlated opposite signed leptons from Z decays in both the SM and in SUSY, but these should be of comparable size. Uncorrelated production of 2 opposite sign leptons from two W's or $\chi^{\pm}$'s will also cancel out statistically since the probability of generating either charge is the same.

In this section we will then go through the mass evolution from the GUT-scale to the weak scale, look at the resulting mass-hierarchies for several mSUGRA points, and find features to look for in the experiment. We will compare a general supersymmetric event to an expected standard model event and base our choice of studying opposite charged di-leptonic supersymmetric events.

## 2.1 Mass evolution

Out of all possible mSUGRA points a few benchmark points have been chosen from cosmological considerations. These belong to regions in the $m_0, m_{1/2}, \tan\beta, A_0$ parameter-space where the relic density is expected to be low corresponding to the measurements of WMAP. [1]. The four free parameters are the $A$-parameters (related to the Yukawa couplings), the scalar masses and the fermion-masses respectively as explained in section 1.4.2

The large masses we expect to see at the weak scale are parametrized by soft SUSY breaking terms. These evolve as does the gauge couplings and the Yuakwa couplings, as we move down from the GUT scale to the weak scale inducing the mass differences between the SM particles and their SUSY partners. Figure 2.1 visualizes the running of the masses.

The evolution for all the supersymmetric particles, the $\mu$-parameter and the A-parameters are described by 26 renormalization group equations (RGE) [2]. These can be solved giving

[1] WMAP measures the Photon Microwave Background Radiation, allowing to study the Universe some 300 000 years after the Big Bang, http://map.gsfc.nasa.gov/

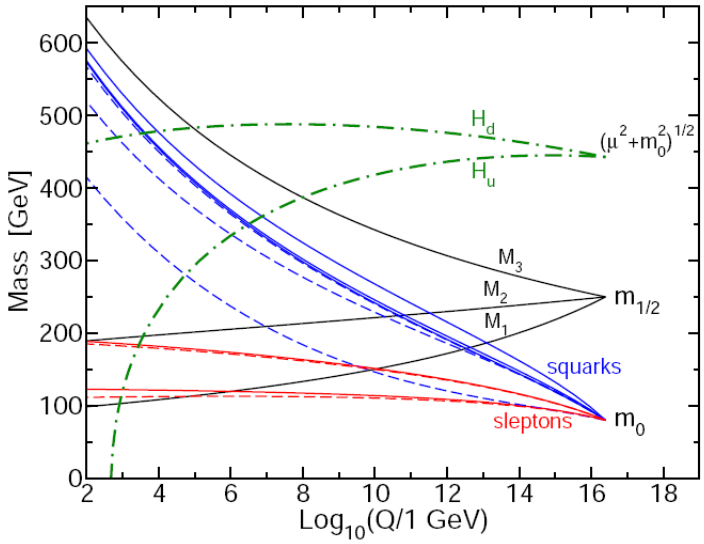


Figure 2.1: Running of masses from the GUT scale to the Weak Scale [15]

initial values of the gauge couplings, the Yukawa couplings, the soft breaking terms and the $\mu$ parameter at a chosen scale $Q_0$ and will completely determine the sparticle masses and their Yukawa interactions at the weak scale. We then understand that by giving different initial values we end up with different sparticles masses, which again will gives us different physics. The various mSUGRA points, some of which will be studied in this thesis, are choices of such initial values.

## 2.2 General sparticle evolution

### 2.2.1 Gauginos

Assuming mass universality which gives us at the GUT scale $\frac{M_1}{\alpha_1} = \frac{M_2}{\alpha_2} = \frac{M_3}{\alpha_3}$ all the gaugino masses $M_i$ evolve following the simple relation [16]

$$M_i(t) = \frac{\alpha_i(t)}{\alpha_0} m_{1/2}$$

which, when we insert values for the various coupling constants $\alpha_i$, results in the mass formulas at the weak scale

$$\begin{aligned} M_3 \equiv M_{\tilde{g}} &\simeq 2.7 m_{1/2} \\ M_2(M_Z) &\simeq 0.8 m_{1/2} \\ M_1(M_Z) &\simeq 0.4 m_{1/2} \end{aligned} \tag{2.1}$$

Under the spontaneous breakdown of $SU(2)_L \times U(1)_Y$ $M_1$ and $M_2$ mix giving us the physical charginos and neutralinos. (M3 does not mix since it is described by an exact gauge symmetry based on the $SU(3)_C$ group, so that $m_{\tilde{g}} = M_3$.) The resulting model-dependent mixing patterns are rather complicated, but they can be roughly divided into scenarios where the gauginos are described by being either gaugino-like or higgsino-like. This is valid if the electroweak symmetry-

breaking effects are small compared to the soft symmetry breaking effects i.e. $M_Z \ll |\mu \pm M_2|$. With this assumption it happens that if $M_2 \ll \mu$ the lightest chargino ($\widetilde{\chi}_1^{\pm}$) and the two lightest neutralinos ($\widetilde{\chi}_1^0, \widetilde{\chi}_2^0$) are gaugino-like (respectively wino-, bino- and wino-like), while the heavier chargino and neutralinos ($\widetilde{\chi}_2^{\pm}$, $\widetilde{\chi}_3^0, \widetilde{\chi}_4^0$) are higgsino-like. For the opposite situation $M_2 \gg \mu$ we have reversed relations, i.e. the lightest neutralino and two lightest charginos are higgsino-like while the heavier neutralinos and charginos are gaugino-like. This affects the gauginos interaction properties: if the gaugino is mostly wino-like it will have a large weak coupling, if it is bino-like, the weak coupling will be very small and so on.

### 2.2.2 Squarks and sleptons

The evolution of the squark and slepton masses is completely determined by the gauge- and Yukawa-interactions, the former increases the mass of the supersymmetric particles, while the latter reduces it. Only 3rd generation sparticles have any significant contribution from the Yukawa interactions, so for the 1st and 2nd generation of sparticles this term is ignored. As the masses evolve they split up from the unification value according to each particle's interaction properties. In this way left handed squarks gain most weight, the right-handed a bit less since these do not interact weakly, while the right-handed sleptons which neither have strong nor weak interactions evolve the least. The 3rd generation squarks and sleptons will be the lightest particles of their sort due to the Yukawa term acting negatively on the mass evolution. A simplified version [2] of the solutions of the renormalization group equations [2]

$$\begin{aligned} m_{\tilde{q}}^2 &\simeq m_0^2 + (5-6)m_{1/2}^2 \\ m_{\tilde{e}_L}^2 &\simeq m_0^2 + 0.5m_{1/2}^2 \\ m_{\tilde{e}_R}^2 &\simeq m_0^2 + 0.15m_{1/2}^2 \end{aligned} \tag{2.2}$$

The range in the first equation depends on the electroweak symmetry breaking energy scale $Q_{EWSB}$.

By these relations we can see that if $m_0 \gg m_{1/2}$ the sfermion masses will be approximately degenerate. If the opposite is the case, the squarks receive a large contribution from the fermion-mass and become much heavier than the sleptons.

Looking at Tables 2.1(b) and 2.1(c) we see that for SU2 (b) where $m_0 \gg m_{1/2}$ the squark and slepton masses are practically degenerate and very much larger than the gluino mass. SU3 (c) has $m_{1/2} > m_0$ and the sleptons are much lighter than the squarks, and follow the relations described in the text above with respect to their different gauge-groups. Table 2.1 and 2.2 will be further discussed in the next sections.

In general we see from relations 2.1 and 2.2 that 1st and 2nd generations squarks are always heavier than gauginos, while the sleptons masses can be heavier or lighter than the gauginos depending on the value of $m_0$ and $m_{1/2}$. We also see that if $m_0$ is very small, the squark and gluino can be approximately degenerate. We will now discuss the various models and the corresponding mass spectra as generated by the ISAJET Monte Carlo program.

## 2.3 SUSY mass spectra from IsaJet

Tools based on IsaJet [3] implement the RGE's and calculate masses and branching ratios that are dependent on the model- parameters. Tables 2.1 and 2.2 show the mass-spectrum as generated from IsaJetV7.69 for the mSUGRA points SU1, SU2, SU3 (table 2.1 (a,b,c)), SU4 and SU6 (2.2 (a,b)) [14]. The corresponding heaviest particles are summarized in table 2.3.

[2] These relations leave out a model-independent D-term $m_{D-term}^2 = M_Z^2 \cos 2\beta (T_3 - Q \sin^2 \theta_W)$ which is the same for all sfermions.

[3] IsaJet [1], a Monte Carlo program generating events for high energy particle collisions

Table 2.1: Ordered mass spectra (a) SU1, (b) SU2 and (c) SU3

(a)

| | |
|---|---|
| $h$ | 115.80 |
| $\widetilde{\chi}_1^0$ | 136.94 |
| $\tilde{\tau}_1$ | 146.58 |
| $\widetilde{e}_R, \widetilde{\mu}_R$ | 154.07 |
| $\tilde{\nu}_{e/\mu}$ | 237.50 |
| $\tilde{\nu}_\tau$ | 237.75 |
| $\widetilde{e}_L, \widetilde{\mu}_L$ | 254.96 |
| $\tilde{\tau}_2$ | 256.78 |
| $\widetilde{\chi}_2^0$ | 263.20 |
| $\widetilde{\chi}_1^\pm$ | 263.57 |
| $\widetilde{\chi}_3^0$ | 460.72 |
| $\widetilde{\chi}_2^\pm$ | 476.89 |
| $\widetilde{\chi}_4^0$ | 477.60 |
| $A$ | 511.55 |
| $H$ | 515.15 |
| $H^\pm$ | 521.06 |
| $\widetilde{t}_1$ | 572.64 |
| $\widetilde{b}_1$ | 698.09 |
| $\widetilde{b}_2$ | 722.83 |
| $\widetilde{d}_R, \widetilde{s}_R$ | 733.54 |
| $\widetilde{u}_R, \widetilde{c}_R$ | 735.41 |
| $\widetilde{t}_2$ | 749.51 |
| $\widetilde{u}_L, \widetilde{c}_L$ | 760.43 |
| $\widetilde{d}_L, \widetilde{s}_L$ | 764.90 |
| $\widetilde{g}$ | 832.33 |

(b)

| | |
|---|---|
| $\widetilde{\chi}_1^0$ | 103.35 |
| $h$ | 119.01 |
| $\widetilde{\chi}_1^\pm$ | 149.42 |
| $\widetilde{\chi}_2^0$ | 160.37 |
| $\widetilde{\chi}_3^0$ | 179.76 |
| $\widetilde{\chi}_2^\pm$ | 286.80 |
| $\widetilde{\chi}_4^0$ | 294.90 |
| $\widetilde{g}$ | 856.59 |
| $\widetilde{t}_1$ | 2131.11 |
| $\widetilde{b}_1$ | 2924.80 |
| $\widetilde{t}_2$ | 2935.36 |
| $\widetilde{b}_2$ | 3500.55 |
| $A$ | 3506.62 |
| $\tilde{\tau}_1$ | 3519.65 |
| $H$ | 3529.74 |
| $H^\pm$ | 3530.61 |
| $\tilde{\nu}_\tau$ | 3532.27 |
| $\tilde{\tau}_2$ | 3533.67 |
| $\tilde{\nu}$ | 3546.32 |
| $\widetilde{e}_R, \widetilde{\mu}_R$ | 3547.46 |
| $\widetilde{e}_L, \widetilde{\mu}_L$ | 3547.50 |
| $\widetilde{u}_L, \widetilde{c}_L$ | 3563.24 |
| $\widetilde{d}_L, \widetilde{s}_L$ | 3564.13 |
| $\widetilde{u}_R, \widetilde{c}_R$ | 3574.18 |
| $\widetilde{d}_R, \widetilde{s}_R$ | 3576.13 |

(c)

| | |
|---|---|
| $h$ | 114.82 |
| $\widetilde{\chi}_1^0$ | 117.91 |
| $\tilde{\tau}_1$ | 150.01 |
| $\widetilde{e}_R, \widetilde{\mu}_R$ | 155.42 |
| $\tilde{\nu}_\tau$ | 216.29 |
| $\tilde{\nu}_{e/\mu}$ | 216.96 |
| $\widetilde{\chi}_1^\pm$ | 218.43 |
| $\widetilde{\chi}_2^0$ | 218.61 |
| $\widetilde{e}_L, \widetilde{\mu}_L$ | 230.47 |
| $\tilde{\tau}_2$ | 232.15 |
| $\widetilde{t}_1$ | 424.14 |
| $\widetilde{\chi}_3^0$ | 463.98 |
| $\widetilde{\chi}_2^\pm$ | 480.13 |
| $\widetilde{\chi}_4^0$ | 480.57 |
| $A$ | 511.53 |
| $H$ | 512.56 |
| $H^\pm$ | 517.85 |
| $\widetilde{b}_1$ | 575.23 |
| $\widetilde{d}_R, \widetilde{s}_R$ | 610.69 |
| $\widetilde{b}_2$ | 610.74 |
| $\widetilde{u}_R, \widetilde{c}_R$ | 611.81 |
| $\widetilde{u}_L, \widetilde{c}_L$ | 631.51 |
| $\widetilde{d}_L, \widetilde{s}_L$ | 636.27 |
| $\widetilde{t}_2$ | 650.50 |
| $\widetilde{g}$ | 717.46 |

Table 2.2: Ordered mass spectra (a) SU4, (b) SU6, (c) SU8

| (a) | | (b) | | (c) | |
|---|---|---|---|---|---|
| $\widetilde{\chi}_1^0$ | 59.84 | $h$ | 116,84 | $h$ | 116.69 |
| $\widetilde{\chi}_1^\pm$ | 113.22 | $\widetilde{\chi}_1^0$ | 149.57 | $\widetilde{\chi}_1^0$ | 142.45 |
| $\widetilde{\chi}_2^0$ | 113.48 | $\tilde{\tau}_1$ | 181.31 | $\tilde{\tau}_1$ | 151.90 |
| $h$ | 113.98 | $\widetilde{\chi}_2^0$ | 287.97 | $\widetilde{e}_R, \widetilde{\mu}_R$ | 253.35 |
| $\tilde{\tau}_1$ | 200.50 | $\widetilde{\chi}_1^\pm$ | 288.29 | $\widetilde{\chi}_2^0$ | 273.95 |
| $\widetilde{t}_1$ | 206.04 | $\tilde{\nu}_\tau$ | 357.26 | $\widetilde{\chi}_1^\pm$ | 274.30 |
| $\widetilde{e}_R, \widetilde{\mu}_R$ | 212.88 | $\widetilde{e}_R, \widetilde{\mu}_R$ | 351.10 | $\tilde{\nu}_\tau$ | 296.98 |
| $\tilde{\nu}_\tau$ | 215.53 | $A$ | 386.47 | $\tilde{\nu}_{e/\mu}$ | 315.29 |
| $\tilde{\nu}$ | 217.92 | $H$ | 388.92 | $\widetilde{e}_L$ | 325.44 |
| $\widetilde{e}_L, \widetilde{\mu}_L$ | 231.94 | $\tilde{\tau}_2$ | 392.58 | $\tilde{\tau}_2$ | 331.34 |
| $\tilde{\tau}_2$ | 236.04 | $H^\pm$ | 401.15 | $A$ | 427.74 |
| $\widetilde{\chi}_3^0$ | 308.94 | $\tilde{\nu}_{e/\mu}$ | 401.89 | $H$ | 430.49 |
| $\widetilde{\chi}_2^\pm$ | 326.59 | $\widetilde{e}_L, \widetilde{\mu}_L$ | 411.89 | $H^\pm$ | 440.23 |
| $\widetilde{\chi}_4^0$ | 327.76 | $\widetilde{\chi}_3^0$ | 477.23 | $\widetilde{\chi}_3^0$ | 463.55 |
| $\widetilde{b}_1$ | 358.49 | $\widetilde{\chi}_4^0$ | 492.23 | $\widetilde{\chi}_4^0$ | 479.01 |
| $A$ | 368.18 | $\widetilde{\chi}_2^\pm$ | 492.42 | $\widetilde{\chi}_2^\pm$ | 479.22 |
| $H$ | 370.47 | $\widetilde{t}_1$ | 641.61 | $\widetilde{t}_1$ | 603.65 |
| $H^\pm$ | 378.90 | $\widetilde{b}_1$ | 716.83 | $\widetilde{b}_1$ | 690.31 |
| $\widetilde{b}_2$ | 399.18 | $\widetilde{b}_2$ | 779.42 | $\widetilde{b}_2$ | 743.09 |
| $\widetilde{u}_R, \widetilde{c}_R$ | 404.92 | $\widetilde{t}_2$ | 797.99 | $\widetilde{t}_2$ | 766.21 |
| $\widetilde{d}_R, \widetilde{s}_R$ | 406.22 | $\widetilde{d}_R, \widetilde{s}_R$ | 840.21 | $\widetilde{d}_R, \widetilde{s}_R$ | 771.91 |
| $\widetilde{u}_L, \widetilde{c}_L$ | 412.25 | $\widetilde{u}_R, \widetilde{c}_R$ | 842.16 | $\widetilde{u}_R, \widetilde{c}_R$ | 773.69 |
| $\widetilde{g}$ | 413.37 | $\widetilde{u}_L, \widetilde{c}_L$ | 866.84 | $\widetilde{u}_L, \widetilde{c}_L$ | 797.09 |
| $\widetilde{d}_L \widetilde{s}_L$ | 419.84 | $\widetilde{d}_L, \widetilde{s}_L$ | 870.79 | $\widetilde{d}_L, \widetilde{s}_L$ | 801.16 |
| $\widetilde{t}_2$ | 445.00 | $\widetilde{g}$ | 894.70 | $\widetilde{g}$ | 856.45 |

| | SU1 | SU2 | SU3 | SU4 | SU6 | SU8 |
|---|---|---|---|---|---|---|
| $\widetilde{g}$ | 831 | 856 | 722 | 894 | 894 | 856 |
| $\tilde{q}$ | 758 | 3576 | 662 | 871 | 862 | 801 |
| $\widetilde{\chi}^0$ | 479 | 294 | 478 | 492 | 493 | 479 |
| $\widetilde{\chi}^\pm$ | 478 | 286 | 476 | e92 | 493 | 479 |
| $\widetilde{l}$ | 254 | 3547 | 233 | 412 | 410 | 325 |

Table 2.3: Heaviest sparticles from each category

According to this mass hierarchy we can now write down some important supersymmetric production and decay-chains, and how the various model points can produce opposite sign di-leptons, and jets. The following subsections will present the various mSUGRA points studied. A

| | SU1 $\sigma_{tot}$ :7.43pb | SU2 $\sigma_{tot}$ :4.86pb | SU3 $\sigma_{tot}$18.59pb | SU4 $\sigma_{tot}$ :262pb | SU6 $\sigma_{tot}$ :4.48pb |
|---|---|---|---|---|---|
| Prod | LO [pb] | LO [pb] | LO [pb] | LO [pb] | LO [pb] |
| $\widetilde{g}\widetilde{g}$ | 6.17E-01 | 6.22E-01 | 1.72 E00 | 51.3E00 | 3.65E-01 |
| $\tilde{q}\bar{\tilde{q}}$ | 1.07 E00 | 4.01E-07 | 2.96 E00 | 26.2 E00 | 5.04E-01 |
| $\tilde{q}\widetilde{g}$ | 3.77 E00 | 4.33E-03 | 9.70 E00 | 130. E00 | 2.08 E00 |
| $\tilde{q}\tilde{q}$ | 1.63 E00 | 1.44E-05 | 3.59 E00 | 21.4 E00 | 9.13E-01 |
| $\widetilde{t}_1\widetilde{t}_1$ | 1.83E-01 | 1.03E-06 | 1.01 E00 | 41.1E00 | 9.30E-02 |
| $\widetilde{t}_2\widetilde{t}_2$ | 3.52E-02 | 1.94E-07 | 8.52E-02 | 7.75E-01 | 2.40E-02 |

Table 2.4: Squark and gluino production cross sections as calculated by prospino 2.0.6 Numbers do not exactly correspond to the SUSY LO cross sections that I use, but will be used as a reference.

summary of squark and gluino production cross sections are given in table 2.4. In chapter 4 table 4.2, the benchmark point parameters together with crossections can be found.

It must be noted that in the branching ratio tables to follow, processes are written e.g. $\widetilde{g} \rightarrow \widetilde{\chi}_1^{\pm}\, t\, b$, without a bar over any of the daughter-particles. Naturally either $t$ or $b$ has to be an antiparticle to conserve charge, but for the sake of minimising notation, this is left out.

## 2.4 Branching ratios for mSUGRA processes leading to leptons and jets

### 2.4.1 Coannihilation point - SU1

In SU1 the scalar masses are fairly low, and the gluino is the heaviest sparticle at 832GeV (table 2.1(a)). Again, since the QCD processes dominate, production of strongly interacting particles are the most important, and in SU1 both the gluino and the squarks are accessible at the collision energies that LHC will operate at. The gluino is the heaviest fermion, and heavier than the squarks, thus decay to real squarks is possible. The total squark and gluino cross sections in SU1 is about 7.3pb at leading order, out of 7.43pb in total (table 2.4). The most probable decay of the gluino ($\sim$ 18%) is through right handed squarks, but these decay promptly to the $\widetilde{\chi}_1^0$ and will not give us leptons. An example decay chains that give us one lepton $\widetilde{g} \rightarrow q\,\overline{\widetilde{q}_L} \rightarrow q\,\overline{q}^{'}\,\widetilde{\chi}_1^{\pm} \rightarrow q\,\overline{q}^{'}\,\nu\widetilde{l}_L^{\pm} \rightarrow q\,\overline{q}^{'}\,l^{\pm}\,\widetilde{\chi}_1^0$ is shown in figure 2.2 while a chain leading to two correlated opposite sign leptons $\widetilde{g} \rightarrow q\,\overline{\widetilde{q}_L} \rightarrow q\,\overline{q}\,\widetilde{\chi}_2^0 \rightarrow q\,\overline{q}\,l^{\pm}\,\widetilde{l}_{L,R}^{\mp} \rightarrow q\,\overline{q}\,l^{\pm}l^{\mp}\,\widetilde{\chi}_1^0$ can be found in figure 2.3.

The process involving decay-chain shown in figure 2.2 can give us two opposite sign leptons if the other leg also involves a lepton.

Both chains decay through a cascade of particles that give us final-state jets.

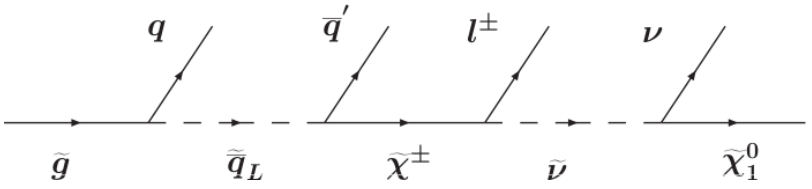


Figure 2.2: Decay of gluino through chargino, leading to a finalstate with a lepton and jets.

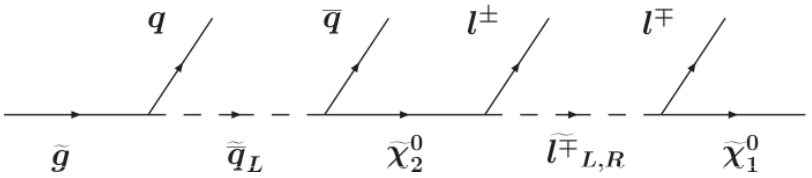


Figure 2.3: Decay of gluino through neutralino, leading to a finalstate with correlated opposite sign di-leptons.

Branching ratios can be found below

| Process | BR % |
|---|---|
| $\widetilde{g} \to \tilde{q}_R\, q$ | 36.8 |
| $\widetilde{g} \to \tilde{q}_L\, q$ | 19.4 |
| $\widetilde{g} \to \widetilde{t}_1\, t$ | 16.2 |
| $\widetilde{g} \to \widetilde{b}_1\, b$ | 15.8 |

| Process | BR % |
|---|---|
| $\tilde{q}_L \to \widetilde{\chi}_1^{\pm}\, q'$ | 60 |
| $\tilde{q}_L \to \widetilde{\chi}_2^0\, q$ | 30 |

| Process | BR % |
|---|---|
| $\widetilde{\chi}_2^{\pm} \to \widetilde{\chi}_2^0\, W$ | 30 |
| $\widetilde{\chi}_2^{\pm} \to \widetilde{\chi}_1^{\pm}\, Z$ | 25 |
| $\widetilde{\chi}_2^{\pm} \to \widetilde{\chi}_1^{\pm}\, h$ | 20 |
| $\widetilde{\chi}_2^{\pm} \to \widetilde{l}_R\, \nu$ | 8 |
| $\widetilde{\chi}_2^{\pm} \to \widetilde{\chi}_1^{\pm}\, W$ | 7 |

| Process | BR % |
|---|---|
| $\widetilde{b}_1 \to \widetilde{\chi}_1^{\pm}\, t$ | 40 |
| $\widetilde{b}_1 \to \widetilde{\chi}_2^0\, b$ | 25 |
| $\widetilde{b}_1 \to \widetilde{\chi}_2^{\pm}\, t$ | 22 |
| $\widetilde{b}_1 \to \widetilde{t}_1\, W$ | 10 |

| Process | BR % |
|---|---|
| $\widetilde{\chi}_1^{\pm} \to \tilde{\nu}\, l$ | 46 |
| $\widetilde{\chi}_1^{\pm} \to \widetilde{\chi}_1^0\, W$ | 7 |
| $\widetilde{\chi}_1^{\pm} \to \widetilde{l}_L \nu$ | 4 |

| Process | BR % |
|---|---|
| $\widetilde{t}_1 \to \widetilde{\chi}_1^{\pm}\, b$ | 48 |
| $\widetilde{t}_1 \to \widetilde{\chi}_2^0\, t$ | 15 |
| $\widetilde{t}_1 \to \widetilde{\chi}_2^{\pm}\, b$ | 12 |

| Process | BR % |
|---|---|
| $\widetilde{\chi}_2^0 \to \widetilde{l}_L l$ | 6 |
| $\widetilde{\chi}_2^0 \to \widetilde{l}_R l$ | 3 |

Once a slepton has been produced it decays 100% to a lepton and the LSP. We can see from the mass table 2.1(a) that both left- and right-handed sleptons are kinetically allowed decays of $\widetilde{\chi}_2^0$. Correlated opposite sign di-leptons can therefore come from both $\widetilde{\chi}_2^0 \to l^{\pm}\, \widetilde{l}_R^{\mp} \to l^{\pm} l^{\mp} \widetilde{\chi}_1^0$ and the equivalent chain with a left-handed slepton instead of a right-handed. A decay-chain leading to a correlated opposite sign di-lepton final state in SU1 is shown in figure 2.2.

### 2.4.2 Focus point SU2

In the Focus point region SU2, $m_0$ is very heavy, resulting in heavy and fairly degenerate squark and slepton masses (table 2.1(b)), and a low produciton crossection. Gluino production is possible in SU2, but because of the heavy scalar masses, the decays through squarks and sleptons must be 3-body and are therefore supressed. The most important sparticle production is therefore

direct gaugino production. A final-state with jets and leptons can be obtained through the 3-body decay $\widetilde{\chi}_2^0 \rightarrow {}^{\pm}\, l^{\mp}\, \widetilde{\chi}_1^0$ in one leg and $\widetilde{\chi}_1^{\pm} \rightarrow u\, \overline{d}\, \widetilde{\chi}_1^0$ in the second leg as illustrated in figure 2.4. We can also see from branching-ratios that decays to Z-bosons have a relatively large probability, and since Z can decay leptonically through $Z \rightarrow l^{\pm} l^{\mp}$ this can give us a large proportion of correlated opposite sign leptons, but not coming directly from a SUSY sparticle.

Important branching fractions which can result in leptons are shown in below.

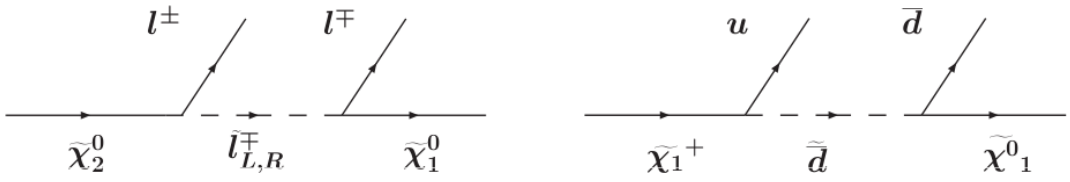


(a) Leg 1 (b) Leg 2

Figure 2.4: Possible decay chain in SU2 leading to jets and correlated opposite sign leptons.

| Process | BR % |
|---|---|
| $\widetilde{g} \rightarrow \widetilde{\chi}_1^{\pm}\, b\, t$ | 24 |
| $\widetilde{g} \rightarrow \widetilde{\chi}_2^{\pm}\, t\, b$ | 20 |
| $\widetilde{g} \rightarrow \widetilde{\chi}_3^0\, t\, t$ | 11 |
| $\widetilde{g} \rightarrow \widetilde{\chi}_2^0\, t\, t$ | 9 |
| $\widetilde{g} \rightarrow \widetilde{\chi}_2^{\pm}\, u\, d$ | 7 |

| Process | BR % |
|---|---|
| $\widetilde{\chi}_4^0 \rightarrow \widetilde{\chi}_1^{\pm}\, W$ | 82 |
| $\widetilde{\chi}_4^0 \rightarrow \widetilde{\chi}_3^0\, Z$ | 11 |
| $\widetilde{\chi}_4^0 \rightarrow \widetilde{\chi}_2^0\, h$ | 6 |

| Process | BR % |
|---|---|
| $\widetilde{\chi}_2^{\pm} \rightarrow \widetilde{\chi}_1^0\, W$ | 38 |
| $\widetilde{\chi}_2^{\pm} \rightarrow \widetilde{\chi}_1^{\pm}\, Z$ | 30 |
| $\widetilde{\chi}_2^{\pm} \rightarrow \widetilde{\chi}_3^0\, W$ | 18 |
| $\widetilde{\chi}_2^{\pm} \rightarrow \widetilde{\chi}_1^{\pm}\, h$ | 8 |
| $\widetilde{\chi}_2^{\pm} \rightarrow \widetilde{\chi}_1^0\, W$ | 5 |

| Process | BR % |
|---|---|
| $\widetilde{\chi}_3^0 \rightarrow \widetilde{\chi}_1^0\, l\, l$ | 7 |

| Process | BR % |
|---|---|
| $\widetilde{\chi}_2^0 \rightarrow \widetilde{\chi}_1^0\, l\, l$ | 7 |

| Process | BR % |
|---|---|
| $\widetilde{\chi}_1^{\pm} \rightarrow \widetilde{\chi}_1^0\, u\, d$ | 70 |
| $\widetilde{\chi}_1^{\pm} \rightarrow \widetilde{\chi}_1^0 \nu\, l$ | 20 |

### 2.4.3 Bulk region - SU3

All the supersymmetric particles are kinematically accessible at the Bulk Region SU3. There will be a large amount of gluino and squark production, as we can see from table 2.4. Opposite sign di-leptons can come from the uncorrelated lepton decays as shown in the figure 2.2. Correlated opposite sign leptons can only come from $\widetilde{\chi}_2^0\, Z\, \widetilde{\chi}_1^0$ or through a right-handed slepton and a lepton as figure 2.3 illustrates. Of the sleptons, only the right-handed is kinematically allowed since the left-handed slepton is heavier than $\widetilde{\chi}_2^0$. Once the slepton has been produced it can only decay to a lepton and the LSP.

| Process | BR % |
|---|---|
| $\widetilde{g} \rightarrow \tilde{q}_L$ | 23 |
| $\widetilde{g} \rightarrow \widetilde{t}_1\ t$ | 16 |
| $\widetilde{g} \rightarrow \widetilde{b}_1\ t$ | 15 |

| Process | BR % |
|---|---|
| $\tilde{q}_L \rightarrow \widetilde{\chi}_1^{\pm}\ q$ | 64 |
| $\tilde{q}_L \rightarrow \widetilde{\chi}_2^0\ q^{'}$ | 32 |

| Process | BR % |
|---|---|
| $\widetilde{b}_1 \rightarrow \widetilde{\chi}_1^{\pm}\ t$ | 36 |
| $\widetilde{b}_1 \rightarrow \widetilde{t}_1\ W$ | 35 |

| Process | BR % |
|---|---|
| $\widetilde{t}_1 \rightarrow \widetilde{\chi}_1^{\pm}\ b$ | 65 |
| $\widetilde{t}_1 \rightarrow \widetilde{\chi}_2^0\ t$ | 10 |

| Process | BR % |
|---|---|
| $\widetilde{\chi}_2^0 \rightarrow \widetilde{l}_R$ | 18 |
| $\widetilde{\chi}_2^0 \rightarrow \widetilde{\chi}_1^0\ Z$ | 3 |

| Process | BR % |
|---|---|
| $\widetilde{\chi}_1^{\pm} \rightarrow \widetilde{\chi}_1^0\ W$ | 29 |

### 2.4.4 Low Mass - SU4

The Low Mass point SU4 has a very large cross section of 262pb and fairly light scalar masses, resulting in large gluino and squark production. Branching ratios of processes leading to leptons are shown below.

| Process | BR % |
|---|---|
| $\widetilde{t}_2 \rightarrow \widetilde{t}_1\ Z$ | 43 |
| $\widetilde{t}_2 \rightarrow \widetilde{\chi}_1^{\pm}\ b$ | 25 |
| $\widetilde{t}_2 \rightarrow \widetilde{\chi}_2^{\pm}\ b$ | 13 |
| $\widetilde{t}_2 \rightarrow \widetilde{\chi}_2^0\ t$ | 8 |

| Process | BR % |
|---|---|
| $\tilde{q}_L \rightarrow \widetilde{\chi}_1^{\pm}\ q^{'}$ | 62 |
| $\tilde{q}_L \rightarrow \widetilde{\chi}_2^0\ q$ | 32 |

| Process | BR % |
|---|---|
| $\widetilde{g} \rightarrow \widetilde{b}_1\ b$ | 47 |
| $\widetilde{g} \rightarrow \widetilde{t}_1\ t$ | 42 |

| Process | BR % |
|---|---|
| $\widetilde{b}_1 \rightarrow \widetilde{t}_1\ W$ | 46 |
| $\widetilde{b}_1 \rightarrow \widetilde{\chi}_2^0\ b$ | 28 |
| $\widetilde{b}_1 \rightarrow \widetilde{\chi}_1^{\pm}\ b$ | 22 |

| Process | BR % |
|---|---|
| $\widetilde{t}_1 \rightarrow \widetilde{\chi}_1^{\pm}\ t$ | 100 |

| Process | BR % |
|---|---|
| $\widetilde{\chi}_2^0 \rightarrow \widetilde{\chi}_1^0\ l\ l$ | 6 |

| Process | BR % |
|---|---|
| $\widetilde{\chi}_1^{\pm} \rightarrow \widetilde{\chi}_1^0\ \nu\ l$ | 23 |

The $\widetilde{t}_1$ is so light that it cannot decay to other than $\widetilde{\chi}_1^{\pm}$ and a b-quark, as the top is not kinematically accessible. The $\widetilde{\chi}_1^{\pm}$ and the $\widetilde{\chi}_2^0$ are the lightest particles after the LSP, and are therefore forced to 3-body-decay through squarks or sleptons in the same way as for SU2 in figure 2.4 a). Production of right-handed squarks is also possible, but these decay almost 100% directly to $\widetilde{\chi}_1^0$+q without giving us any leptons, and have therefore not been listed.

### 2.4.5 Funnel region - SU6

$\widetilde{\chi}_1^{\pm}$ almost always decay directly to $\tilde{\tau}_1$ and is not included in the table, as the $\tilde{\tau}_1$ is not one of the signal-leptons. The $\widetilde{\chi}_2^0$ has a similar behaviour and decays to $\tilde{\tau}\ \tau$. This is due to the masses being

very low, and only the $\tilde{\tau}$ is kinematically allowed decay-mode. Decays from the heavier gauginos will give us some signal-leptons, as can be seen in the decay-modes below.

| Process | BR % |
|---|---|
| $\widetilde{g} \rightarrow \widetilde{b}_1\ b$ | 39 |
| $\widetilde{g} \rightarrow \widetilde{t}_1\ t$ | 20 |
| $\widetilde{g} \rightarrow \widetilde{b}_2\ b$ | 19 |
| $\widetilde{g} \rightarrow \tilde{q}_L\ q$ | 4 |

| Process | BR % |
|---|---|
| $\widetilde{b}_1 \rightarrow \widetilde{\chi}_2^0\ b$ | 28 |
| $\widetilde{b}_1 \rightarrow \widetilde{\chi}_3^0\ b$ | 11 |
| $\widetilde{b}_1 \rightarrow \widetilde{\chi}_2^{\pm}\ t$ | 7 |

| Process | BR % |
|---|---|
| $\widetilde{t}_1 \rightarrow \widetilde{\chi}_2^{\pm}\ b$ | 23 |

| Process | BR % |
|---|---|
| $\widetilde{b}_2 \rightarrow \widetilde{\chi}_2^{\pm}\ t$ | 47 |
| $\widetilde{b}_2 \rightarrow \widetilde{\chi}_4^0\ b$ | 15 |
| $\widetilde{b}_2 \rightarrow \widetilde{\chi}_3^0\ b$ | 14 |
| $\widetilde{b}_2 \rightarrow \widetilde{t}_1\ W$ | 8 |
| $\widetilde{b}_2 \rightarrow \widetilde{\chi}_2^0\ b$ | 7 |

| Process | BR % |
|---|---|
| $\tilde{q}_L \rightarrow \widetilde{\chi}_1^{\pm}\ q^{'}$ | 61 |
| $\tilde{q}_L \rightarrow \widetilde{\chi}_2^0\ q^{'}$ | 31 |

| Process | BR % |
|---|---|
| $\widetilde{\chi}_2^{\pm} \rightarrow \widetilde{\chi}_2^0\ W$ | 24 |
| $\widetilde{\chi}_2^{\pm} \rightarrow \widetilde{\chi}_1^{\pm}\ Z$ | 20 |
| $\widetilde{\chi}_2^{\pm} \rightarrow \widetilde{\chi}_1^{\pm}\ h$ | 17 |
| $\widetilde{\chi}_2^{\pm} \rightarrow \widetilde{\chi}_1^0\ W$ | 8 |

| Process | BR % |
|---|---|
| $\widetilde{\chi}_4^0 \rightarrow \widetilde{\chi}_1^{\pm}\ W$ | 42 |
| $\widetilde{\chi}_4^0 \rightarrow \widetilde{\chi}_2^0\ h$ | 15 |

| Process | BR % |
|---|---|
| $\widetilde{\chi}_3^0 \rightarrow \widetilde{\chi}_1^{\pm}\ W$ | 39 |
| $\widetilde{\chi}_3^0 \rightarrow \widetilde{\chi}_2^0\ W$ | 15 |
| $\widetilde{\chi}_3^0 \rightarrow \widetilde{\chi}_1^0\ Z$ | 8 |

| Process | BR % |
|---|---|
| $\widetilde{\chi}_2^0 \rightarrow \widetilde{\chi}_1^0\ Z$ | 8 |

## 2.5 General feature of SUSY

For all the decay-chains above there will be less jets if the decay-chain is shorter, e.g. starting from a squark instead of a gluino when the gluino is heavier than the squark, or for example by direct gaugino production. In general we aquire large missing transverse energy due to two $\widetilde{\chi}_1^0$ produced in each event, and many jets. Leptons are produced through decay of the various neutralinos, charginos, and W and Z bosons. In many of the mSUGRA points the leptonic decay of Z competes with producing correlated opposite signed leptons.

## 2.6 Conclusion

We have seen that many of the decay-modes of the various models can give us two leptons with correlated opposite sign, large $\not{E}_{\mathrm{T}}$ and many jets. In order to study these events we must find a way to distinguish our signal-events from both the supersymmetry background-events and in particular the large Standard model background. Our methods of selecting these interesting events have to be able to perform well in the highly complicated collision-enviroment. We will now turn our focus on how this will be done experimentally, by introducing the Monte Carlo datasamples, and then study the performance of our methods.

# Chapter 3

# The Atlas Detector and commissioning

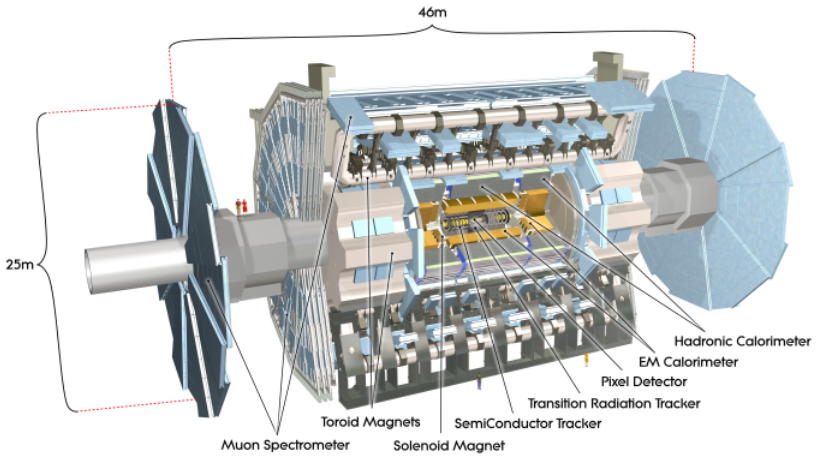


Figure 3.1: The ATLAS Detector [10]

Todays high energy particle physics experiments are performed in particle accelerators. The Large Hadron Collider (LHC) at the European Organization for Nuclear Research: CERN, is about to be turned on and thousands of physicist are eager to start analyzing results. With powerfull detectors such as the ATLAS detector: A Toroid LHC ApparatuS (figure 3.1) one will record the collisions that take place. The large energy of the colliding beams at LHC will possibly allow "new" physics to play a role, but since the manifestation of this "new" physics is not yet known ALTAS has been built as a multi-purpose detector and will pick up a wide range of particles and signatures whatever these might be.

In this chapter we will give a rough overview of the ATLAS detector and describe its various detector-components and trigger, dataaquisition and monitoring tasks necessary for its operation.

## 3.1 Proton collisions

The LHC is a hadron collider, allowing proton-proton but also lead-lead collisions for specific studies. Two beams running parallell in the 27km long underground tunnel cross at interaction points where the detectors are placed. At the nominal integrated luminosity of 100 $fb^{-1}$ a year, there will on averge be 23 interactions each 25ns. The detectors task is to register these collisions as precisely as possible but not more precisely than necessary. For this the detector and also a trigger and dataaquisition system (DAQ) has been developed and built in order to pick out collisions of interest.

The ATLAS detector consists of the following subsystems:

- Magnet
- Inner Detector tracking system
- Electromagnetic Calorimeter
- Hadronic Calorimeter
- Muon system
- Trigger and Data Acquisition

## 3.2 Coordinate system

The LHC coordinate system is a right handed coordinate system with z along the beam axis and the x-y plane transverse to the beam direction. Figure 3.2 shows the coordinate system in xyz. Polar coordinates are used for physics purposes, these are pseudorapidity $\eta$, the azimuthal angle $\phi$, and z. Pseudorapidity $\eta$ is related to the polar angle $\theta$ through

$$\eta = -\ln\left[\tan\left(\frac{\theta}{2}\right)\right]$$

The azimuthal angle $\phi$ runs around the z-axis. $x$ and $y$ are related to the polar angles in the usual way with $x = \cos\theta$ and $y = \cos\theta$. We will also use the angular distance R, where $\Delta R$=$\sqrt{\Delta\eta^2 + \Delta\phi^2}$.

The transvese momentum $p_T$, the transverse energy $E_T$ and the transverse missing energy $\not{E}_{\mathrm{T}}$ are defined in the x-y plane.

## 3.3 Magnet system

To be able to measure the particles momentum a magnet system has to be in place. The magnetic field bends the particles trajectory and the radius of the bending is then used for particle identification. The ATLAS magnet system consists of a solenoid magnet encapsulating the inner detector, 1 outer toroidal magnet placed around the barrel plus one toroid magnet for each end-cap. Each toroid is made up of 8 coils, see figure 3.3. The solenoid magnet provides a fairly uniform 2T central magnetic field parallel to the beam pipe and encapsulating the inner detector. The ATLAS toroids makes up a less uniform magnetic field co-centric to the barrel. The toroid fields in the barrel and end-cap are approximately 0.5 and 1 Tesla respectively.

## 3.4 The inner detector - the tracker

The inner detector (see figure 3.4) is contained within the solenoid and is a high resolution detector build up of 3 main parts: The Pixel detector, the Silicon Strip detector and the Transition radiation tracker (TRT). The inner detector provides excellent momentum resolution, primary and

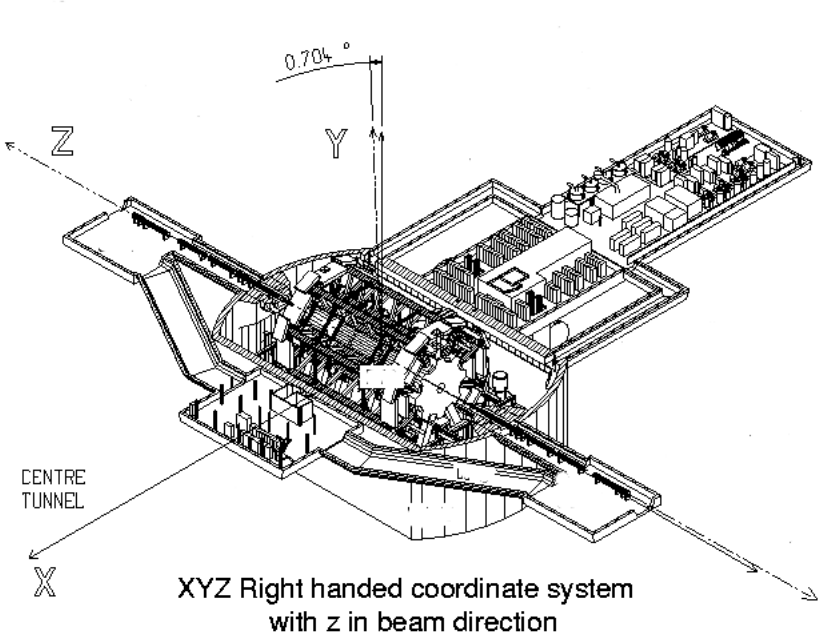


Figure 3.2: The ATLAS coordinate system [10]

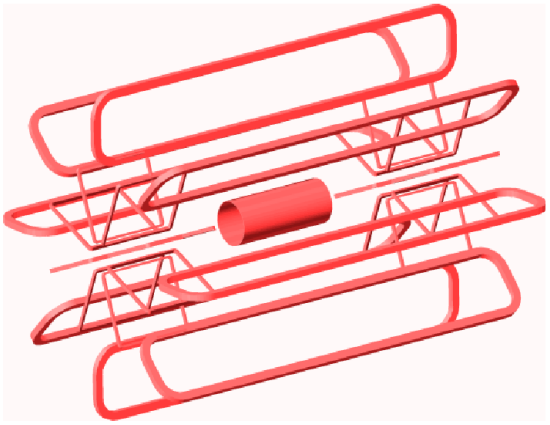

Figure 3.3: The Atlas Magnet system, build up of 3 toroids and 1 solenoid. Each toroid consists of 8 coils, and the magnetic field follows cocentric circles to the beam axis.

secondary vertex measurements pattern recognition and electron identification. Required momentum resolution for the tracking system is $\sigma_{P_T}/p_T$ = 0.05% with an uncertainty on the momentum $p_T$ of 1% [8].

It is built hermetically and serves over a range 0$<|\eta|<$2.5.

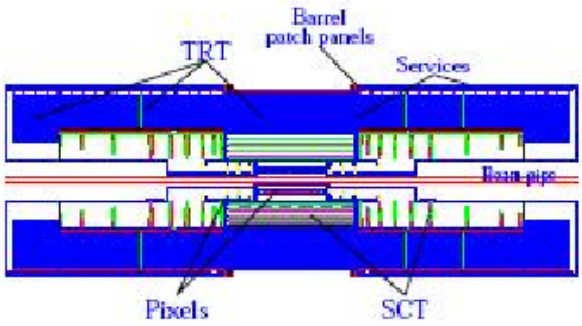


Figure 3.4: Layout of the inner detector showing the positioning of the pixel detector, the silicon strip detector (SCT) and the transition radiation tracker (TRT).

### 3.4.1 Pixel detector

The silicon pixel tracker is placed as close to the interaction point as possible. The granularity and precision is very high, and balance between performance and material density has been met by only allowing 3 layers around the barrel. They are placed concentrically at radii of 4, 11 and 14 cm. There are 5 layers at each end-cap placed perpendicular to the beam pipe. Intrinsic accuracies in the barrel are 10 $\mu$m in (R-$\phi$) and 115 $\mu$m in z. Each pixel of 50 $\mu$m $\times$ 300$\mu$m has its own circuit

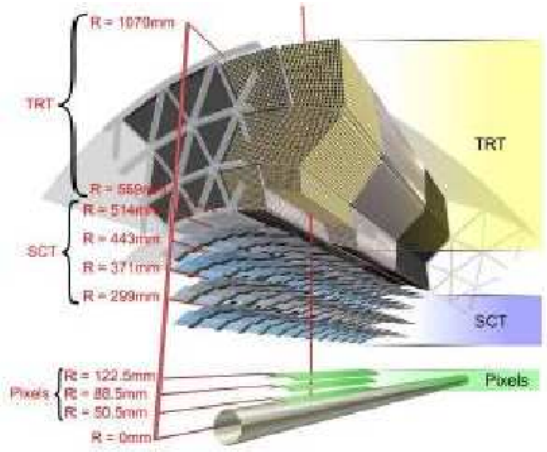


Figure 3.5: Layout of the inner detector showing the positioning of the pixel detector, the silicon strip detector and the transition radiation tracker.

placed on chips on the pixel detector. This chip also contains buffers storing data until a level 1 trigger decision has been made. There are 140million pixel elements in total. Main physics tasks are vertexing and b-tagging, where finding secondary vertexes are important.

### 3.4.2 Silicon Strip Tracker

The middle part of the inner detector is the Semiconductor tracker (SCT) and is made up of silicon micro-strips. The Four barrel layers and 9 disk layers make up 61$m^2$ of silicon and 6.2million channels. The 9 layers provide 9 precision measurements per track. One module has two detector pairs glued back to back at an angle of 40 mradians. A pich of 80 $\mu$m gives a spatial resolution of 16 $\mu$m in the R$\phi$ plane and 580 $\mu$m in the z direction. The readout electronics is mounted above the detectors and as for the pixel detector contains a system for storing data until the Level 1 trigger decision has been made. The SCT is the most important tracker in the perpendicular plane since it measures a traversing particle over a much larger area than the Pixel Detector and sample more points with about the same accuracy as the Pixel Detector.

### 3.4.3 Transition Radiation Tracker

A straw detector filled with a gas-mixture of Xenon-$CO_2$ and $0_2$ makes up the last layers of the inner detector. Its precision is lower than the Pixel and SCT detectors, but it is capable of a very large number of measurements, typically as many as 36 per track. Each straw is 4mm in diameter and has a 30 $\mu$m diameter gold-plated wire in the center. A total of 500000 straws make up the TRT barrel detector, while another 420000 equip the end-caps. Drift-time measurement give a spatial resolution of 170 $\mu$m per straw. The TRT functions as a combination of a straw tracker and a transition radiation detector. Each straw use separate low- and high- thresholds in the read-out electronics to separate the tracking pulses (low threshold) and the transition radiation pulses (high threshold). The transition radiation produced when a particle traverses the different materials depends on the mass of the particles and this is used for particle identification.

## 3.5 The Calorimetry

The calorimetry is placed outside of the solenoidal magnet and consists of the Electromagnetic and the Hadronic Calorimeter. The calorimeters main task is to measure the energy of particles. It does this by measuring energies of the particle showers that are caused when the traversing particles interact with the absorbing material in the detectors. Purely electromagnetic particles like the electron, positron and photon are absorbed in the electromagnetic calorimeter while the heavier hadrons which also interact strongly pass through the ECAL and are absorbed in the hadronic calorimeter. Both calorimeters are sampling detectors which mean that they sample the shape of the particle showers and from this infer the energy of the original particle. All calorimeters have a full $\eta$ coverage up to $|\eta|$ <4.9, and the electromagnetic and the hadronic calorimeter have both barrel components and end-cap components.

### 3.5.1 The Electromagnetic Calorimeter

An accordion shaped geometry with layers of lead as absorbing material in between liquid argon as the active detector material is used for the electromagnetic calorimeter (ECAL). The accordion waves in the barrel are parallel to the beam-pipe and run in the $\phi$ direction. In the end-caps the waves are parallel to the r direction and run in z. The ECAL operates at high precision, both in energy resolution and location of energy deposit. Since the particles already suffer from energy loss due to interaction with the material in the inner detector the electromagnetic calorimeters have an innermost pres-ampler layer which measure energy lost in front of the ECAL. Coverage is divided into precision sections at 0< $\|\eta\|$ <2.5 and a higher -$\eta$ region 2.5< $\|\eta\|$ <3.2. Required energy resolution in the electromagnetic calorimeter is $\sigma E/E =$ 10% $\sqrt{E}$ with an uncertainty in $E$ of 0.7%.

### 3.5.2 The Hadronic Calorimeter

The hadronic calorimeter is divided into 3 main parts: the central barrel region, the end-cap calorimeter (HEC) and the forward calorimeter (FCAL). The coverage-range for the barrel part of hadronic calorimeter is 0$<\|\eta\|<$1.7. The end-cap section covers the ranges 1.5$<\|\eta\|<$3.2 and the forward hadronic calorimeter FCAL extends out to $\|\eta\|$4.9. Both the HCAL and FCAL use liquid argon as scintillating material, the HCAL uses copper as absorbing material, while the FCAL uses a copper/tungsten combination. The central barrel hadronic calorimeter uses tiles of scintillator sampling medium and steel plates as absorbing material. Required energy resolution in the barrel and end-cap hadronic calorimetry is $\sigma_E/E = 50\% \sqrt{E}$ with an uncertainty in $E$ of 3%. The forward hadronic calorimeter is required to have an energy resolution of $\sigma_E/E = 100\% \sqrt{E}$ with an uncertainty in $E$ of 10%.

## 3.6 Muon system

It is the muon system that reaches out to the 22x46 meters of ATLAS. It is also divided into a barrel part and an end-cap part. The muon chambers in the barrel are placed in between the toroid magnets and are made out of 3 layers at radii about 5, 7 and 10 meters. The muon chambers in the end-cap form 4 circular disks placed at 7.4, 10, 13 and 21 m from the center of the detector and perpendicular to the beam axis. They are placed both in front and behind the end-cap toroids. The muon system has coverage up to $|\eta| <$2.7 and can measure the momentum of a muon to a precision of 10% for a 1TeV muon. Required momentum resolution is $\sigma_{p_T}/p_T = 10\% \sqrt{E}$.

The muon system uses 4 different detectors. For precision measurements: the Monitored Drift Tube Chamber (MDT) and the Cathode Strip Chambers (CSC). For trigger: the Resistive Plate Chambers (RPC) and the Thin Gap Chambers (TGC). The MDT have high measuring accuracy, about 80 $\mu$m per tube and are the most important for precise measurements of momentum. The CSCs are placed to cover the very forward region 2$<\|\eta\|<$2.7. The CSC's have high rate capability and time resolution. For fast triggering on muon tracks the RPC's are used in the barrel and the TGCs used for the end-cap. Within 15-20ns a signal of a muon track is delivered, and this makes the two muon systems capable of bunch tagging.

## 3.7 Trigger and Data Acquisition

The Triggers purpose is to reduce the 40MHz rate to about 100Hz for final storage. ATLAS' trigger performs online event selection in 3 stages, the Level 1 Trigger (L1), the Level 2 Trigger (L2) and the Event Filter (EF). L2 and EF make up the High Level Trigger.

The Level 1 hardware trigger must deliver its trigger decision each 25ns and the overall time of the whole process from receiving data to sending the decision back has to be less than 2.5$\mu$s. The Level 1 trigger reduces the rate to about 100kHz triggering on high-$p_T$ muons, electrons/photons, jets, hadronic decays of $\tau$-leptons and it also triggers on large missing transverse energy ( $\not{E}_{\mathrm{T}}$ ).

The Level 2 trigger uses information from the L1 trigger to select Regions of Interest (RoI). It then extracts full-granularity and full-precision data from the appropriate detector parts and uses dedicated algorithms for its decision. The L2 trigger sends 3.5 kHz of events along to the Event Filter, and on average the each event is evaluated in 10ms.

To reduce the rate to the requested 100Hz which is the allowed permanent storage rate for ATLAS, the Event Filter uses offline algorithms on fully built events.

The L1 trigger uses coarse event-data and the High Level Trigger uses the full-granularity and -precision data. A sketch of the ATLAS Trigger and DataAquisition system is shown in figure 3.6.

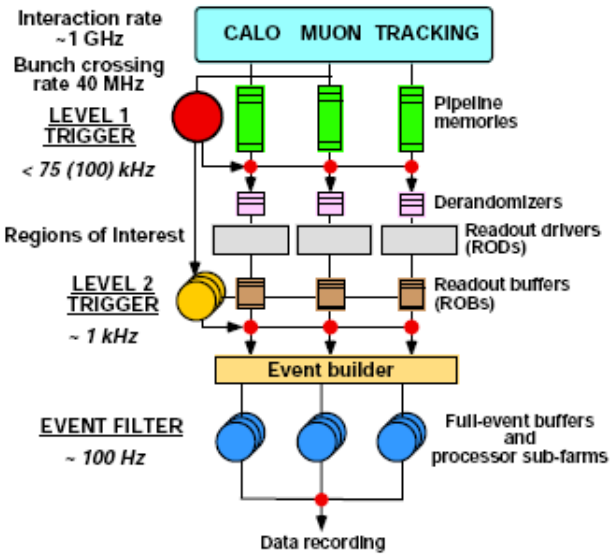


Figure 3.6: The Dataflow from detector components through trigger and to data acquisition.

## 3.8 Commisioning of the ATLAS detector systems

An important part of studying high energy particle physics is contributing to the ongoing preparations and commissioning of the experiment and the detector. The completion of the detector is dependent on this type of involvement, and the chance to gain practical and technical experience is highly valued amongst experimentalists. In order to test the detector as it bit by bit has gotten installed, cosmic test-runs have frequently taken place. In these tests one switches on parts of the detector and run the full data acquisition chain from detecting cosmic muons traversing the detector to final storage of the data, and analysis of these. During these runs shift-work is needed as the experiments run continuously over some days. Students as well as experienced physicists are encouraged to join and valuable experience is gained which will be of great benefit when LHC starts up and the data starts flowing.

## 3.9 The Online Global Inner Detector Monitoring

The Inner Detector consisting of the Pixel detector, the Semi-Conductor Tracker (SCT) and the Transition Radiation Tracker (TRT) are of particular interest to the Norwegian particle physicist community since a large amount of the SCT modules were developed and produced here. The Norwegian community has continued their involvement also after all the SCT modules have been installed. One of these involvements is in online monitoring tasks, and during cosmic runs in November of 2007 and March of 2008 Oslo's particle physics students joined in the preparations and shift-work. The Global Inner detector monitoring, including the Pixel, the SCT and the TRT, was under implementation and needed to be included in to the overall run-configuration [1].

### 3.9.1 Preparing the monitoring for online implementation

The testing and preparation of the Global Inner Detector monitoring was done offline. Part of this work consisted of making sure histograms were filled and that they could be published to an online histogram repository for the online monitoring services to subscribe to. Once the histograms were

[1] under supervision of Heidi Sandaker and Arshak Tonoyan, University of Bergen

available in the server, the Online monitoring applications could display the histograms for the end-user, here: shifter, to evaluate.

Working on this implementation meant getting acquainted to the not trivial tools and options under continuous change and development. The Global Inner Detector Monitoring uses Atlas based monitoring tools. These are standard offline tools that also can be used online via a so-called Processing Tool (PT).

The Atlas Trigger and Data Acquisition (TDAQ) controls the trigger and data flow when the detector is turned on. In the main run-control, the detector components that are included are called as a whole a partition. One can naturally have different partitions depending on the kind of run i.e. which detector components that are implemented and for example if the run is a cosmic run or a technical run. For the end-configuration this partition will be the whole of the ATLAS detector, but for the commissioning only parts are implemented at the time. A certain sub-system in the whole partition is called a segment, for instance the Global Inner Detector monitoring. A test partition and segment had to be built using job-option files and a PT-monitoring build-partition tool. The job-option files specify, among other things which histograms to use, and where to find them. Once the partition has been built files are produced which specify the partition and the segments have been produced, and these are directly fed into the TDAQ system for running, see figure 3.8(a) showing the display of the TDAQ application. Once the partition and segment were connected using a xml-editor tool, the final test of a working configuration could be done by starting the off-line Trigger and Data Acquisition (TDAQ) run controller. This was set in run-mode with the partition that was just built. Data input was from a prepared data-file instead of data from the detector as would be the online situation. As the run proceeded histograms showed up in the histogram server as histograms were filled. Once the Online Histogram Display was set up to subscribe to relevant histograms, these could then be seen in the Online Histogram Presenter used by monitoring shifters. Figure 3.8(b) shows a typical screen with some shifter histograms loaded.

The Global Inner Detector monitoring was implemented online for the first time during the cosmic run in March, and main features worked successfully. As an example histograms showing number of tracks in the SCT detector are shown in figure 3.9(a), while figure 3.9(b) show an Atlantis shot of a cosmic muon going through the TRT and SCT of the Inner Detector. These were all taken during shifts in March in the so called Milestone 6 (M6) cosmic run.

The work refining the Online Global Inner Detector Monitoring is still ongoing, but now that the main functionalities are working, these are mainly improving histogram readability and deciding which histograms are of most importance for the shifter to evaluate.

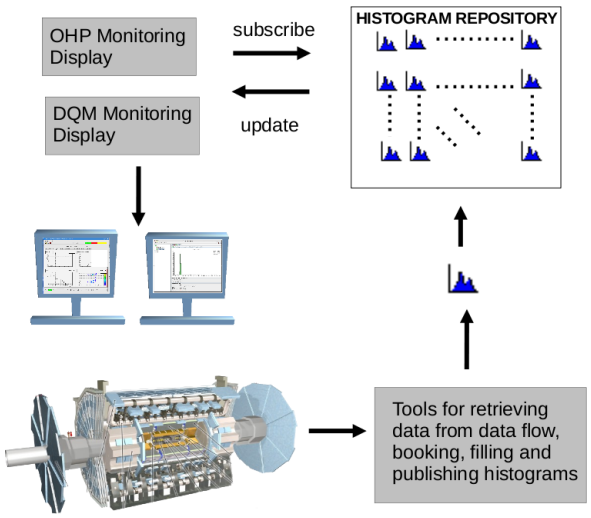


Figure 3.7: Scetch of the online monitoring setup.

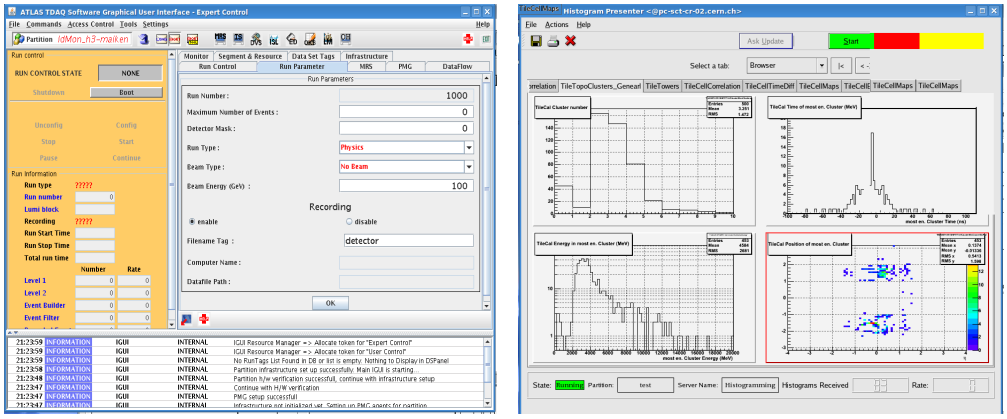

(a) TDAQ (b) OHP

Figure 3.8: The Trigger and Data Acquisition Tool and the Online Histogram Presenter

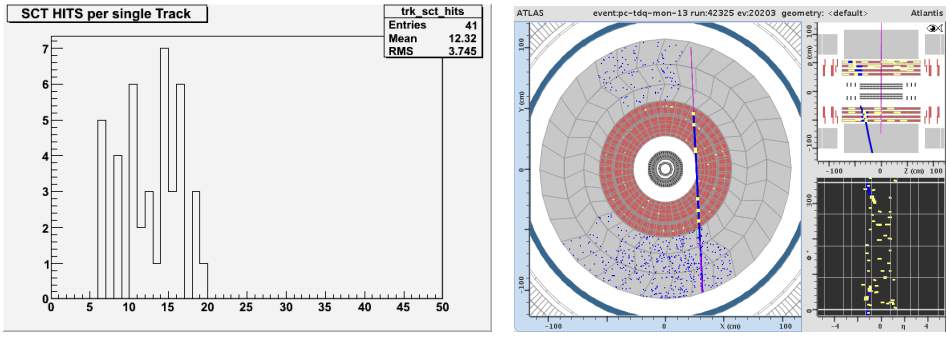


(a) Number of hits per track in SCT (b) Atlantis Event View track through TRT and SCT

Figure 3.9: Number of hits per track and track through SCT and TRT

# Chapter 4

# Analysis Tools and Monte Carlo data

## 4.1 Using simulated data

LHC is yet to start, and in the mean-time all analysis have been done using Monte Carlo simulated data.

The simulated data is produced using event generators like ISAJET [1], HERWIG [11] and PYTHIA [17]. These are computer programs that simulate high energy particle collisions, depending on the chosen physics model. Once the events have been generated and strongly interacting particles have been hadronized [1], the interaction and journey through the detector needs to be simulated. The Athena Framework takes care of this. It incorporates the geometry of the detector and takes into account interactions with the detector. GEANT4 [9] is used for the simulation of the particles' interaction with the matter in the detector. The passing of the particles through the detector are then digitized to mimic detector behaviour, and in the end reconstructed based on this digitization. Reconstruction means running algorithms to retrace and identify the particle based on the digital signals that were generated. This creates Analysis Object Data (AOD) which contains all the kinematics of particles that were reconstructed. To analyze the data one then creates data structures called Ntuples from the AOD data sample. These allow practical analysis of data event by event. They are ROOT-files [3], and this analysis uses ROOT in conjunction with C++ and Python. In the production of these, one can put constraints on which objects one chooses to include, and how they should be defined. This analysis uses ntuples produced according to the SUSYView [5] CSC[2] note 5 [7] note production. All samples are run with an integrated luminosity of $1 fb^{-1}$ throughout the analysis.

## 4.2 Background and signal data samples

This analysis studies the dilepton channel in SUSY events. SUSY events in mSUGRA are, as we have seen characterized by containing many jets, a large amount of missing transverse energy and many leptons. Important SM backgrounds will therefore be QCD, t-ttbar production, Z+hadron and W+hadron production and di-boson production. QCD will dominate at the interaction-energies that LHC will operate at and is therefore in any way an important background that has to be studied

[1] forming hadrons out of quarks and gluons
[2] Computing System Commissioning

and tackled. Ttbar production gives missing energy in form of neutrinos and also jets and leptons, as does the Z and W production.

The crossections of the SM background samples used for this analysis are shown in table 4.1. The data set name together with the numbering of the physics process, the crossection and number of events expected when running at an integrated luminosity of $1\,fb^{-1}$.

| Name | PhysicsProcess | Crossection [pb] | Events at 1fb$^{-1}$ |
|---|---|---|---|
| T1 | 5200 | 449.820 | 449820 |
| TTbar | 5204 | 370.685 | 370685 |
| WW | 5985 | 24.500 | 24500 |
| ZZ | 5986 | 2.100 | 2100 |
| WZ | 5987 | 0.0226 | 22.6 |
| Zee | 8194 | 46.200 | 46200 |
| Zmumu | 8195 | 9.604 | 9604 |
| Ztautau | 8191 | 4.500 | 4500 |
| Znunu | 8190 | 41.328 | 41328 |
| Wenu | 8270 | 49.049 | 49049 |
| Wmunu | 8271 | 28.640 | 28640 |
| Wtaunu | 8272 | 43.500 | 43500 |
| J4 | 8090 | 916.4 | 916400 |
| J5 | 8091 | 356.250 | 356250 |
| J6 | 8092 | 6.742 | 6742 |
| J7 | 8093 | 5.300 | 5300 |
| J8 | 8094 | 0.0221 | 22.1 |

Table 4.1: Background samples.https://twiki.cern.ch/twik i/bin/view/Atlas/SusyCscMcProduction. https://twiki.cern.ch/twiki/bin/view/A tlas/HiggsWGCSCHG5Dataset

The non all-hadronic or (semi) leptonic $t\bar{t}$ background T1, is by far our most important. There will be a large multiplicity of two leptons of opposite sign and in addition missing transverse energy $\not{E}_{\mathrm{T}}$ due to the neutrino from the W-boson decay through $t \rightarrow \bar{b}W^{+} \rightarrow l^{+}\,\nu$ showing in figure 4.1. Since the second leg with $\bar{t}$ decays analogously, but with opposite signs, we end up with two jets, opposite sign di-leptons and $\not{E}_{\mathrm{T}}$ from the two $\nu$'s.

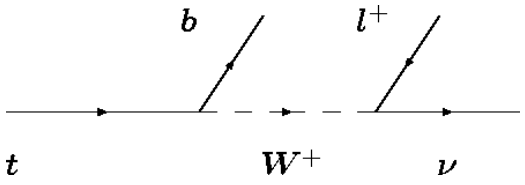


Figure 4.1: Decay of the top-quark leading a jet, lepton and $\not{E}_{\mathrm{T}}$ .

The fully hadronic ttbar sample TTbar makes up the rest of the whole $t\bar{t}$ SM background. From the two W-bosons created through $t \rightarrow b\,W \rightarrow b\,q\,\overline{q'}$ we get as many as 3 jets in each leg. With a preselection of two leptons most of these events should be removed, so it will not be an important background in this analysis.

Single Z boson production plus either a plus either a quark or a gluon. The Z-boson then decays leptonically, giving us missing transverse energy, $\not{E}_{\mathrm{T}}$ , or leptons through $Z \rightarrow \nu\,\bar{\nu}$, or

$Z \rightarrow l^+ l^-$. Generator level cuts requiring as above two jets, with $p_T^{1,2}$ 80,40GeV respectively, and an $\not\!\!E_{\rm T}$ filter >=80GeV have been applied.

Single W boson production with the second leg either being a quark or a gluon. Through leptonic decay it is also a relevant background when studying di-lepton events. From the W-boson leptonic decay $W \rightarrow l\,\nu$ one lepton is obtained, together with missing transverse energy. Another lepton can come from e.g. jets, mimicking a signal event. The single W-boson production has generator level pre-cuts, requiring two jets with minimum transverse momentum $p_T$ of 80 and 40 for the hardest and second hardest jet. A missing transverse energy filter at $\not\!\!E_{\rm T}$ >=80GeV is also used.

Double vector boson samples, WW, ZZ and WZ will naturally mimic our signal by leptonic final-states and $\not\!\!E_{\rm T}$ , and also jets which can all be contained in the production. Generator level cuts have also here been made, requiring as above two jets, with $p_T^{1,2}$ 80,40GeV respectively, and an $\not\!\!E_{\rm T}$ filter >=80GeV.

QCD production give us many jets, and leptons related to jets. $\not\!\!{\rm E}_{\rm T}$ filter of 100GeV and a minimum of two jets are required at generator level.

The SUSY signal mSUGRA points used in this analysis together with parameters and crossections are shown in table 4.2

| Point | $\mathbf{m_0}$ [GeV] | $\mathbf{m_{1/2}}$ [GeV] | A0 | $\tan(\beta)$ | sgn $\mu$ | x-sec [pb] | Events 1fb$^{-1}$ |
|---|---|---|---|---|---|---|---|
| Coannihil.SU1 | 70 | 350 | 0 | 10 | + | 7.43 (a) | 7430 |
| Focus Point SU2 | 3550 | 300 | 0 | 10 | + | 4.86 (a) | 4860 |
| Bulk SU3 | 100 | 300 | -300 | 6 | + | 18.59 (a) | 18590 |
| Low Mass SU4 | 200 | 160 | -400 | 10 | + | 262 (b) | 262000 |
| Funnel SU6 | 320 | 375 | 0 | 50 | + | 4.48 | 4480 |
| Coannihil. SU8.1 | 210 | 360 | 0 | 40 | + | 6.44 (a) | 6440 |

Table 4.2: Notes: (a) From the Herwig output of csc11 production (b) Rome cross-section information. https://twiki.cern.ch/twiki/bin/view/Atlas/SusyEventFilesInfo

# Chapter 5

# Selecting and defining signal leptons, jets and $\not{E}_{\mathrm{T}}$

There are many complicated steps on the way from electrical pulses in a wire in some part of the detector to the identification and reconstruction of an actual particle. All the electrical signals produced in the detector after a collision need to be read out and reconstructed based on our more or less good understanding of the detector and on the way matter behaves. Since this process is not straightforward we need to set up some criteria as to what we call a particle, or clarify the so-called object definitions. The object definitions are applied in two steps, first from the algorithms used to reconstruct the particles in the AODs, secondly from analysis-specific requirements can be put on the objects when creating the ntuples. The first step is done centrally and is not up to the end-user to change, while the second step is where the end-user can put limits on the definition of the objects to suit his or her analysis.

This analysis puts most emphasis on how the leptons are defined. Varying the criteria for what we call a good lepton will give us more or less confidence that we are actually looking at a lepton produced in the way our analysis is focused on. In our case this is a final-state lepton produced when a slepton decays. Actually we would like to rule out all leptons coming from either quarkonia-decay, $\gamma \rightarrow e^{+}e^{-}$ or produced inside a jet such as leptonic or semi leptonic decays of mesons. We are only interested in the leptons produced from decay of heavier elementary particles/sparticles like gauge-bosons or SUSY particles like sleptons or gauginos. A suitable naming convention is to call all leptons decaying from the heavy particles above as *primary* leptons, while the leptons coming from the other processes mentioned above will be called *secondary*. We will also define a class of leptons as "not matched" meaning the reconstructed leptons that do not find a match in the generator-level leptons, for generator level leptons that are not matched to a reconstructed lepton. Another way of naming the leptons that will be used is *prompt*, which contains the same selection as *primary*, and *extra* which contain all the rest, i.e. *secondary* and *not matched* leptons.

The following sections will first look at the $\eta$ and $p_T$ distributions of leptons at the generator-level. Since we are operating with Monte-Carlo produced data we have access to the true particle production information. We can use this to individually study distributions and reconstruction and matching efficiencies of the prompt and extra leptons. We will then go on to look at the standard object definitions and isolation criteria used for identifying the reconstructed leptons, and compare these with an alternative definition. The chosen selection criteria will then be used in the end-analysis.

## 5.1 Generated leptons

The $\eta$ and $p_T$ distributions of electrons and muons can be seen in figure 5.1 for the mSUGRA bulk region SU3. At this point no cuts or selection on the leptons have been used. The distributions are shown for generator level leptons that are primary and have a match to a reconstructed lepton (entry "Prim M" in the legend), secondary and matched to a reconstructed lepton (entry "Sec M" in the legend) and leptons that are not matched (entry "Not M"). In this section we will mostly discuss the generator-level leptons that do not get reconstructed, as discussion of the reconstructed leptons will come in the following section. The distributions of the generated leptons that are reconstructed are shown for completeness.

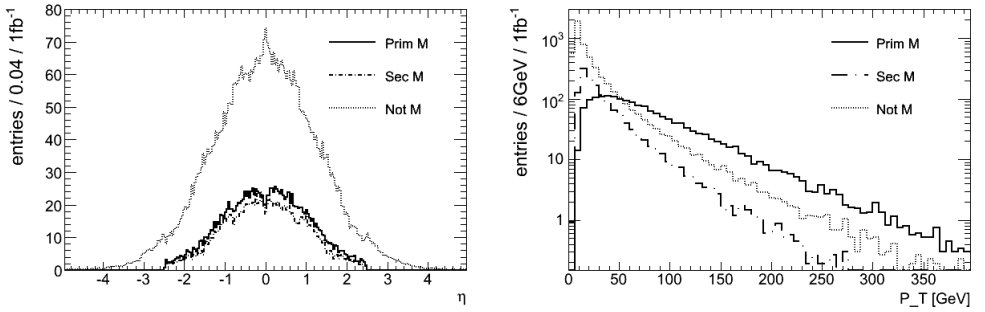


(a) Electron eta coverage

(b) Electron pt range

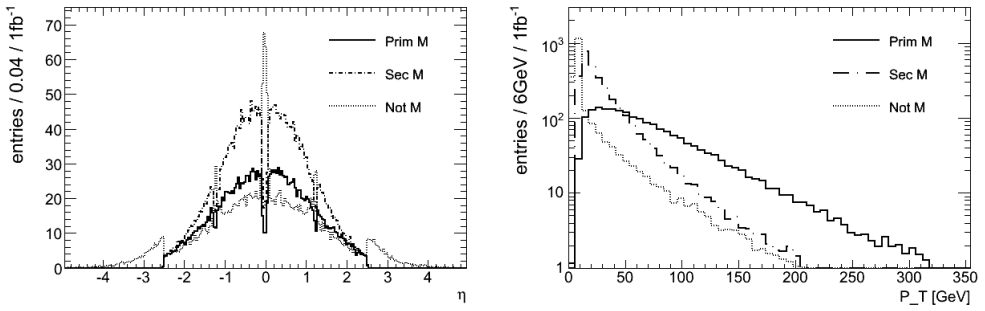


(c) Muon eta coverage

(d) Muon pt range

Figure 5.1: Lepton $\eta$ and $p_T$ distributions for generated leptons. Primary (Prim M) and secondary (Sec M) leptons shown in these plots have a match (M) to a reconstructed lepton, while the leptons that are not matched (Not M) contain all not-reconstructed leptons. Signal sample SU3.

In figure 5.1 we can the multiplicity of electrons (a,b) and muons (c,d) as function of $\eta$ and $p_T$. The $|\eta|$ distribution reflects the detector geometry as various regions with poor detector coverage show up as peaks for the leptons that do not get reconstructed, and as a consequence, dips the distributions of the generator-level leptons that *do* get reconstructed. Both for the electrons and muons there is a crack region at $\eta$=0. The liquid argon detector has a 6mm wide gap between the two half barrels [10] which affects reconstruction of electrons, while the muon detectors have a crack at $|\eta|$=0 due to passage of service cables [10]. The not - reconstructed muons also show a clear peak at $|\eta|$ =1.2. According to the Muon Working Group [18] there is low detector coverage around this area, which explains the lower reconstruction rate. Both distributions of electrons and muons as function of $\eta$ show that leptons in the are $|\eta|$ >2.5 do not get reconstructed. This is due to the lepton definitions which will be discussed in the section on reconstruction, 5.2.

In general we can see from figures 5.1(a) and 5.1(c) that more electrons than muons do not get reconstructed. Table 5.1 lists the total amount of generated leptons and how many of these are reconstructed, for all lepton types as defined above (row 1-3), and for the sub-group of primary leptons (row 4-6). From this table we can read the overall reconstruction efficiency, which is then

71.5% for primary electrons, and 85.8% for primary muons. These reconstruction efficiencies as function of $\eta$ and $p_T$ will be discussed in more detail in the next section.

The $p_T$ distributions for both electrons and muons 5.1(b) and 5.1(d) show that extra leptons (Sec M and Not M) dominate at low $p_T$ values. 72% of the electrons and 47% of the muons that are not reconstructed can be found in the region $p_T$<10GeV which is the threshold of reconstruction. We also observe that the secondary leptons overall have a smaller $p_T$ than primary leptons.

| | Electrons | % | Muons | % |
|---|---|---|---|---|
| Total All | 8280 | | 7124 | |
| Matched to Recon | 3043 | 36.8 | 5024 | 70.5 |
| Not Matched to Recon | 5237 | 63.2 | 2100 | 29.5 |
| Total Primary | 2338 | | 2304 | |
| Matched to Recon prim | 1671 | 71.5 | 1977 | 85.8 |
| Not Matched to Recon prim | 667 | 28.5 | 327 | 14.2 |

Table 5.1: Number of leptons generated, matched and not matched for the Bulk region SU3.

A graphical interpretation of the multiplicity of generated leptons are shown in figures 5.2 and 5.3 in form of scatter plots in $\eta$ vs $p_T$. Figure 5.2(c) shows that a large amount of the not-reconstructed electrons have a low transverse momentum and high value of $|\eta|$ which can explain the failure of reconstruction.

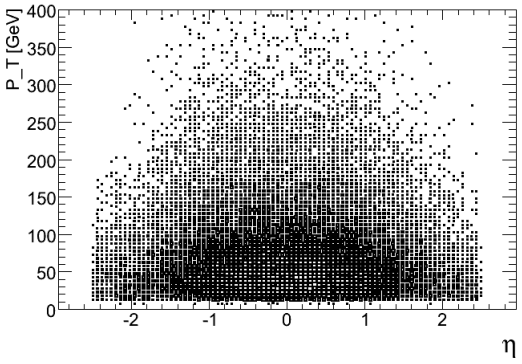


(a) Primary electrons matched to reconstructed electrons. Total: 1671

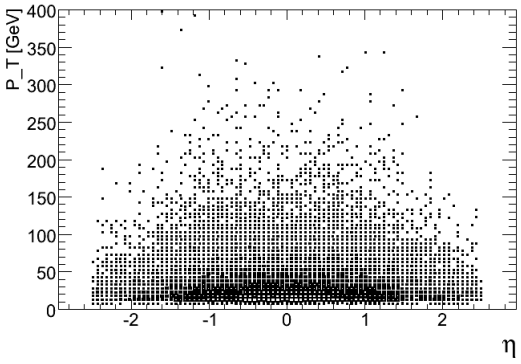


(b) Secondary electrons matched to reconstructed electrons. Total: 1372

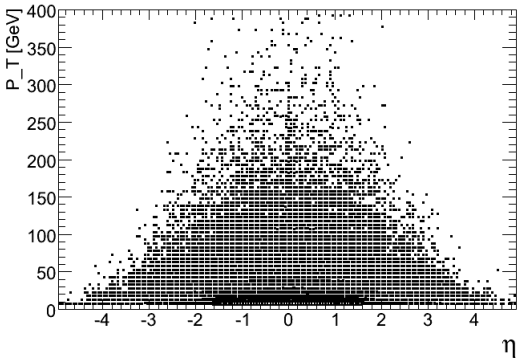


(c) Not matched to reconstructed electrons. Total: 5237

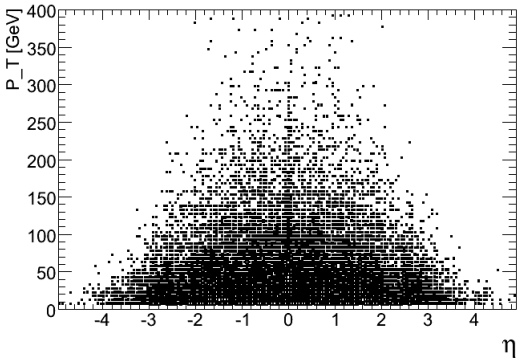


(d) Primary electrons not mached to reconstructed electrons. Total: 667

Figure 5.2: Pt vs Eta distribution for Bulk Region SU3 MC generated electrons.

One can see a tendency of higher multiplicity of electrons that are not reconstructed in the crack region around $\eta$=0. Out of all the electrons that are not reconstructed there are also some primary leptons, and their distributions are shown in figure 5.2(d). In general these electrons have a lower transverse momentum than the primary electrons that are actually reconstructed. But there is also a substantial spread both in high pt regions and low $\eta$ regions where ultimately, the electron should have been reconstructed. As a comparison we see in figures 5.2(a) and 5.2(b) primary and secondary electrons respectively. We see that for primary electrons the spread in $\eta$ and $p_T$ is large, and fairly uniform, without any large peaks or cracks. The bulk of the distribution is between $\eta$<2.2 and $p_T$<150GeV. The secondary electrons are mostly found at $p_T$< 50GeV, but have a similar uniform distribution.

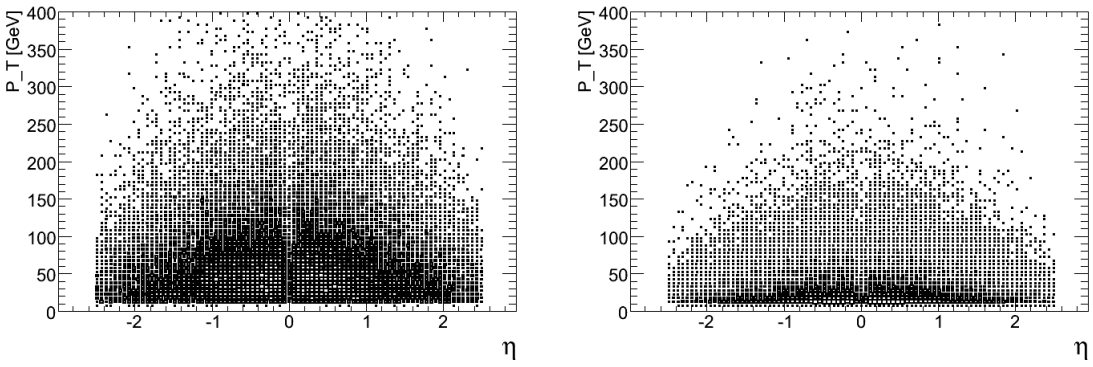


(a) Primary muons matched to reconstructed muons. Total: 1977

(b) Secondary muons matched to reconstructed muons. Total: 3048

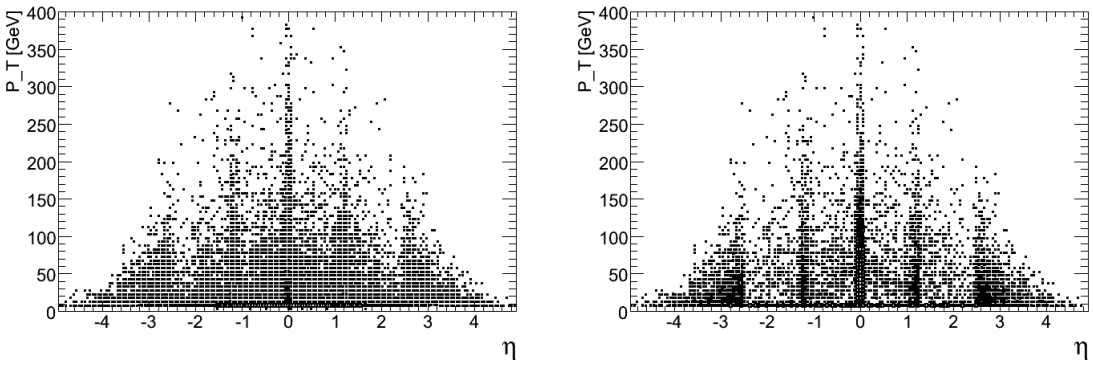


(c) Muons not matched to reconstructed muon. Total: 2100

(d) Primary muons not matched to reconstructed muon. Total: 327

Figure 5.3: Pt vs Eta distribution for Bulk Region SU3 MC generated muons.

The muons in figure 5.3 (c,d) show a similar trend as the electrons in addition to a more evident pattern around the regions with poor detector coverage at $|\eta| \sim 0.0$ and 1.2 as discussed above. Most of the muons that are not reconstructed can be found in these areas of $\eta$ or in low pt-regions and are therefore not reconstructed.

## 5.2 Reconstructed leptons and jets

### 5.2.1 Leptons

A set of requirements have been defined by the Atlas eGamma Working Group [13] and the Atlas Muon Working Group [18] in order to properly select electrons and muons. These requirements are introduced so that one with a large certainty will select leptons produced through heavy particle decay, rather than e.g. as a part of a jet. Leptons from heavy particle decay will hereafter be called *primary* or *prompt* leptons, while all other leptons will be referred to as *extra*. We will in this section study the $\eta$ and $p_T$ distributions of the reconstructed leptons, calculate reconstruction and matching efficiencies and compare these with results reported in the CSC5 Note [7] and the Atlas Detector Paper [8].

#### Lepton definitions

The Atlas eGamma Working Group [13] defines how electrons are reconstructed in the AODs. In general, the electrons are reconstructed using either cluster based or track based algorithms. The cluster based algorithms use information from the electromagnetic calorimeters while the track based use information from the tracking detectors. High $p_T$ (>10GeV) electrons are more likely to be reconstructed with the cluster based algorithms while soft electrons are reconstructed using the track based ones. In the production of the ntuples used in this analysis, only electrons reconstructed by the cluster based algorithms are chosen, i.e. hard electrons that are reconstructed with the `egamma` algorithm.

The muons are defined by the Atlas Muon Working Group [18]. Since the muons leave footprints from the inner part of the detector to the outermost part, algorithms used to reconstruct muons must therefore incorporate information from all the detector subsystems. Various strategies are used for this, and this analysis uses STACO muons which are reconstructed by the STACO (STAtistical COmbination) algorithm. The STACO algorithm combines information from the inner detector track and the muon spectrometer track and tries to merge these at the interaction point.

To measure the separation between particles, the angular distance $\Delta R$ is used and is defined as

$$\Delta R = \sqrt{\Delta\eta^2 + \Delta\phi^2} \tag{5.1}$$

The standard set of selection criteria used to pick out primary electrons and muons are as follows

1. $|\eta|$<2.5 and $p_T$ > 10 GeV
2. Transverse calorimeter energy $E_T$ in a cone of $\Delta R$ =0.2 is required to be smaller than 10 GeV. Energy is measured in the calorimeter and the isolation variable will be referred to as *etcone20*
3. Angular distance $\Delta R$ to closest jet >0.4, to be referred to as the *lepton-jet veto*

Table 5.2: Lepton definition and isolation requirements

The lepton jet veto together with the etcone20 criteria are isolation requirements. A prompt

lepton is expected to have less activity in its surroundings than an extra lepton, and this is measured both in energy, through the etcone and through the angular distance $\Delta R$ to the closest jet. The latter is called the lepton-jet veto and is applied only for leptons and jets that already have passed $p_T$, $\eta$ and etcone isolation cuts.

We will also look at a alternative lepton definition, using

| |
|---|
| 1. $p_T^{hardest}$ >20 GeV and $p_T^{second}$ >10GeV |
| 2. Transverse calorimeter energy $E_T$ in a cone of $\Delta R$=0.2 normalized to the $p_T$ of the lepton itself <0.05. Energy measured in the calorimeter. This isolation variable will be referred to as *netcone20*. |

Table 5.3: Alternative lepton definition

The choice of using both higher lepton $p_T$ cut and normalized etcone20 isolation is based on the enhanced ability of rejecting to reject extra electrons.

In addition to these requirements we remove the whole event if there is an electron in the so called crack region 1.37 < $|\eta|$ < 1.52. This is due to an overestimation in the Monte-Carlo simulations of the reconstructed electrons, and not based on physics. The crack-region is a region between the barrel and end-cap where the material density is very high [8], and one should therefore expect degraded reconstruction efficiency in this area. However, the number of electrons reconstructed in this area are highly overestimated and show up as peaks when plotting the number of electrons as function of the pseudo - rapidity $\eta$. The procedure has therefore been to remove the whole event if an electron is found in this region in order not to propagate the overestimation. The ratio of events that are discarded due to this are about 5 per mill.

**Reconstruction of leptons as function of $p_T$ and $\eta$.**

In this section leptons are put into categories of primary and matched ("Prim M"), secondary and matched ("Sec M"), and not matched ("Not M"). "Prim M" are primary (or prompt) reconstructed leptons that have a match to a generator level lepton, "Sec M" are leptons coming from all other processes than decay from gauge bosons and SUSY particles, and that have a match to a generator level lepton, while "Not M" are all particles that do not have a match to a generator level lepton. Together the 3 groups contain the whole lepton reconstruction sample.

Figures 5.4 and 5.5 show the number of electrons and muons reconstructed as function of $\eta$ and $p_T$ respectively. Figure 5.4(a) shows an excess of not matched electrons in the region around $\eta$=1. We do not see the same effect for the muons in figure 5.4(b). This particular region is the transition region between the barrel and the extended barrel hadronic calorimeter. Studies done on isolated leptons in multi-jet events [12] have shown that the efficiency of the `egamma` algorithm ensuring rejection of jets faking to be electrons is lower in this region, as we also observe. The excess in number of not matched electrons is therefore explained by this faulty reconstruction. The detector crack at $\eta$=0 as described in section 5.1 is also reflected in the number of reconstructed electrons.

Figure 5.4(b) shows the $\eta$ distribution for the muons. The detector geometry is reflected by a dip in number of reconstructed muons around $\eta$ =0 and $|\eta|$=1.2 for all categories of muons. This is due to the crack region at $\eta$=0 and poor detector coverage at $|\eta|$=1.2 as discussed in section 5.1. We must also point out that compared to the electrons there are much more secondary muons relative to primary that are reconstructed. This could be due to the large amount of muons related to jets.

From figure 5.5 we see that a large amount of extra leptons (secondary and not matched) have a low $p_T$ relative to primary leptons, even after using the standard cut of $p_T$>10GeV. The ratio of secondary electrons below 20GeV to all electrons is 38%, while only 7% of the primary electrons

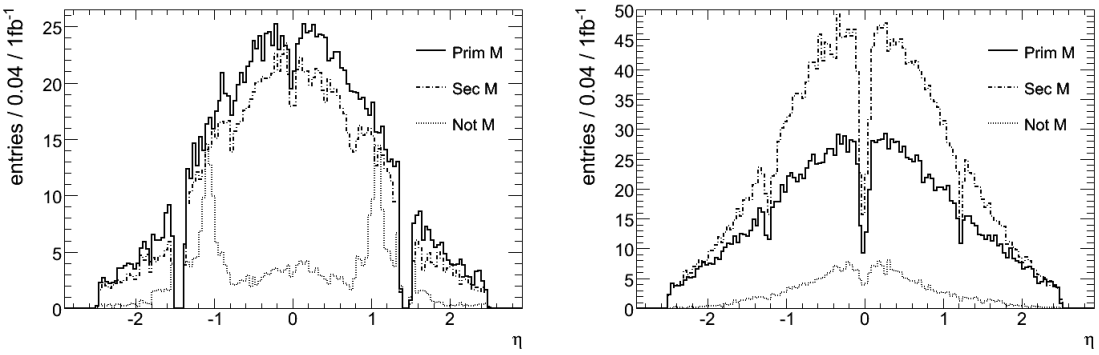


(a) Electrons (b) Muons

Figure 5.4: Number of leptons reconstructed as function of eta for electrons and muons respectively for the signal point SU3. Prim M and Sec M are respectively primary and secondary leptons that have a match to a generator-level lepton, while Not M are all leptons that do not have a generator level match.

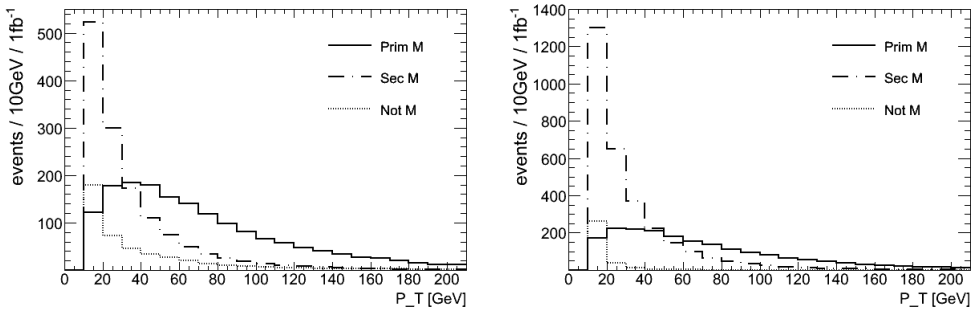


(a) Electrons (b) Muons

Figure 5.5: Transverse momentum $p_T$ for various categories of leptons as described in text.

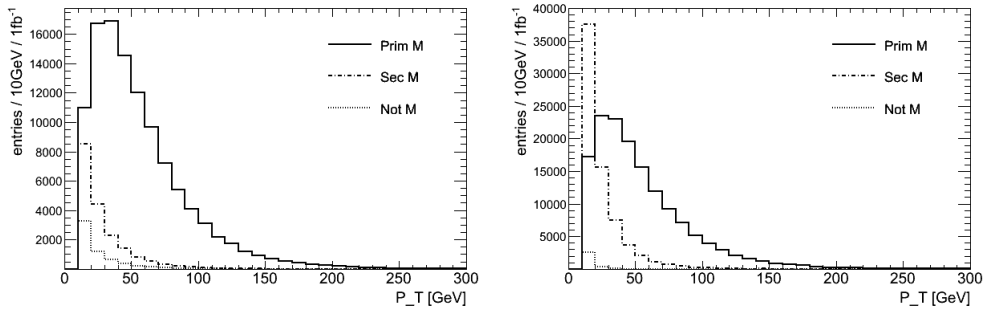


(a) Electrons (b) Muons

Figure 5.6: Transverse momentum $p_T$ for various categories of leptons for the leptonic $t\bar{t}$ sample T1

are in this $p_T$ region. 43% of the secondary muons and 9% or the primary muons have a $p_T$ <20GeV. For the not matched leptons we have 45% of the electrons and 80% of the muons below 20GeV. This could suggest that requiring the hardest lepton to have $p_T$>20GeV could be a good way of supressing extra leptons. A harder lepton $p_T$ cut will be applied later on in this analysis, in order to compare our signal with the signal using standard cuts.

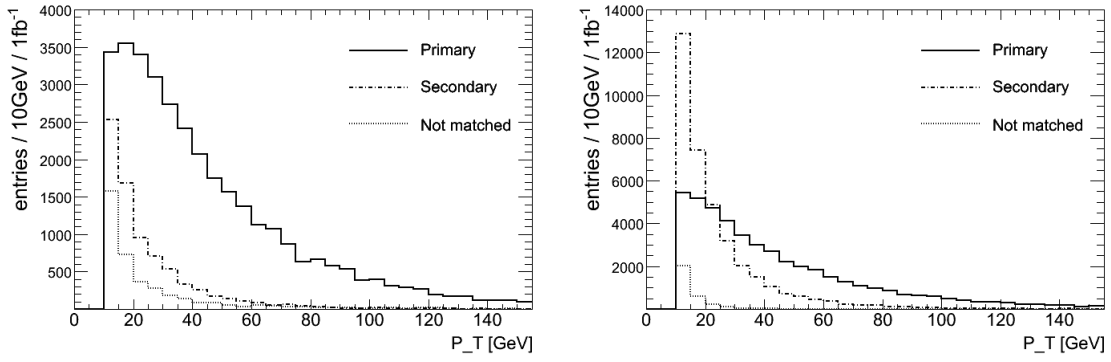


(a) Electrons (b) Muons

Figure 5.7: $p_T$ of reconstructed primary, secondary or not matched leptons for the low mass point SU4. $p_T$ cut on 10GeV is applied

In general the tendencies in $\eta$ are independent on the data sample, since the reconstruction as function of $\eta$ is dependent on the detector geometry. In the $p_T$ distribution, the background samples and the low mass signal samples will have a large portion of primary leptons in the low $p_T$ range, see figures 5.6 and 5.7.

### Lepton Reconstruction efficiency

Lepton reconstruction efficiency is defined as

$$\mathcal{E}_l \equiv \frac{N_{REC}^{prim}}{N_{GEN}^{prim}}$$

or in other words the number of generator level leptons that have a match to a reconstructed lepton normalized to the total number of generator level leptons (MC). Depending on the analysis done, one defines the generator level leptons accordingly. This analysis deals with leptons coming from heavy particle decay, the so called *primary* leptons. We have therefore defined the reconstruction efficiency as the ratio of generator level matched primary leptons by all generated primary leptons [7]. The efficiencies $\mathcal{E}_l$are shown in figure 5.8 and as a function of $\eta$ and $p_T$ for electrons and muons respectively. The distributions correspond well to similar efficiency studies done in [7].

We can again see that the crack regions in $\eta$ mentioned above are reflected as drops in reconstruction efficiency both for the electrons and for the muons.

The $p_T$ efficiency plots, figure 5.8(b) and 5.9(b) show a drop at $p_T \sim<$ 10GeV. We can see a increase in the efficiency from very low values up to a plateau, where the efficiency stays practically stable.

The Atlas CSC5 Note [7] report electron reconstruction efficiency as function of $\eta$ to be around 80% in the region $|\eta|$ < 1, and drop down to 50% from $|\eta| \sim$ 1 to $|\eta|$=2.5. The efficiency as function of $p_T$ has been measured to around 75% from $p_T$ >60GeV, where it drops substantially for lower $p_T$ values. The muon efficiency as function of $\eta$ are more stable around 90%, while the efficiency as function of $p_T$ reaches a stable value of 90% at $p_T$>20GeV. These results correspond very well with the results of this analysis.

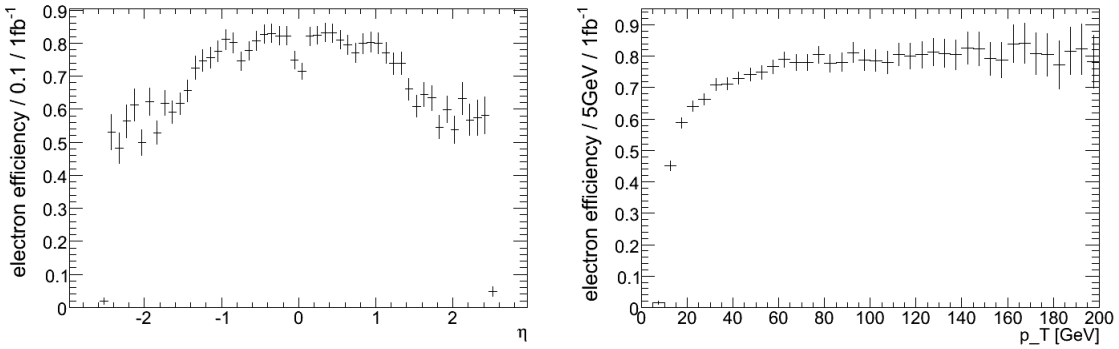


(a) Electrons (b) Electrons

Figure 5.8: Reconstruction efficiency, reconstructed electrons/ generated electrons

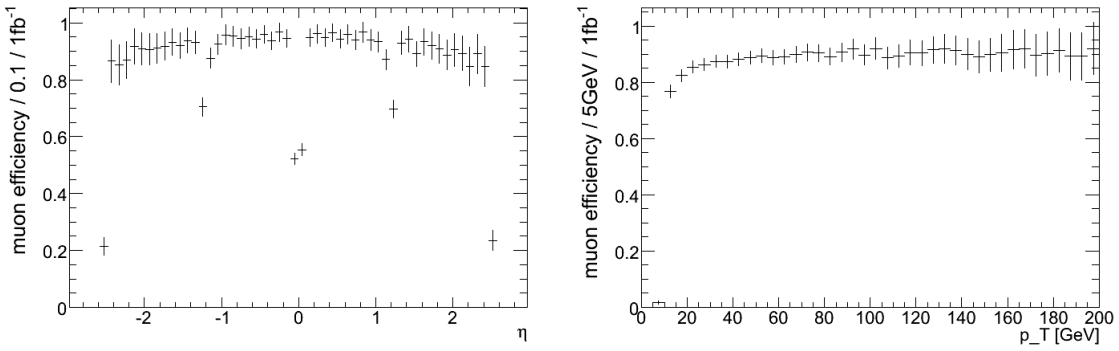


(a) Muons (b) Muons

Figure 5.9: Reconstruction efficiency, reconstructed muons/ generated muon

### 5.2.2 Jets

The jets used in this analysis are so called "Cone4Tower" jets, identified by a jet algorithm using an iterative process of collecting particles within a $\Delta R$ cone = 0.4 until a satisfactory jet has been reconstructed. The energy towers in the hadronic calorimeters are used as input for this iterative process. Jets fulfil the following requirements

- Cone4TowerJets
- $|\eta|$ < 2.5 and pT > 20 GeV

The identification of a jet has a complication. The algorithms responsible for reconstructing respectively jets and electrons can reconstruct one physical object as both an electron and a jet. If this is the case we, for technical reasons, define the object in question as an electron and remove the jet, confident that the jet was wrongly reconstructed. This is the so-called electron-jet overlap removal and it is done by removing all jets passing requirements above that are closer to an electron, passing lepton requirements in 5.2 than an angular distance $\Delta R$ < 0.2.

Figure 5.10 shows the angular distance between electrons and jets after overlap removal has been done. No electron isolation has been required in this figure, and in particular not the lepton jet overlap removal which removes all leptons within a con $\Delta R$ =0.4. By the clear two peak structure with one foot around $\Delta R$ 0.4, we can reason for the overlap removal defining leptons below this area as not isolated.

To a good approximation $\mu$ - jet misidentification is negligible.

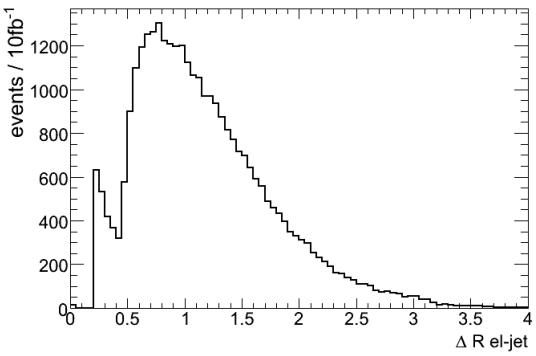


Figure 5.10: Angular distance $\Delta$R between the electron and the closest jet after electron-jet overlap removal but before lepton isolation.

## 5.3 Missing Transverse Energy

A large missing transverse energy, $\not\!\!E_{\mathrm{T}}$ , is expected in R-parity conserving SUSY scenarios such as mSUGRA which we study here. The missing transverse energy used in this analysis is based on algorithms which output is `MET_RefFinal_et`. This is recommended from the ATLAS Missing Et Group [6]. We do not take into account or study $\not\!\!E_{\mathrm{T}}$ inefficiencies or miscalculation, neither sources for fake $\not\!\!E_{\mathrm{T}}$ , but will assume that both resolution and scale is understood.

## 5.4 Looking closer at lepton isolation criteria

### 5.4.1 Calorimeter based lepton isolation

The calorimeter based lepton isolation measures the transverse energy $E_T$ (energy towers) in the electromagnetic calorimeter [1], in a given cone around the lepton, while subtracting the energy of the lepton itself. The performance of cone widths 0.2 and 0.3 are investigated here, and two different isolation values will be considered. These are

$$\text{etconeX} = \sum_{\Delta R=0}^{0.X} E_T^{\Delta R} \tag{5.2}$$

$$\text{netconeX} = \frac{\sum_{\Delta R=0}^{0.X} E_T^{\Delta R}}{p_T^{\text{lepton}}} \tag{5.3}$$

where etconeX is the standard etcone value, netconeX is the normalized value, and X is the radius of of the cone around the lepton. $E_T$ and $p_T$ are the transverse energy and transverse momentum respectively.

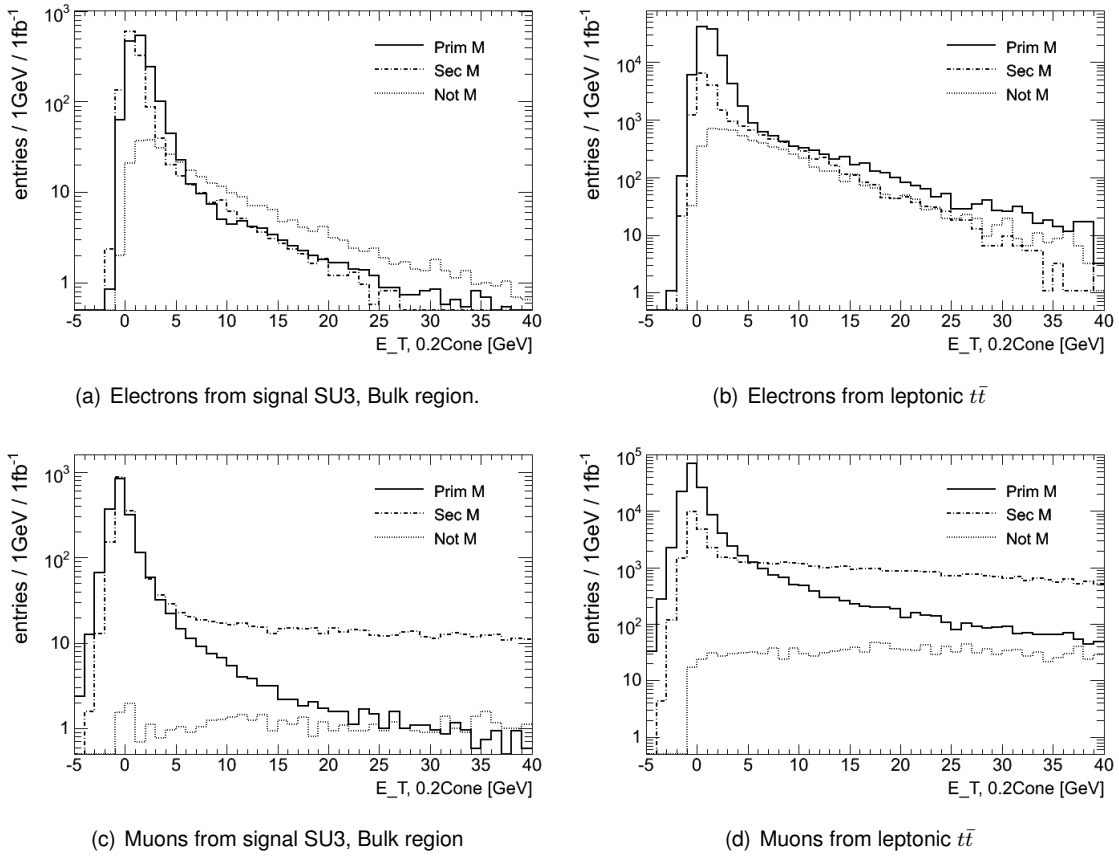


(a) Electrons from signal SU3, Bulk region.

(b) Electrons from leptonic $t\bar{t}$

(c) Muons from signal SU3, Bulk region

(d) Muons from leptonic $t\bar{t}$

Figure 5.11: Transverse energy in a cone of 0.2 around the lepton, the leptons energy has been subtracted.

[1] Track based isolation is another alternative, which was studied but not reported here. There are indications that the track-based isolation performs better than the calorimeter-based. Further studies are needed, and will be continued beyond this thesis.

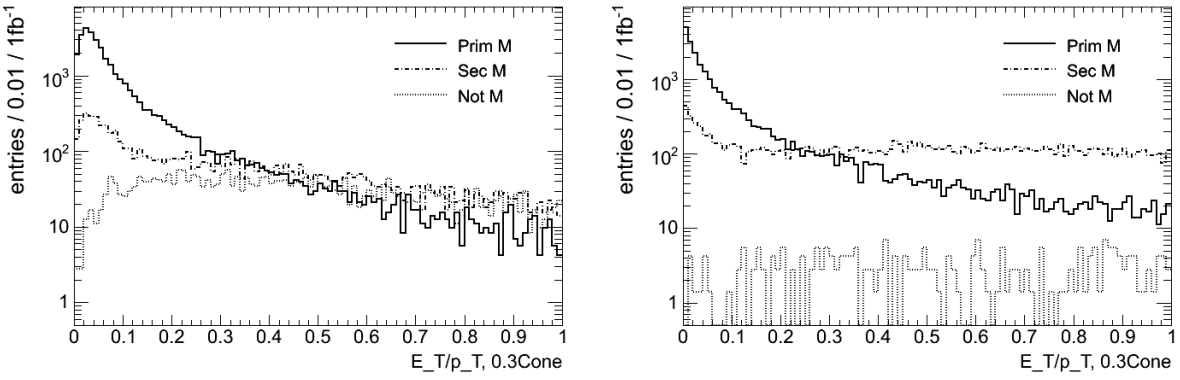


(a) Electrons (b) Muons

Figure 5.12: Distributions for the normalized transverse energy in a cone of 0.3 from electrons and muons respectively. Normalization is done by dividing the transverse energy in a cone around the lepton with the transverse momentum of the lepton itself. Signal sample SU3.

The distributions of the transverse energy in a cone of 0.2 and of the normalized transverse energy in a cone of 0.3 are shown in figures 5.11 and 5.12. We see that both for electrons and for muons, there is a peak at low values for prompt leptons (Prim M). For the extra muons (Sec M and Not M) we can in addition see a dominance at higher energies. The trend is the same for etcone30, but since the cone is larger for etcone30, the energies are in general also higher.

### 5.4.2 Investigating the isolation cut

The standard cut on leptons is to require the transverse energy in a cone around the lepton of 0.2 to be less than 10GeV, i.e. etcone20<10GeV on leptons that pass the $\eta$ and $p_T$ cut mentioned above. We will see that cutting on a etcone normalized with the $p_T$ of the lepton itself (netconeX) gives better results. We will therefore compare the variables etconeX and netconeX to see how well they perform. In order to help us evaluate the effect of the calorimeter isolation cuts, we use the following quantities

$$\epsilon_P = \frac{\text{\# selected primary leptons}}{\text{\# tot primary leptons}}$$

$$r_E = 1 - \frac{\text{\# selected extra leptons}}{\text{\# tot extra leptons}}$$

where $\epsilon_P$ is the efficiency of selecting prompt leptons, while $r_E$ describes the cuts ability to reject extra leptons. We naturally want both $\epsilon_P$ and $r_E$ to be as high as possible, and therefore a product of the two can give a good measure of how well the cuts perform. We will let the cut run over a range of values and plot efficiencies, rejection factors and the product of the two.

According to figure 5.14 which plots the product of the efficiency $\epsilon_P$ and rejection factor $r_E$, the type of cut that performs best are the normalized etcone cuts, since $\epsilon_P \cdot r_E$ reaches the highest values both for electrons and muons. $\epsilon_P \cdot r_E \sim 0.25$ for electrons and 0.48 for muons for etcone20, against 0.40 for electrons and 0.51 for muons with netcone20 or netcone30. By choosing the alternative cut of netcone20 <0.05, where the product $\epsilon_P \cdot r_E$ peaks, we see from figure5.13 that we get a signal efficiency of 90% for both electrons (e) and muons (f), while we are able to reject 40% of the extra electrons (g) and 57% of the extra muons (h). This should be compared to the performance of the standard etcone20 cut at 10GeV which gives an equally large efficiency (a,b), but only a rejection factor of 10% for electrons (c) and 50% for muons (d).

A simple illustration of the number of primary or extra leptons passing the standard isolation

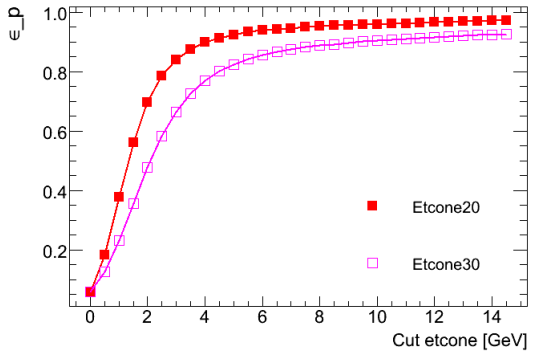


(a) $\epsilon_p\ e$

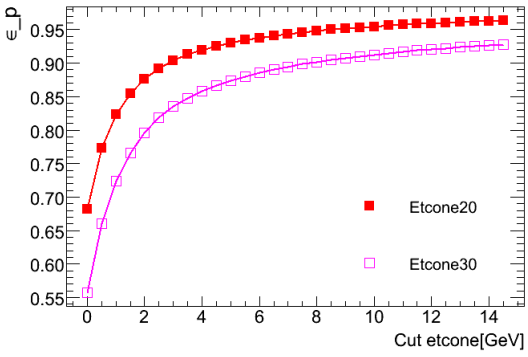


(b) $\epsilon_p\ \mu$

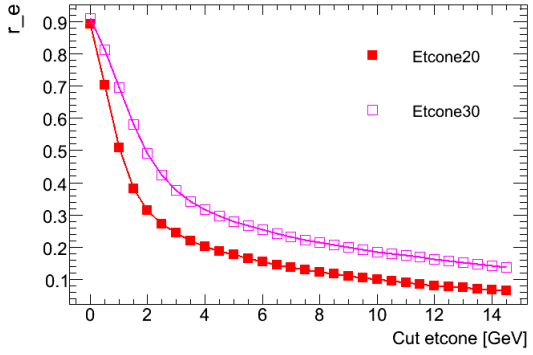


(c) $r_E; e$

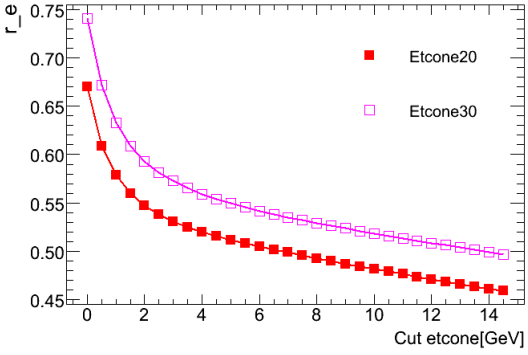


(d) $r_E \mu$

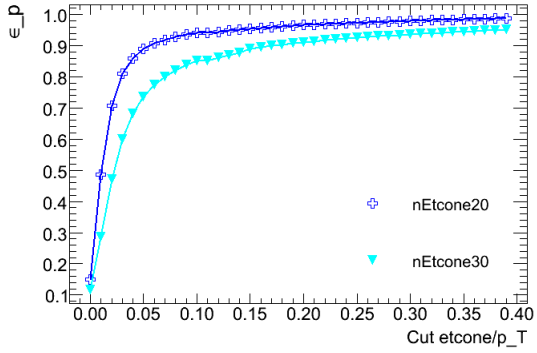


(e) $\epsilon_p\ e\ norm$

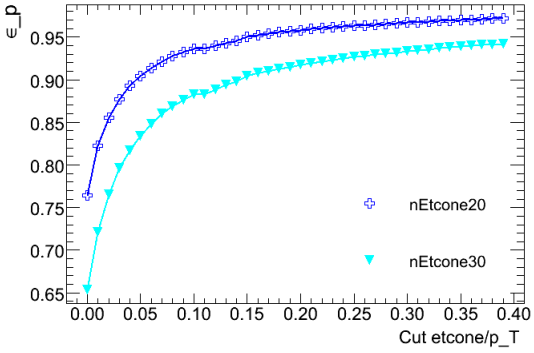


(f) $\epsilon_p\ \mu\ norm$

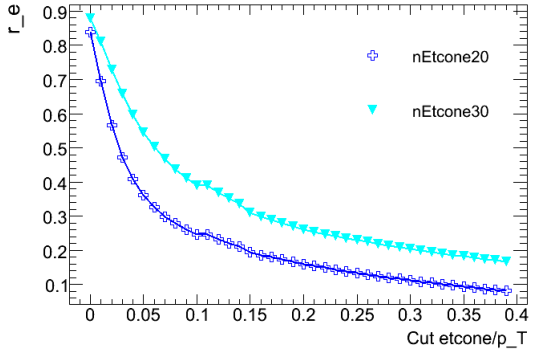


(g) $r_E; e\ norm$

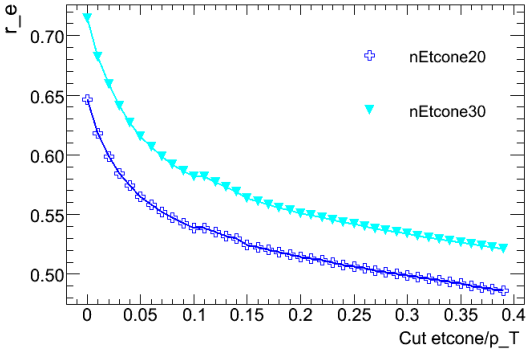


(h) $r_E \mu\ norm$

Figure 5.13: First two rows show the pure etcone disttributions, while the next two rows show the normalized values. Efficiency $\epsilon_P$ of selecting primary leptons and the rejection $r_E$ of extra leptons, both as function of the cut in etcone value are shown. Lepton pt>10GeV, $|\eta|$<2.5.

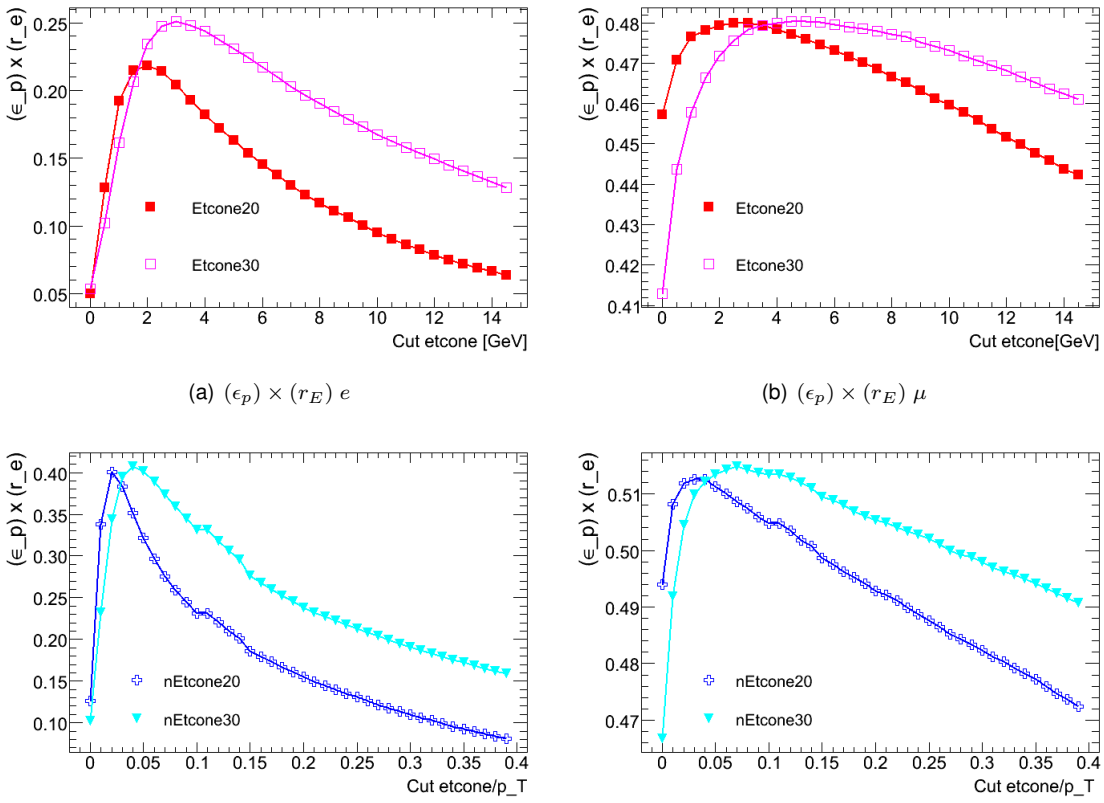


(a) $(\epsilon_p) \times (r_E)$ $e$

(b) $(\epsilon_p) \times (r_E)$ $\mu$

(c) $(\epsilon_p) \times (r_E)$ $e$ $norm$

(d) $(\epsilon_p) \times (r_E)$ $\mu$ $norm$

Figure 5.14: $(\epsilon_P) \times (r_E)$ as function of the cut in etcone value.

cut and the normalized isolation cut is shown in figure 5.15. The solid line shows how the primary and extra leptons respond to the standard etcone20 <10GeV cut, while the dotted line shows the same for the normalized etcone, netcone20<0.05. The leptons with bin label "iso" are the ones passing lepton isolation, and will be included in the sample, while the leptons in the bin labeled "not iso" will be discarded. Plot (a) shows number of primary and secondary leptons for all events, before requiring two isolated leptons of opposite sign. We see that with the standard etcone20 more primary leptons pass the isolation requirement than the normalized netcone20. As expected from the efficiency and rejection studies done above, netcone20 rejects more extra leptons. Plot 5.15(b) and 5.15(c) show results after the event is required to contain at least two isolated leptons of opposite sign. We see that the overall number of leptons has decreased for both of the isolation types. Of all primary leptons that pass the two lepton requirement both methods keep relatively the same amount $\sim$ 98%, although the etcone20 overall keeps more. 17% of the extra leptons get rejected with etcone20 against 32% for netcone20. The numbers when using $p_T$>20GeV for the hardest lepton are similar, but we see that the total number of secondary leptons has decreased by about 30%. This corresponds to the studies earlier in this section showing that a large proportion of the secondary leptons can be found at low $p_T$, so by raising the $p_T$ requirement on the hardest lepton, a substantial amount of the secondary leptons are rejected. The rejection power within the lepton sample for both etcones is lower with higher $p_T$ threshold, 23% for etcone20 and 29% for netcone20.

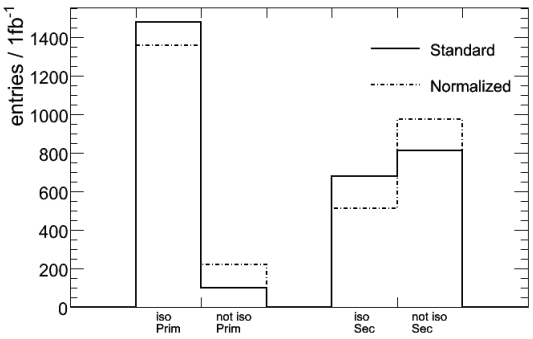


(a) Before event selection, $p_T^{1,2}$ > (20,10)GeV

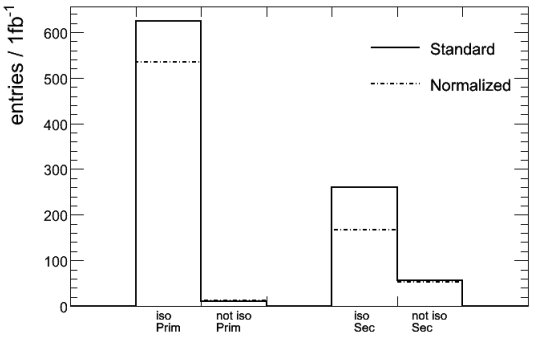


(b) 2 os isolated leptons required, $p_T^{1,2}$ >(10,10)GeV

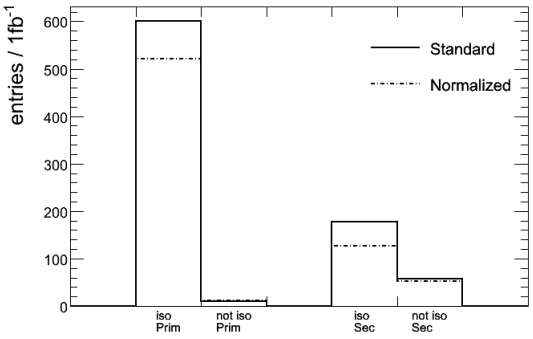


(c) 2 os isolated leptons required, $p_T^{1,2}$ >(20,10)GeV

Figure 5.15: Number of prompt (Prim) and secondary and not matched (Sec) leptons that pass or fail isolation requirements. The Standard isolation cut is etcone20<10GeV, while the Normalized isolation is etcone20/$p_T(lep)$<0.05. The two bottom plots have required 2 isolated leptons of opposite sign, while the first takes into account all events. The bottom left plot have a lepton $p_T$ requirement $lep^{hardest}, lep^{second}$ > (10,10), while the bottom right plot uses (20,10).

### 5.4.3 Lepton-jet veto

The lepton - jet veto removes leptons that have passed the calorimeter isolation requirement, $p_T$ and $\eta$ cut as described above in section 5.2, and are closer than an angular distance $\Delta R$ =0.4 to a well defined jet with $Jet_{PT} > 20GeV, |eta| < 2.5$.

Figure 5.16 shows $\Delta R$ between the leptons and jets before using the calorimeter cone isolation. The electron-jet overlap removal has been applied. The plots show clearly that before doing any calorimeter isolation, the $\Delta$ R cut at 0.4 would have a large effect, especially on the muons. We would in particular loose a lot of primary muons.

In more detail we can see a clear dip in the distributions around $\Delta$R =0.4 which corresponds to the usual cut-value. There are not many electrons in this area, only 5-6% of the primary and the secondary electrons can be found here, while about 10% of the electrons without a match are in this region. For the muons, however, a cut at $\Delta$R=0.4 would be very effective in order to remove muons without a match and secondary muons, numbers are respectively 98% and 58%, in total 62% of all the extra muons. However, a fairly large amount of primary muons suffer from this cut, as many as 32% would be removed by it.

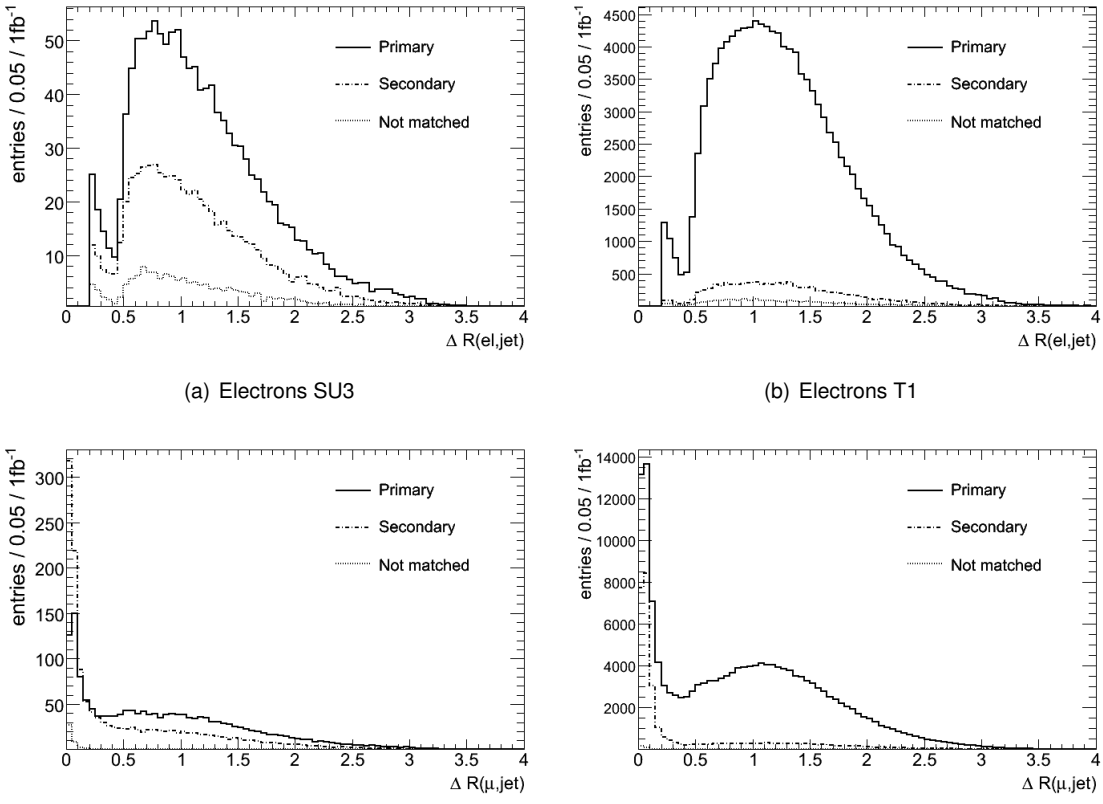


(a) Electrons SU3

(b) Electrons T1

(c) Muons SU3

(d) Muons T1

Figure 5.16: Angular distance $\Delta R$ between the lepton and the closest jet without any calorimeter isolation requirements.

The usual procedure is to apply the lepton - jet veto *after* the calorimeter cone isolation. In figure 5.17 we can see that the cut is not very efficient. Only a small number of extra leptons are below the cut region when the calorimeter cone isolation cut has been applied. For the electrons we can even see that cutting on $\Delta R$>0.4 would remove more primary than extra electrons. For the muons the ratio of extra muons in the cut region is slightly larger than for primary muons, but still very small compared to the whole sample.

The calorimeter cone isolation cut and the lepton jet veto are related since a small separation

to a jet would imply larger amount of energy deposits around the lepton. Therefore the order of application matters, and one should first apply the isolation requirement that best conserves primary leptons. Following the standard order by first applying the calorimeter isolation seems like a good strategy since we saw that the efficiency of keeping primary leptons was around 90%, and if cutting on $\Delta R$ first we would cut away a large proportion of primary muons especially.

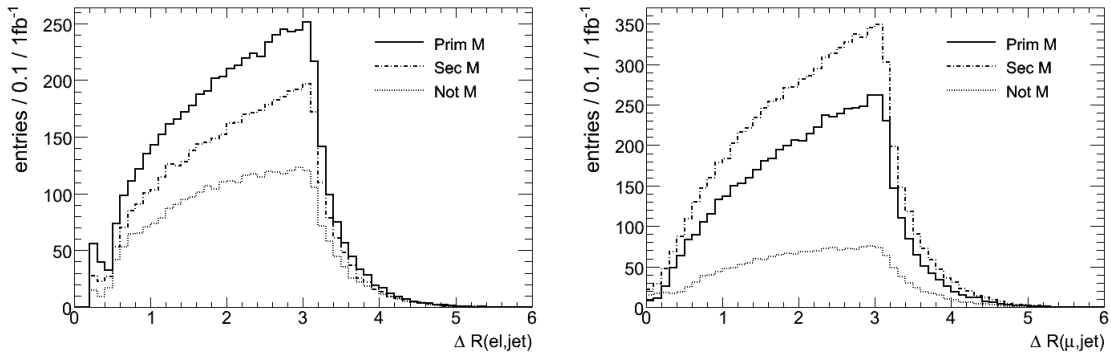


(a) Electrons (b) Muons

Figure 5.17: Angular distance $\Delta R$ between lepton and jet after electron jet overlap removal, and after all particle definition cuts have been applied. SU3 signal sample.

## 5.5 Conclusions

We have studied ways of selecting primary leptons for our analysis. The studies suggest a requirement of $p_T$ >20GeV for the hardest lepton, and use of the normalized etcone20 instead of the standard etcone20. This would possibly give us a cleaner signal event, where a large proportion of the leptons are really primary leptons. The total number of signal events might be smaller, but the purity could be enhanced, and this will be important when performing measurements on our signal, such as invariant mass measurements of two opposite sign, same flavour leptons coming from $\widetilde{\chi}_2^0$ decay. In the following analysis we will study cuts on basis of the standard etcone20, but apply a leptons $p_T$ cut of 20GeV for the hardest lepton in the event. At the end we will compare the two calorimeter isolation requirements, to see if applying the normalized etcone20 could have a positive effect on our signal.

# Chapter 6

# Selecting the SuperSymmetric event

After having studied how to select single primary leptons by using isolation cuts, we can apply further requirements on the event. These cuts are designed in order to select opposite sign dilepton SUSY events out of all the SM background events. For this, we use expected features that dominate for SUSY. In mSUGRA this is high $\not{E}_{\mathrm{T}}$ , a large proportion of hard jets from cascade decays of squarks and gluinos, and in general a large effective mass Meff as defined earlier as Meff $= \not{E}_{\mathrm{T}} + \sum_{i=1}^{4} p_T^{jet_i}$. Usual selection requirements or cuts for a dilepton opposite sign SUSY search are [7], [10]

| |
|---|
| 1. at least two leptons with opposite sign, $l_1^+$, $l_2^-$<br>only leptons within $\|\eta\|$<2.5 and with $p_T$>10 GeV are considered |
| 3. Minimum missing transverse energy, $\not{E}_{\mathrm{T}}$ >100 GeV |
| 4. Minimum ratio $\not{E}_{\mathrm{T}}$ to effective mass: $\not{E}_{\mathrm{T}}$ /Meff>0.2 |
| 5. 4 jets with $p_T$>50 GeV and hardest jet with a $p_T$ >100 GeV<br>only jets within $\|\eta\|$<2.5 and with $p_T$>20 GeV are considered |

Table 6.1: Common cuts in a dilepton SUSY search

All events that are studied in this chapter have already passed requirement 1. in the list above. We have used a standard and fairly loose isolation cut so as to be able to compare results found in other dilepton studies. This is the calorimeter based isolation requirement which demands a transverse energy in a cone of $\Delta R$ 0.2 around the lepton less than 10 GeV (etcone20<10 GeV). In the end we will compare with the alternative isolation suggested in the previous chapter. It must be noted that generator level cuts on the Pythia background data samples J4-J8, single W and single Z are $\not{E}_{\mathrm{T}}$ > 0 GeV and two jets with $p_T^{1,2}$ >80,40 GeV. In order to compare data samples that do not have such generator level cuts we make a preselection on our event requiring all events to have $\not{E}_{\mathrm{T}}$ > 100 GeV, and two jets with $p_T^{1,2}$ > 100,50 GeV. We set the limits higher than the

generator values in order to account for reconstruction resolution. Chapter 4 on Analysis Tools and Monte Carlo Data lists which data samples have generator level cuts. The $t\bar{t}$ sample T1 which is our most important background, and the SUSY samples used in this analysis do not come with generator level cuts, and will therefore be shown as a reference before the event preselection is done.

## 6.1 Two leptons with opposite sign

As earlier discussed we expect many leptons with correlated opposite signs in a Supersymmetric event. This in particular means two leptons of opposite sign and same flavour coming from $Z \rightarrow l^+l^-$ or $\widetilde{\chi}_2^0 \rightarrow \ l^{\pm}\ \widetilde{l}^{\mp} \rightarrow \ l^{\pm}\ l^{\mp}\widetilde{\chi}_1^0 l^+l^-$ decays. An illustration of this can be seen in figure 6.1, where events with two leptons are put in categories of flavour and sign for the signal sample SU3, and for the most important SM background - the leptonic or semi leptonic decays of $t\bar{t}$, the "T1" sample. In this selection, the leptons have undergone the usual etcone20 isolation cut. We can see that the SUSY sample clearly has a much larger multiplicity of leptons with opposite sign and same flavour (OSSF) relative to leptons of opposite flavour (OSOF), while the "T1" sample has an ideally identical amount of both. Due to this feature a powerful additional cut can be used to suppress the SM background. This is the so called *flavour subtraction*. Since there in background processes should be an equal amount of uncorrelated opposite sign dilepton-pairs such as $e^+e^-$, $\mu^+, \mu^-$, $e^+\mu^-$ or $\mu^+e^-$, subtracting the opposite sign, opposite flavour pairs will then be statistically the same as subtracting opposite sign same flavour pairs that are produced by chance. This is a particularly useful technique when looking at the invariant mass of the two leptons in order to extract sparticle masses from end-point measurements.

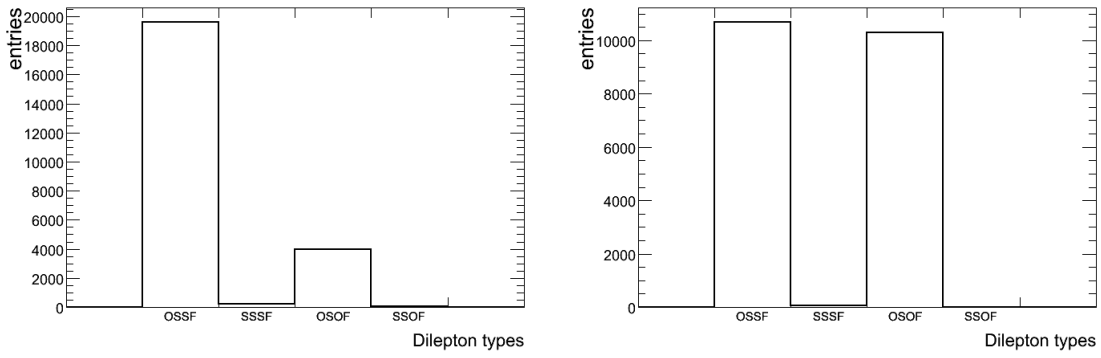


(a) Signal SU3

(b) TTbar Background

Figure 6.1: Multiplicity of dilepton types in event according to sign and flavour. SU3 signal sample and the most important background sample, the T1 sample.

## 6.2 Lepton pt

Cuts on $\eta$ and $p_T$ on the leptons mentioned in section 5.2 on "Lepton Definitions", are due to the detector performance. The region $|\eta|$<2.5 is defined as a precision measurement region and is the reason for the cut used in SUSY analysis. [1]. Requiring the lepton to have $p_T$>10 GeV is motivated by the amount of secondary versus primary leptons in this $p_T$ range. We already saw in section 5.2 that a large amount of the extra leptons could be found in region of $p_T$<20

[1] See Detector chapter 3

GeV. Figure 6.2 shows the $p_T$ distribution of primary, secondary and not matched leptons after an event-selection of two isolated leptons of opposite sign. Different $p_T$ cut has been used for the hardest lepton. The first row shows leptons when the hardest lepton is required to have $p_T$>10 GeV, while in the second row the hardest lepton is required to have $p_T$>20 GeV. With the second requirement we reject 32% of the extra electrons, while keeping 95.9% of the primary electrons. The corresponding numbers for muons are 30.6% (rejection) and 96.6% (efficiency).

As increasing the lepton $p_T$ requirement has shown to have a good effect on rejecting extra leptons, we will take this in to consideration when selecting the final cuts for the analysis. We will then choose the set of standard cuts so as to compare with results reported in [7], and compare with the cuts that could possibly give us a cleaner signal sample. These will be the normalized etcone isolation, and the lepton $p_T$ cut.

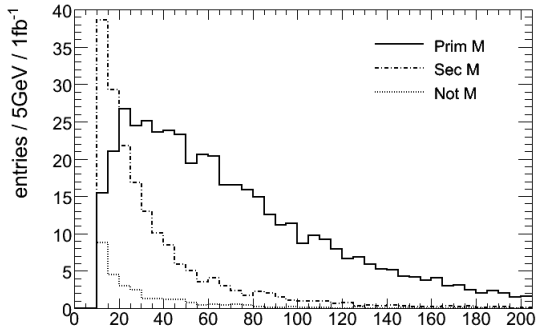


(a) Electrons $p_T^{1,2}$>10GeV etcone20<10GeV

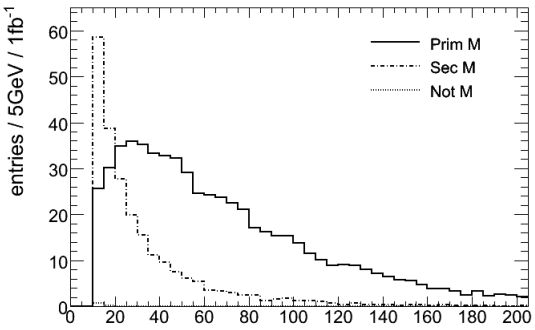


(b) Muons $p_T^{1,2}$>10GeV etcone20<10GeV

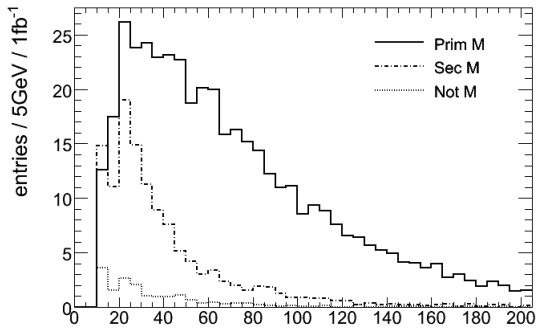


(c) Electrons $p_T^1$>20GeV, $p_T^2$>10GeV, etcone20<10GeV

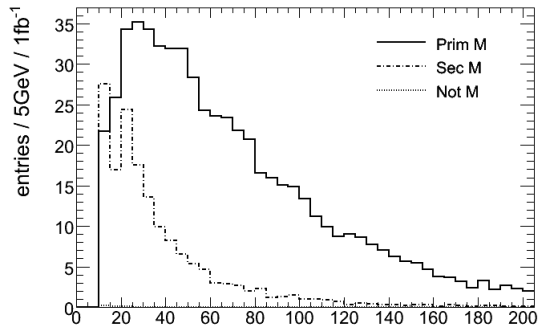


(d) Muons $p_T^1$>20GeV, $p_T^2$>10GeV, etcone20<10GeV

Figure 6.2: $p_T$ of reconstructed primary, secondary or not matched leptons for the bulk region signal point SU3. Event has 2 leptons of opposite sign. $P_T$ cut on the leptons of 10 or 20GeV is applied.

## 6.3 MissET

Figure 6.3 shows the distribution of the missing transverse energy $\not{E}_{\mathrm{T}}$ before (a) and after (b,c) the extra generator based cuts have been applied. All events have two isolated leptons of opposite sign. Applying equal generator based cuts on all samples greatly reduces the SM background, as we can see by comparing figure 6.3 a) which is without precuts, and b) and c) where precuts are applied. As expected the Standard Model background dominates at low values, with the (semi) leptonic $t\bar{t}$ sample T1 as the most important background. Figure 6.3(c) shows that all the SM

backgrounds that are left peak at small $\not\!\!E_{\mathrm{T}}$ , with a tail due to neutrinos from decay of top quarks, W and Z bosons.

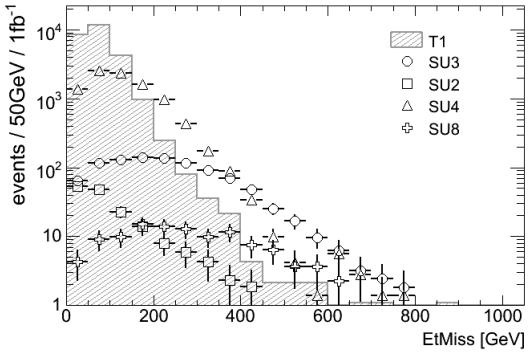


(a) Without extra generator-based cuts

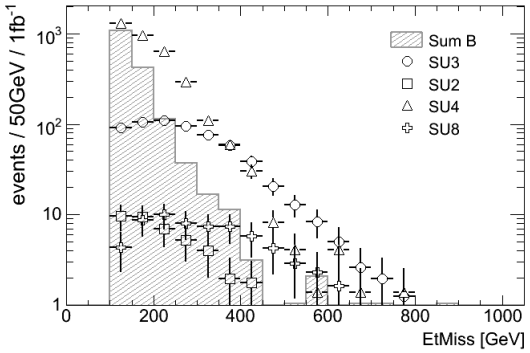


(b) With extra generator-based cuts

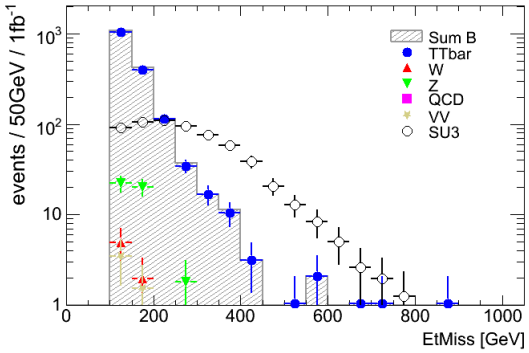


(c) With extra generator-based cuts

Figure 6.3: Missing transverse energy for a) the $t\bar{t}$ (semi) leptonic background and various signal samples. 2 isolated opposite sign leptons required, no generator level cuts, b) and c) have the generator based cuts applied $\not\!\!E_{\mathrm{T}}$ > 100 GeV, $p_T^{jet1,jet2}$> 100, 50GeV in addition to 2 isolated opposite sign leptons, b) shows various signal samples and the total background and c) signal sample SU3 and the various classes of backgrounds.

Also the low mass signal point SU4, and the focus point region SU2 have a relatively lower $\not\!\!\mathrm{E}_{\mathrm{T}}$ . This is explained by the mass-relations in the two signal-points. SU4 have fairly light squarks, and the mass difference between the gluino and the squarks is small, see table 2.2. SU2 is dominated by direct gaugino production, and the energy-scale will be smaller, resulting in relatively lower $\not\!\!E_{\mathrm{T}}$ .

The effective mass (Meff) for three $\not\!\!\mathrm{E}_{\mathrm{T}}$ cut values, 100, 150 and 200 GeV is shown in figure 6.4.

The resulting relative signal efficiencies and background rejection factors, and significances when cutting on $\not\!\!E_{\mathrm{T}}$ are shown in table 6.2. Efficiency is here defined as the ability to select a SUSY event, while rejection is the ability to discard SM background. Significance is defined as

$$\mathcal{S} = \frac{\mathrm{S}}{\sqrt{\mathrm{B}}} \tag{6.1}$$

where S is number of signal events, and B the number of background events. The significance $\mathcal{S}$ if a measure of the discovery potential. A significance larger than 5 is considered as discovery.

The generator based cuts have already been applied for these numbers, and are a preselection

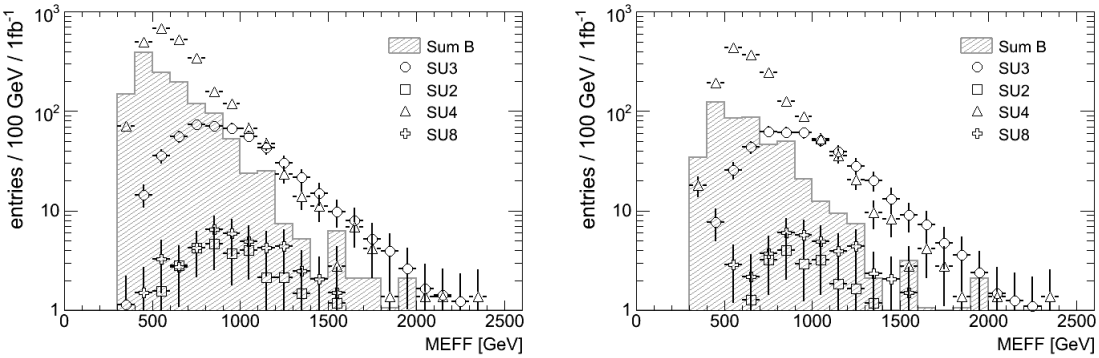


(a) $\not{E}_{\mathrm{T}}$ >100GeV

(b) $\not{E}_{\mathrm{T}}$ >150GeV

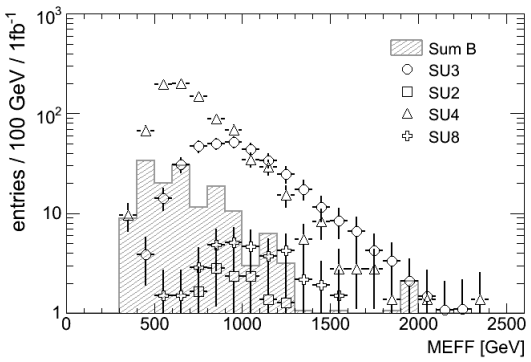


(c) $\not{E}_{\mathrm{T}}$ >200GeV

Figure 6.4: Effective mass when cutting on 3 values of $\not{E}_{\mathrm{T}}$ . 2 isolated leptons with opposite sign and extra generator-level cuts, a preselection of $\not{E}_{\mathrm{T}}$ > 100 GeV, $p_T^{jet1,jet2}$ > 100, 50 GeV have been applied.

of events with $\not\!\!E_{\rm T}$ >100 GeV, and two jets with $p_T^1$>100 GeV and $p_T^2$>50 GeV. Increasing the $\not\!\!E_{\rm T}$ cut has a great effect on the background, requiring $\not\!\!E_{\rm T}$ >150 GeV rejects as much as 68% of the background. We also see that increasing $\not\!\!E_{\rm T}$ to 250 GeV enhances the significance $\mathcal{S}$ for all signal points expect SU2 and SU4 which acquire highest significance at $\not\!\!E_{\rm T}$ >250 and 100 GeV respectively, before it decreases. At the same time, increasing the $\not\!\!E_{\rm T}$ requirement to 250 GeV results in a substantial drop in signal efficiency, from around 70% at $\not\!\!E_{\rm T}$ >150 GeV to 50% or below at 250 GeV.

Figure 6.4 gives a visualization on the effect of the $\not\!\!E_{\rm T}$ cut. Wee see that signal points SU3 and SU4 already at $\not\!\!E_{\rm T}$ >100 GeV have a discovery potential, as we already saw from table 6.2. The figure also visualizes the effect on the other signal points as they get a better separation from the SM background as the $\not\!\!E_{\rm T}$ requirement gets harder. A higher integrated luminosity than $1fb^{-1}$ would be needed to study models such as for instance SU2.

(a) 2 os leptons, gen. cuts

| $\not\!\!E_{\rm T}$ | SU1 | | | SU2 | | | SU3 | | |
|---|---|---|---|---|---|---|---|---|---|
| > | S / $\epsilon_s$ | B / $r_b$ | S/$\sqrt{B}$ | S / $\epsilon_s$ | B / $r_b$ | S/$\sqrt{B}$ | S / $\epsilon_s$ | B / $r_b$ | S/$\sqrt{B}$ |
| 100 | 227.22 | 1704.88 | 5.50 | 41.07 | 1704.88 | 0.99 | 627.29 | 1704.88 | 15.19 |
| 150 | 0.71 | 0.71 | 7.30 | 0.54 | 0.71 | 1.00 | 0.71 | 0.71 | 20.07 |
| 200 | 0.62 | 0.91 | 11.36 | 0.38 | 0.91 | 1.26 | 0.57 | 0.91 | 29.09 |
| 250 | 0.51 | 0.96 | 14.53 | 0.25 | 0.96 | 1.29 | 0.43 | 0.96 | 33.37 |
| 300 | 0.41 | 0.98 | 16.14 | 0.16 | 0.98 | 1.15 | 0.30 | 0.98 | 32.58 |

(b) 2 os leptons, gen. cuts

| $\not\!\!E_{\rm T}$ | SU4 | | | SU6 | | | SU8 | | |
|---|---|---|---|---|---|---|---|---|---|
| > | S / $\epsilon_s$ | B / $r_b$ | S/$\sqrt{B}$ | S / $\epsilon_s$ | B / $r_b$ | S/$\sqrt{B}$ | S / $\epsilon_s$ | B / $r_b$ | S/$\sqrt{B}$ |
| 100 | 3409.79 | 1704.88 | 82.58 | 104.86 | 1704.88 | 2.54 | 64.26 | 1704.88 | 1.56 |
| 150 | 0.47 | 0.71 | 72.71 | 0.72 | 0.71 | 3.39 | 0.70 | 0.71 | 2.04 |
| 200 | 0.26 | 0.91 | 71.59 | 0.61 | 0.91 | 5.17 | 0.61 | 0.91 | 3.15 |
| 250 | 0.12 | 0.96 | 50.02 | 0.51 | 0.96 | 6.72 | 0.47 | 0.96 | 3.76 |
| 300 | 0.05 | 0.98 | 31.02 | 0.42 | 0.98 | 7.57 | 0.37 | 0.98 | 4.15 |

Table 6.2: Relative efficiency and rejection factors and significances when running over the $\not\!\!E_{\rm T}$ requirement. All events are required to have 2 isolated leptons of opposite sign, and extra generator-based requirements, but no additional requirement. First row, $\epsilon_S$ column states total number of signal events, first row $r_B$ column states total number of background events.

## 6.4 Number of jets and $p_T$ of hardest jet

The standard number of jets to require in an event with two leptons of opposite sign is 4 jets with $p_T$>50 GeV, and the hardest jet with $p_T$>100 GeV [7]. Figure 6.5 show the number of jets that have $p_T$>50 GeV with (b, c ) and without (a) the extra generator based cuts for a) the various signal points and the T1 background and b) various signal points and the sum of backgrounds, and c) SU3 signal-sample and all the backgrounds. Isolated opposite sign di-leptons have been required for all events. All the SUSY points shown in figure 6.5 a) except for SU2 have a large proportion of events with 4 jets. SU2 has as we saw in chapter 2.3 very large scalar masses and is expected to have low QCD activity, it is therefore not the optimal point for discovery using methods in this analysis. We see clearly, that the overall number of hard jets is higher in a typical SUSY event than in a SM event. Using a jet-requirement is therefore beneficial as it will remove a significant part of the background.

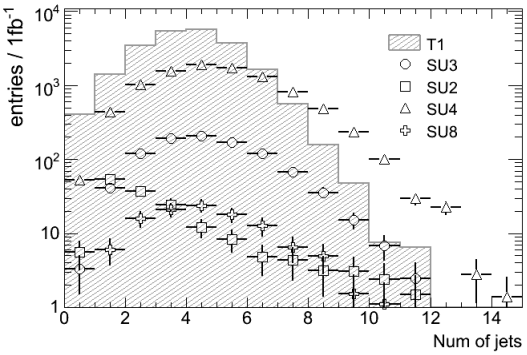


(a) Without generator based cuts

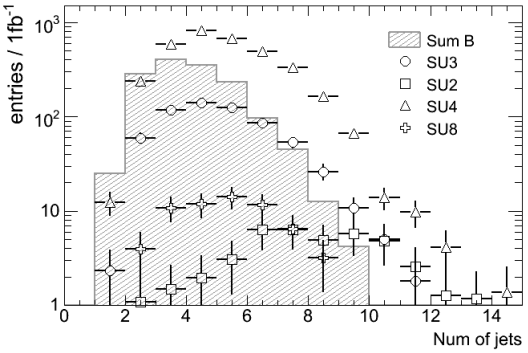


(b) With extra generator-based cuts

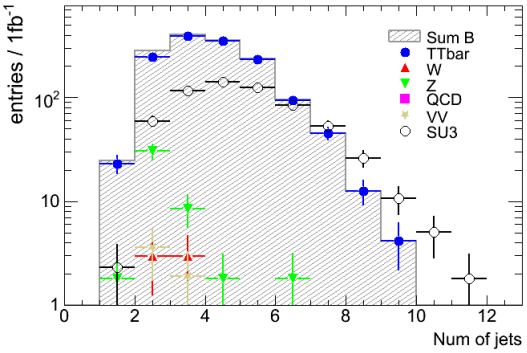


(c) With extra generator-based cuts

Figure 6.5: Number of jets with $p_T$> 50 GeV. 2 isolated leptons of opposite sign have been required for all plots. Plot a) shows the $t\bar{t}$ (semi) leptonic SM background sample T1 together with various SUSY signal samples. Event has no other requirements than 2 isolated leptons of opposite sign, in particular no generator based cuts. Plot b) shows the sum of backgrounds and various signal samples, plot c) shows the sum of backgrounds, all background samples and the signal sample SU3. Plot b) and c) have applied the generator based cuts: $\not{E}_T$ > 100GeV, $p_T^{jet1,jet2}$> 100, 50 GeV.

Figure 6.6 show a distribution of the $p_T$ of the hardest well-defined jet in the event with and without the extra generator based cuts respectively. When applying the extra cuts for all samples we see that the peak of the $p_T$ distributions have been slightly shifted to the right for both the SM background and for the SUSY signal. Cutting at $p_T$>100 GeV seems to be safe for all our signal samples, while we are able to reject part of the SM $t\bar{t}$ background. SU2 and SU4 is are exceptions, since the cut would have a similar affect as for the SM background. For SU4 this is not so important, as the crossection is very high, and the discovery potential would not fall dramatically. SU2 does suffer, and another treatment would be needed to take into account SU2.

Cutting at 100 GeV seems like a good compromise as we already cut away a large proportion of the SM background, and are able to conserve much of the SUSY signal.

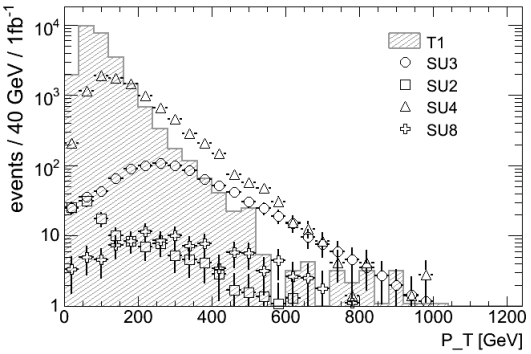


(a) Without generator based cuts

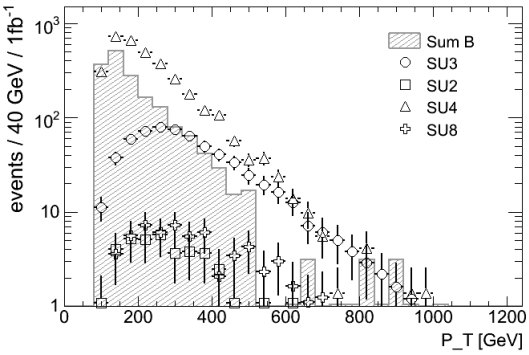


(b) With extra generator-based cuts

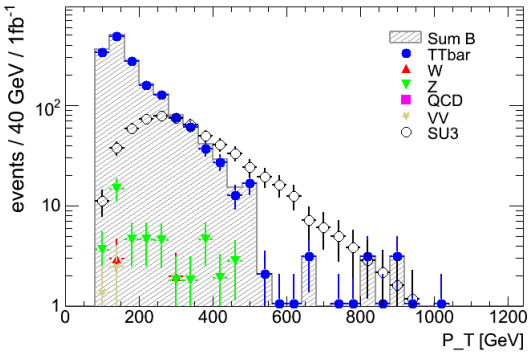


(c) With extra generator-based cuts

Figure 6.6: Transverse momentum $p_T$ of the hardest jet in the event. Plot a) show SM (semi) leptonic $t\bar{t}$ sample "T1" and for the various SUSY signal samples. Only requirement on event is at least 2 opposite signed well-defined leptons required. Plot b) shows various signal samples versus the sum of all backgrounds, plot b) shows the signal sample SU3 together with the sum of all backgrounds, and also each class of backgrounds seperately. Event requirements for all 3 plots are at least 2 isolated opposite sign leptons, and for plot (b,c) additional generator-based cuts $\not{E}_{\mathrm{T}}$ > 100 GeV, $p_T^{jet1,jet2}$ > 100, 50 GeV. SU1 and SU6 have similar distribtutions as SU3 and are therefore not shown.

Table 6.3 shows results when choosing a certain number of jets, with $p_T$ constraint on the hardest jet having $p_T$>100 GeV . Overall we observe that except for SU4, we gain the highest significance if we require 4 jets. But if we at the same time consider the efficiencies we see a substantial drop most of the SUSY points when going from 3 to 4 jets, and for e.g. SU3 the efficiency drops from 70% to 36%.

For comparison, the 4, 3 and two-jet cut with $p_T$ configuration $p_T^{Jetall}$>50 GeV and $p_T^{Jet1}$>100 GeV are shown in figure 6.7. The 4-jet case gives us according to table 6.3 the largest signifi-

(a) 2 os leptons, gen. cuts

| Jet cut | SU1 | | | SU2 | | | SU3 | | |
|---|---|---|---|---|---|---|---|---|---|
| > | S / $\epsilon_s$ | B / $r_b$ | S/$\sqrt{B}$ | S / $\epsilon_s$ | B / $r_b$ | S/$\sqrt{B}$ | S / $\epsilon_s$ | B / $r_b$ | S/$\sqrt{B}$ |
| 2 | 227.22 | 1704.88 | 5.50 | 41.07 | 1704.88 | 0.99 | 627.29 | 1704.88 | 15.19 |
| 3 | 0.70 | 0.65 | 6.44 | 0.90 | 0.65 | 1.50 | 0.70 | 0.65 | 17.82 |
| 4 | 0.37 | 0.91 | 6.68 | 0.78 | 0.91 | 2.54 | 0.36 | 0.91 | 17.82 |

(b) 2 os leptons, gen. cuts

| Jet cut | SU4 | | | SU6 | | | SU8 | | |
|---|---|---|---|---|---|---|---|---|---|
| > | S / $\epsilon_s$ | B / $r_b$ | S/$\sqrt{B}$ | S / $\epsilon_s$ | B / $r_b$ | S/$\sqrt{B}$ | S / $\epsilon_s$ | B / $r_b$ | S/$\sqrt{B}$ |
| 2 | 3409.79 | 1704.88 | 82.58 | 104.86 | 1704.88 | 2.54 | 64.26 | 1704.88 | 1.56 |
| 3 | 0.63 | 0.65 | 87.57 | 0.80 | 0.65 | 3.40 | 0.75 | 0.65 | 1.96 |
| 4 | 0.27 | 0.91 | 73.26 | 0.50 | 0.91 | 4.14 | 0.44 | 0.91 | 2.24 |

Table 6.3: Relative efficiency and rejection factors, and significances when requiring 2, 3 or 4 jets in the event. All events are required to have 2 leptons of opposite sign, and generator level preselection cuts: $\not\!\!E_{\mathrm{T}}$ >100GeV, $p_T^{jet1,jet2}$>100,50 GeV. First row, $\epsilon_S$ column states total number of signal events, first row $r_B$ column states total number of background events.

cance, but also loss off efficiency as the figures illustrate. The background rejection is very high for the 4-jet requirement, 91% of the background gets rejected, compared to 65% when requiring 3 jets. If requiring 4 jets especially the low mass point SU4 suffers as the signal efficiency drops from 63% to 27%.

## 6.5 Optimizing $\not\!\!E_{\mathrm{T}}$ and jet cut

When considering the $\not\!\!E_{\mathrm{T}}$ cut and the jet cut at the same time we see that the 3-jet requirement overall performs best for combinations shown in tables 6.4 and 6.5.

Figure 6.8 shows the distributions of the effective mass Meff for various $\not\!\!E_{\mathrm{T}}$ cuts and when requiring 3 jets. We can in particular see that increasing the $\not\!\!E_{\mathrm{T}}$ requirement from 150 GeV to 200 GeV reduces the SM background by a large amount. Again, the low mass signal point SU4, as well as SU8 suffer but the other signal samples seem not to be too affected by this cut. In table 6.4 we can read that requiring $\not\!\!E_{\mathrm{T}}$ >200 GeV reduces the background by 85% in the 3 - jet case and 82% in the 4 - jet case. The efficiencies stay around 70-80% for all points except SU2 and SU4. In SU2 we experience a large drop in signal efficiency from around 60 % to around 30 % for both the 3 and 4 - jet configuration. SU4 also has a large drop in efficiency but still has a significance of 72 for $\not\!\!E_{\mathrm{T}}$ cut of 200 GeV.

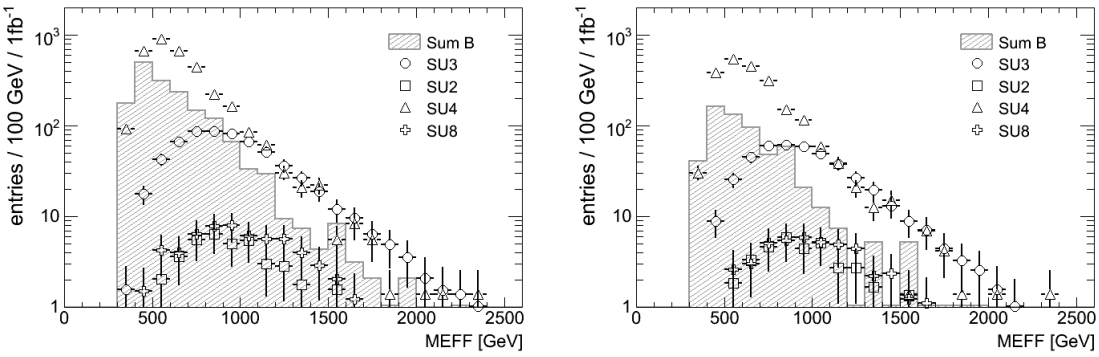


(a) Requiring 2 jets

(b) Requring 3 jets

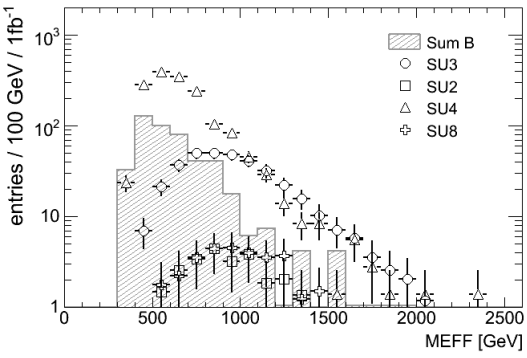


(c) Requiring 4 jets

Figure 6.7: Effective mass when requiring event to contain 2 leptons of opposite sign, $\not{E}_{\mathrm{T}}$ > 100 GeV and 2, 3 or 4 jets with $p_T^{All}$ > 50 GeV, $p_T^1$ > 100 GeV

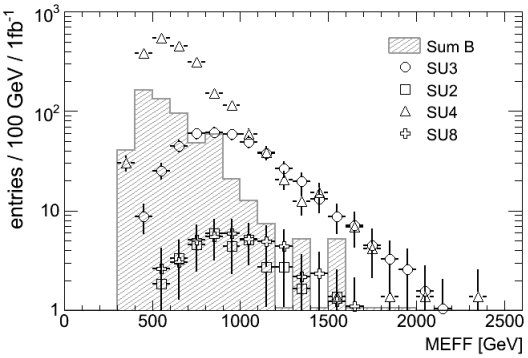


(a) 3 jets, $\not\!\!E_{\mathrm{T}}$ >100GeV

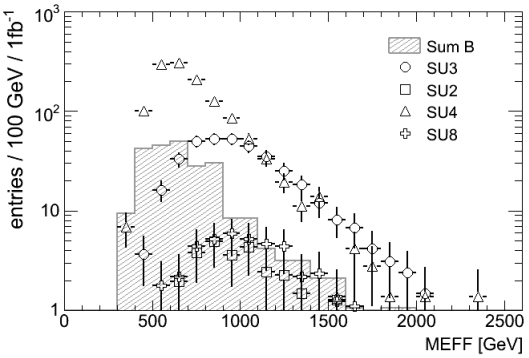


(b) 3 jets, $\not\!\!E_{\mathrm{T}}$ >150GeV

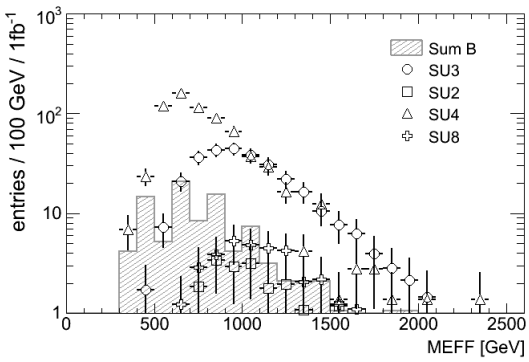


(c) 3 jets, $\not\!\!E_{\mathrm{T}}$ >200GeV

Figure 6.8: Effective mass distributions after 2 leptons of opposite sign have been required, and in addition 3 jets satisfying $p_T^{JetAll}$ > 50 GeV, $p_T^{Jet1}$ > 100 GeV. Plots show effect of $\not\!\!E_{\mathrm{T}}$ cut for $\not\!\!E_{\mathrm{T}}$ > (100,150,200) GeV

(a) 2 os leptons, 3 jets, gen. cuts

| $\not{E}_{\mathrm{T}}$ | SU1 | | | SU2 | | | SU3 | | |
|---|---|---|---|---|---|---|---|---|---|
| > | S / $\epsilon_s$ | B / $r_b$ | S/$\sqrt{B}$ | S / $\epsilon_s$ | B / $r_b$ | S/$\sqrt{B}$ | S / $\epsilon_s$ | B / $r_b$ | S/$\sqrt{B}$ |
| 100 | 157.95 | 601.11 | 6.44 | 36.87 | 601.11 | 1.50 | 436.85 | 601.11 | 17.82 |
| 150 | 0.89 | 0.60 | 9.02 | 0.80 | 0.60 | 1.89 | 0.85 | 0.60 | 23.97 |
| 200 | 0.76 | 0.85 | 12.51 | 0.56 | 0.85 | 2.14 | 0.69 | 0.85 | 31.07 |
| 250 | 0.63 | 0.92 | 14.34 | 0.38 | 0.92 | 2.04 | 0.51 | 0.92 | 31.92 |
| 300 | 0.51 | 0.95 | 14.79 | 0.25 | 0.95 | 1.68 | 0.36 | 0.95 | 28.72 |

(b) 2 os leptons, 3 jets, gen. cuts

| $\not{E}_{\mathrm{T}}$ | SU4 | | | SU6 | | | SU8 | | |
|---|---|---|---|---|---|---|---|---|---|
| > | S / $\epsilon_s$ | B / $r_b$ | S/$\sqrt{B}$ | S / $\epsilon_s$ | B / $r_b$ | S/$\sqrt{B}$ | S / $\epsilon_s$ | B / $r_b$ | S/$\sqrt{B}$ |
| 100 | 2146.95 | 601.11 | 87.57 | 83.47 | 601.11 | 3.40 | 47.96 | 601.11 | 1.96 |
| 150 | 0.59 | 0.60 | 81.73 | 0.95 | 0.60 | 5.08 | 0.93 | 0.60 | 2.88 |
| 200 | 0.32 | 0.85 | 71.51 | 0.80 | 0.85 | 6.90 | 0.79 | 0.85 | 3.95 |
| 250 | 0.14 | 0.92 | 42.08 | 0.67 | 0.92 | 8.04 | 0.65 | 0.92 | 4.46 |
| 300 | 0.06 | 0.95 | 23.70 | 0.54 | 0.95 | 8.36 | 0.53 | 0.95 | 4.69 |

Table 6.4: Relative efficiencies and rejection factors, and significances when running over the $\not{E}_{\mathrm{T}}$ cut. All events have 2 isolated leptons of opposite sign, and 3 jets with $p_T^{JET1} \geq 100$, $p_T^{all} \geq 50$. First row, $\epsilon_S$ column states total number of signal events, first row $r_B$ column states total number of background events.

(a) 2 os leptons, 4 jets, gen. cuts

| | SU1 | | | SU2 | | | SU3 | | |
|---|---|---|---|---|---|---|---|---|---|
| $\not{E}_{\mathrm{T}}$ > | S / $\epsilon_s$ | B / $r_b$ | S/$\sqrt{B}$ | S / $\epsilon_s$ | B / $r_b$ | S/$\sqrt{B}$ | S / $\epsilon_s$ | B / $r_b$ | S/$\sqrt{B}$ |
| 100 | 78.94 | 158.17 | 6.28 | 36.45 | 158.17 | 2.90 | 230.52 | 158.17 | 18.33 |
| 150 | 0.88 | 0.54 | 8.20 | 0.83 | 0.54 | 3.57 | 0.84 | 0.54 | 22.86 |
| 200 | 0.84 | 0.82 | 12.40 | 0.63 | 0.82 | 4.34 | 0.71 | 0.82 | 30.58 |
| 250 | 0.62 | 0.87 | 11.03 | 0.38 | 0.87 | 3.13 | 0.51 | 0.87 | 26.46 |
| 300 | 0.54 | 0.93 | 12.58 | 0.28 | 0.93 | 3.04 | 0.38 | 0.93 | 25.46 |

(b) 2 os leptons, 4 jets, gen. cuts

| $\not{E}_{\mathrm{T}}$ | SU4 | | | SU6 | | | SU8 | | |
|---|---|---|---|---|---|---|---|---|---|
| > | S / $\epsilon_s$ | B / $r_b$ | S/$\sqrt{B}$ | S / $\epsilon_s$ | B / $r_b$ | S/$\sqrt{B}$ | S / $\epsilon_s$ | B / $r_b$ | S/$\sqrt{B}$ |
| 100 | 921.30 | 158.17 | 73.26 | 58.80 | 158.17 | 4.68 | 36.23 | 158.17 | 2.88 |
| 150 | 0.57 | 0.54 | 61.73 | 0.95 | 0.54 | 6.59 | 0.93 | 0.54 | 3.98 |
| 200 | 0.30 | 0.82 | 51.52 | 0.82 | 0.82 | 9.05 | 0.78 | 0.82 | 5.30 |
| 250 | 0.14 | 0.87 | 29.94 | 0.66 | 0.87 | 8.66 | 0.69 | 0.87 | 5.59 |
| 300 | 0.07 | 0.93 | 18.66 | 0.46 | 0.93 | 7.92 | 0.60 | 0.93 | 6.40 |

Table 6.5: Relative efficiencies and rejection factors, and significances when running over the $\not{E}_{\mathrm{T}}$ cut. All events have 2 isolated leptons of opposite sign, and 4 jets with $p_T^{JET1} \geq 100$, $p_T^{all} \geq 50$. First row, $\epsilon_S$ column states total number of signal events, first row $r_B$ column states total number of background events.

## 6.6 $\not\!\!E_{\mathrm{T}}$ / MEFF

The last cut to investigate is the $\not\!\!E_{\mathrm{T}}$ over effective mass Meff. If we were to apply the standard cut of $\not\!\!E_{\mathrm{T}}$ / Meff >0.2 as listed in 6.1 we can see directly from the distributions in figure 6.9 that we loose a large proportion of signal events, both if applying the cut before any other requirements than the standard generator level requirements and two leptons of opposite sign in figure 6.9(a), or when requiring 3 or 4 jets, figure 6.9(b) and 6.9(c). In particular cutting on $\not\!\!E_{\mathrm{T}}$ / Meff will not do a good job since it does not manage to discriminate between signal and background.

Table 6.6 confirms this as we see that significances are lower when in addition to the standard $\not\!\!E_{\mathrm{T}}$ > 100 GeV cut require $\not\!\!E_{\mathrm{T}}$ /Meff.

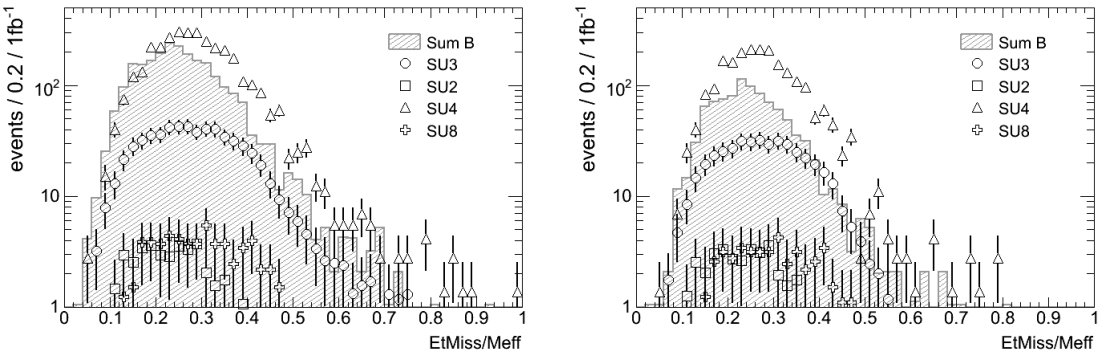


(a) Requiring 2 jets

(b) Requiring 3 jets

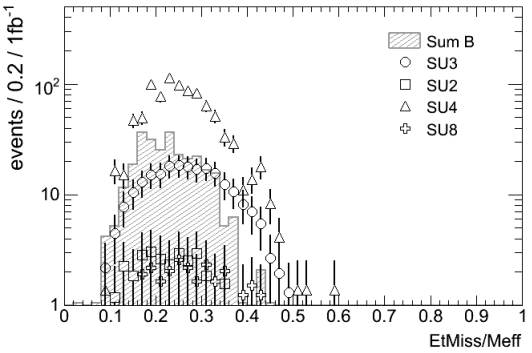


(c) Requiring 4 jets

Figure 6.9: $\not\!\!E_{\mathrm{T}}$ / (MEFF), both plots require 2 leptons of opposite sign, and (b) requires in addition 2, 3 or 4 jets with $p_T^{JetAll}$ > 50 GeV$p_T^{Jet1}$ > 100GeV and $\not\!\!E_{\mathrm{T}}$ >100 GeV

(a) 2 os leptons, 3 jets, gen. cuts

| $\not{E}_{\mathrm{T}}$ /Meff | SU1 | | | SU2 | | | SU3 | | |
|---|---|---|---|---|---|---|---|---|---|
| > | S / $\epsilon_s$ | B / $r_b$ | S/$\sqrt{B}$ | S / $\epsilon_s$ | B / $r_b$ | S/$\sqrt{B}$ | S / $\epsilon_s$ | B / $r_b$ | S/$\sqrt{B}$ |
| 0.00 | 157.95 | 601.11 | 6.44 | 36.87 | 601.11 | 1.50 | 436.85 | 601.11 | 17.82 |
| 0.10 | 0.98 | 0.02 | 6.36 | 0.98 | 0.02 | 1.48 | 0.98 | 0.02 | 17.68 |
| 0.15 | 0.92 | 0.09 | 6.21 | 0.84 | 0.09 | 1.32 | 0.91 | 0.09 | 16.98 |
| 0.20 | 0.82 | 0.23 | 6.03 | 0.65 | 0.23 | 1.11 | 0.78 | 0.23 | 15.80 |
| 0.25 | 0.68 | 0.50 | 6.25 | 0.46 | 0.50 | 0.98 | 0.61 | 0.50 | 15.32 |
| 0.30 | 0.52 | 0.72 | 6.34 | 0.23 | 0.72 | 0.65 | 0.43 | 0.72 | 14.49 |

(b) 2 os leptons, 3 jets, gen. cuts

| $\not{E}_{\mathrm{T}}$ / Meff | SU4 | | | SU6 | | | SU8 | | |
|---|---|---|---|---|---|---|---|---|---|
| > | S / $\epsilon_s$ | B / $r_b$ | S/$\sqrt{B}$ | S / $\epsilon_s$ | B / $r_b$ | S/$\sqrt{B}$ | S / $\epsilon_s$ | B / $r_b$ | S/$\sqrt{B}$ |
| | 2146.95 | 601.11 | 87.57 | 83.47 | 601.11 | 3.40 | 47.96 | 601.11 | 1.96 |
| 0.10 | 1.00 | 0.02 | 87.92 | 0.99 | 0.02 | 3.41 | 0.99 | 0.02 | 1.96 |
| 0.15 | 0.95 | 0.09 | 86.95 | 0.93 | 0.09 | 3.33 | 0.95 | 0.09 | 1.95 |
| 0.20 | 0.81 | 0.23 | 80.77 | 0.83 | 0.23 | 3.23 | 0.82 | 0.23 | 1.83 |
| 0.25 | 0.59 | 0.50 | 73.44 | 0.68 | 0.50 | 3.30 | 0.66 | 0.50 | 1.83 |
| 0.30 | 0.35 | 0.72 | 57.55 | 0.51 | 0.72 | 3.28 | 0.49 | 0.72 | 1.82 |

Table 6.6: Relative efficiency and rejection factors, and significances when running over the $\not{E}_{\mathrm{T}}$/Meff cut. All events have 2 isolated leptons of opposite sign, and 3 jets with $p_T^{JET1} \geq 100$, $p_T^{all} \geq 50$ and $\not{E}_{\mathrm{T}}$ >100GeV. First row, $\epsilon_S$ column states total number of signal events, first row $r_B$ column states total number of background events.

## 6.7 Conclusion

We have seen that the different mSUGRA benchmark points behave differently under the various cuts. Especially the Focus Region point SU2 and the Low Mass point SU4 are sensitive to the chosen cut values for both cuts on $\not{\mathrm{E}}_{\mathrm{T}}$ and on number of jets. SU3, SU6 and SU8 are more robust, and seem to respond fairly similarly to cuts, although optimal values vary for different signal points. In searches for SUSY several strategies will be used exactly for this reason.

Knowing our SM exactly, as assumed when calculating significance as $S/\sqrt{B}$, one could allow focus more towards keeping signal event, i.e. keeping the signal efficiency high, than towards suppressing SM background. A fairly loose set of cuts could then be chosen.

However, the uncertainty, particularly on the size of the QCD background is very large. We can account for this by using a more refined significance $S = S/\sqrt{(B + (f \cdot B)^2)}$, where $f$ is some number, here chosen to be 0.5. By using this significance instead of the naive $S/\sqrt{(B)}$, and for example choosing 3 jets and $\not{\mathrm{E}}_{\mathrm{T}}$ >100GeV, for the SU3 sample we go from a significance of 17.82 to a considerably lower 1.5, which we can calculate from the number of signal and background events in the first two rows of table 6.4. Taking into account the alternative and more realistic significance, would possibly lead to a different set of cut-choices, since instead of being careful not to remove the signal events, we should consider the importance on removing the background events. For the further analysis, we will, though, stay with our considerations already made [2], and instead compare significances as we proceed. The final cut choices are then:

| |
|---|
| 1. Two isolated opposite sign leptons 2. $p_T$ of hardest lepton >20 GeV |
| 3. Three jets with $p_T^1$>100Gev, $p_T^{2,3}$>50 GeV |
| 4. $\not{\mathrm{E}}_{\mathrm{T}}$ >150 GeV |

Table 6.7: Final choice of event cuts

The generator level cuts are also applied, i.e. $\not{\mathrm{E}}_{\mathrm{T}}$ >100 GeV, and two jets with $p_T^{jet1,jet2}$> 100, 50 GeV, but cut 3. and 4. in the table above are stronger, so these are not listed.

In addition we have studied the isolation of single leptons. We will use the standard isolation criteria etcone20< 10 GeV, but use a harder lepton $p_T$ cut which is 20 GeV for the hardest lepton, and keep the second requirement to $p_T$ >10 GeV. We will also use the alternative isolation, the normalized etcone20, which following the discussion in chapter 5.2 found to be optimal at 0.05 and compare the performance of the two lepton isolation cuts.

[2] due to time restrictions

# Chapter 7

# Final analysis using effective mass and invariant mass

So far our focus has been on selecting general SUSY events with a pair of opposite sign leptons. Although our base of choice was the decay $\widetilde{\chi}_2^0 \rightarrow \widetilde{\chi}_1^0 \, l^+ \, l^-$ expecting to give an excess of events with two leptons of opposite sign, we have not studied features of specific decay chains, or tried to extract observables such as particle masses. Selecting specific decay-chains is classified as an exclusive search, while the focus of the analysis so far has been inclusive. In this chapter we will apply our cuts and plot the effective mass distribution in order to calculate discovery potential, the significance $\mathcal{S}$. We will also make an exclusive application of our cuts, plotting the invariant mass of two leptons of opposite sign, $M_{ll}$ to possibly be able to make some preliminary guesses on the mass relations of the sparticles in the decay chain 7.1.

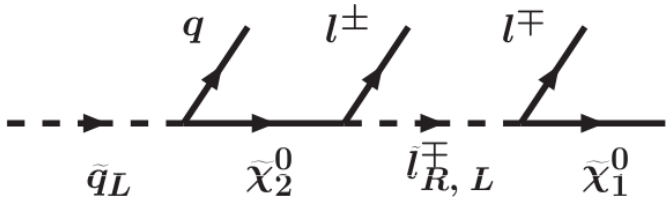


Figure 7.1: Signal decay chain for mass measurement of $\widetilde{\chi}_2^0$

We must be aware that there are large uncertainties in the SM background, in particular the QCD background which could be much larger than what has been considered here. We will therefore make a simple approximation of the background uncertainty when calculating significances, and compare with the significances without the background uncertainties. Four different significances will be used

$$S1 = \frac{\mathrm{S}}{\sqrt{\mathrm{B}}} \tag{7.1}$$

$$S2 = \frac{\mathrm{S}}{\sqrt{\mathrm{B} + (0.5 \cdot \mathrm{B})^2}} \tag{7.2}$$

$$S3 = \frac{\text{SF-OF}}{\sqrt{\text{SF + OF}}} \tag{7.3}$$

$$S4 = \frac{\text{SF-OF}}{\sqrt{2 \cdot \text{OF}}} \tag{7.4}$$

The first significance, $S1$ is used in the tables in the previous chapter, and give a simple approximation to discovery potential. The next, $S2$ takes into account background uncertainty. The two last are alternative ways of calculating significance using the flavour subtracted event as signal, and the whole event sample as background. SF-OF corresponds to the number of signal events, and SF+OF to the number of background events. $S3$ then corresponds to $\mathrm{S}/\sqrt{\mathrm{B}}$, and $S3$ to $\mathrm{S}/\sqrt{(\mathrm{S+B})}$, where the last is yet another significance measure.

Understanding our SM background is crucial in this exercise. Precise prediction on the background is the only way we can be able to measure any deviations since we obviously will not have access to truth information as we do for this analysis. If the SM background is well understood even small deviations can indicate new physics.

We will start by performing the inclusive analysis, applying the selected cuts and isolation to the effective mass distribution and calculate significances. We will extract an additional cut which is a cut on the effective mass, chosen from significance considerations. In the end we will apply this cut and all others previously discussed including the lepton isolation to the invariant mass of two opposite sign same flavour leptons $M_{ll}$. We will compare the two lepton isolation methods and finally make a conclusion of our study.

## 7.1 Effective Mass and significances

Figure 7.2 shows the effective mass for the Bulk Region point SU3 and the sum of all backgrounds applying consecutive cuts. In the first plot no other event preselections have been done other than the generator based cuts $\not{E}_{\mathrm{T}}$ >100 GeV, and two jets with $p_T^{1,2}$ >100 ,50 GeV, in particular, no leptons are required. We see that our SU3 signal is completely covered by the background, but still the SU3 signal does make a small difference on the distribution of the sum of the SM background and SU3. This we see by the red hashed histogram which shows the sum of SU3 and the SM background, rising above the black hashed histogram which is the SM background alone. Tables 7.4(a) and 7.5(a) give us the number of events for all our signal samples, and our SM background respectively. From this we can see that for SU3, 1374 events are left after applying only the generator based cuts. Corresponding number for the SM background 12281.This give us a significance $S1$ of 12.4, already very good for discovery presuming we exactly know our SM background. If the uncertainty on the SM background is taken into account by using the significance $S2$ defined as $S2 = S\sqrt{(B + (0.5 \cdot B)^2)}$, we arrive at 0.22, which implies that there will be absolutely no experimental evidence of supersymmetry. Now, when we start by applying our preselections and cuts, we see from figures 7.2(b)-7.2(d) that the deviation from the SM background has increased by a large amount. The lepton requirement already makes a large difference, in figure 7.2(b). This is using the standard etcone20 < 10 GeV, and with a $p_T^{1,2}$ >20,10 GeV for the two hardest opposite sign leptons. Requiring 3 jets with $p_T^1$ >100 GeV and $p_T^{2,3}$ > 50 GeV in figure 7.2(c), and finally $\not{E}_{\mathrm{T}}$ >150 GeV if figure 7.2(c) has left us with a clear signal.

Figure 7.3 shows the equivalent final plots for all the SUSY signal samples discussed in this analysis.

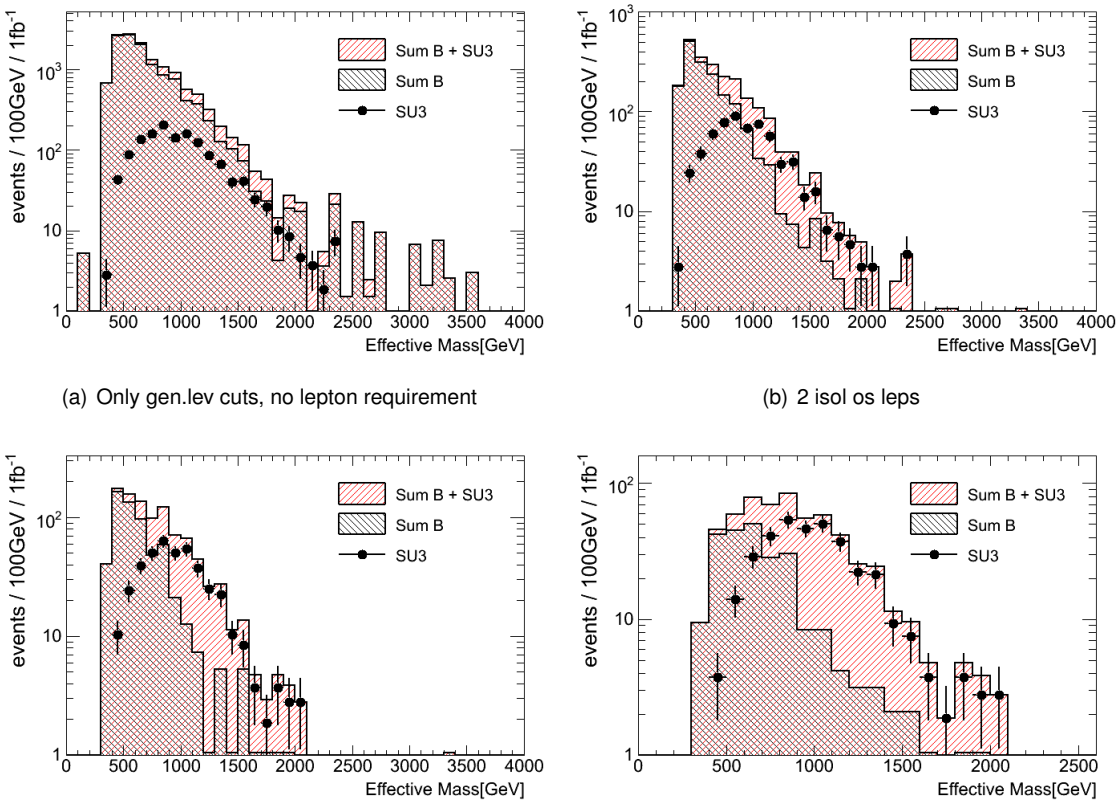


(a) Only gen.lev cuts, no lepton requirement

(b) 2 isol os leps

(c) 3 jets with $p_T$ req.

(d) $\not{E}_{\mathrm{T}}$ >150GeV

Figure 7.2: Effective mass after consequetive cuts. Etcone20<10GeV lepton isolation

Significances as function of cut in effective mass is shown in figure 7.4 for two types of background estimations (left, right plots) and the two different lepton isolation requirements (top, bottom plot).

First we must note that applying the normalized lepton isolation gives us in general lower significances than the standard etcone20 isolation for low values of the effective mass cut, as we see by comparing figures 7.4 a) and b) with figures 7.4 c) and d). This is also reflected in number of signal and background events in tables 7.4 and 7.5, where we see that our SUSY event selection is smaller when using normalized etcone lepton isolation. Even though the SM event selection also is lower, it is comparably not low enough to give a positive effect on the significance. For higher cut values though, the two isolation requirements are comparable. The use of normalized etcone20 needs optimization in order to be applied correctly, and given a fair chance to compete with the standard etcone20 isolation.

We also see that especially the two SUSY signal points SU3 and SU4 with best significance in figures 7.4 a) and c) suffer most when correcting for the uncertainty of the background in figures 7.4 b) and d). Considering cuts at Meff >1000GeV suggests that harder cuts are needed when we take into account the background uncertainty.

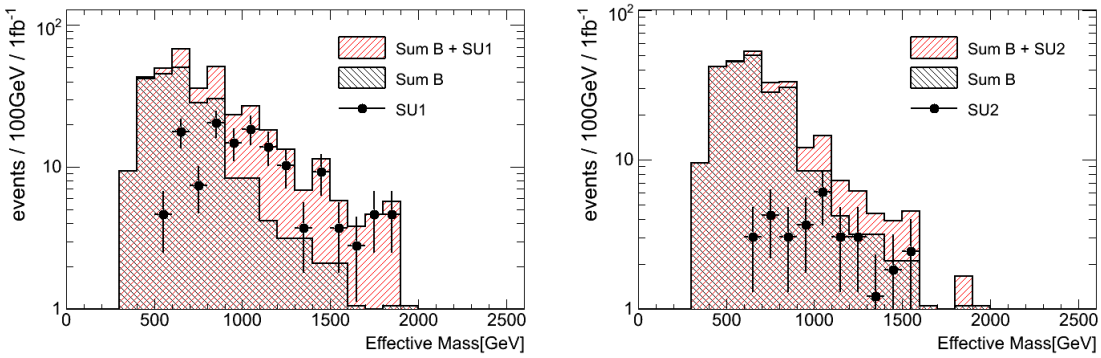


(a) SU1




(b) SU2

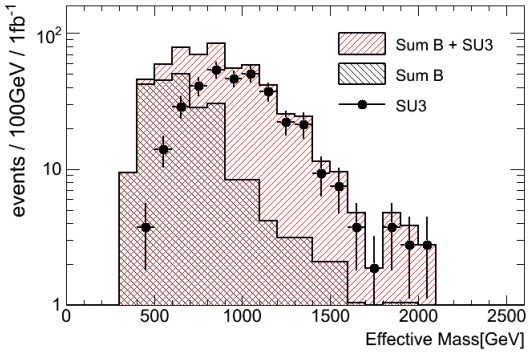


(c) SU3

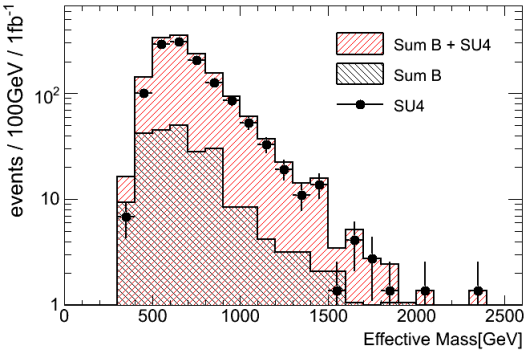


(d) SU4

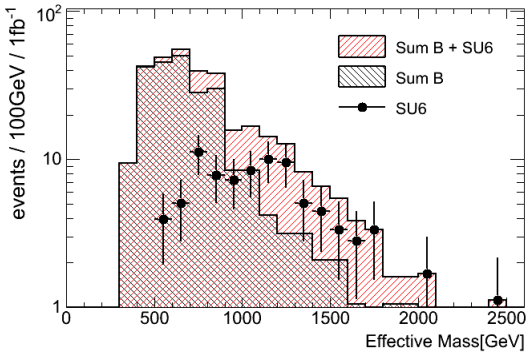


(e) SU6

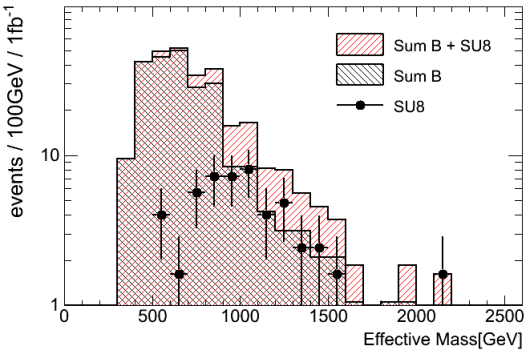


(f) SU8

Figure 7.3: Effective mass Meff for all SUSY signal points discussed and SM background after all cuts have been applied.

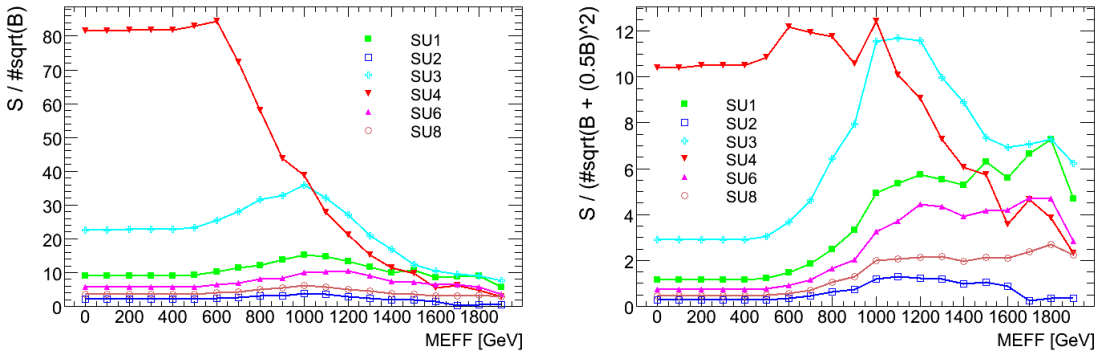


(a) Etcone20<10 GeV,Background uncertainty $\sqrt{B}$

(b) Etcone20<10 GeV, Background uncertainty $\sqrt{B+(0.5B)^2}$

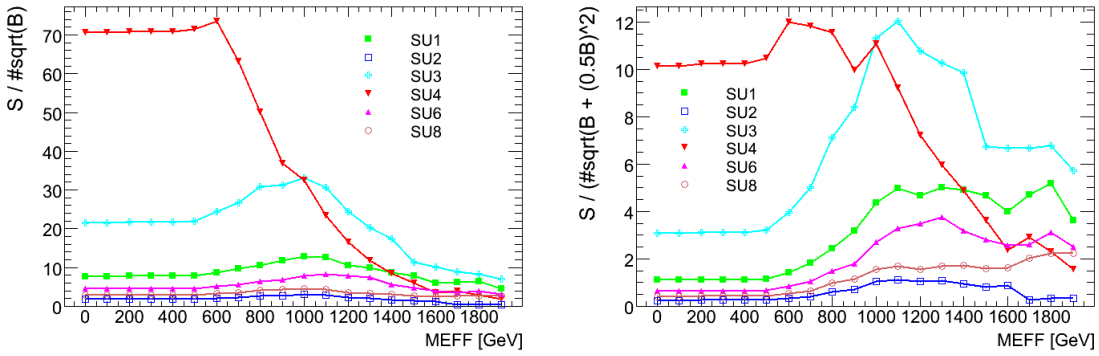


(c) Netcone20<0.05,Background uncertainty $\sqrt{B}$

(d) Netcone20<0.05, Background uncertainty $\sqrt{B+(0.5B)^2}$

Figure 7.4: Significances as function of cut in effective mass Meff. The first row show results using the etcone20 isolation algorithm, while the second row uses the normalized netcone20. All other cuts are identical: $\not{E}_{\mathrm{T}}$ > 150 GeV, 3 jets $p_T^1$>100 GeV, $p_T^{2,3}$> 50 GeV, lepton $p_T^{1,2}$> 20,10 GeV

A more elaborate list of significances and the total number of signal and background events when cutting on effective mass can be found in tables 7.1 - 7.3 for all SUSY signal points discussed. The first two columns report the cut value and number of background events, while the first column of each signal points reports number of signal events. The top tables lists results when using the standard lepton isolation etcone20, while the bottom tables are for the normalized etcone20 isolation. Again we can see the overall lower significance for all types of background estimations and significance types when using the normalized etcone isolation. For the flavour subtracted significances ($S3,\ S4$), cutting om effective mass just deteriorates our discovery potential, while it has a positive effect on the two others ($S1,\ S2$). As mentioned earlier there is a large uncertainty on the SM background. Using the significance $S1$ is therefore in the best case naive, and possibly completely misleading. We see by comparing $SU1$ and $SU2$ in tables 7.1 - 7.3, that for SU1 and SU6 we go from clear discovery to total loss of significance. All the other points also have a much worse discovery potential. $S3$ and $S4$ which use flavour subtraction for calculating the significance could be interesting alternatives to use, but needs to be studied further.

It must be noted that we have concentrated on an integrated luminosity of $1fb^{-1}$, and optimized our search using $S/\sqrt{B}$. As expected taking into account the uncertainties on the SM background by using significance $S2$ deteriorates the significance. In order to do the work correctly a new optimization is needed. This is already suggested by cutting high in Meff. Other cuts, if optimized on the new significances might give better results. This work will be continued beyond this master thesis.

Table 7.1: Significances as function of cut in Meff. Top table use lepton isolation etcone20 < 10 GeV, while bottom table uses the normalize netcone20 < 0.05. Significances are: $S1$ $S/\sqrt{B}$, $S2$ : $S/\sqrt{(B+(0.5B)^2)}$, $S3$ : $(SF-0F)/\sqrt{(SF+OF)}$ and $S4$ : $(SF-0F)/\sqrt{(2\cdot OF)}$. Second column of the table reports number of background events (B), while first column of each SUSY sample is number of Signal (S) events.

(a) ETcone20<10 GeV

| Cut | B | SU1 | | | | | SU2 | | | | |
|---|---|---|---|---|---|---|---|---|---|---|---|
| | | S | $S1$ | $S2$ | $S3$ | $S4$ | S | $S1$ | $S2$ | $S3$ | $S4$ |
| 500 | 230.01 | 141.17 | 9.31 | 1.22 | 4.27 | 4.81 | 32.81 | 2.16 | 0.28 | 2.63 | 2.86 |
| 600 | 188.11 | 140.24 | 10.23 | 1.48 | 4.09 | 4.62 | 32.81 | 2.39 | 0.35 | 2.38 | 2.59 |
| 700 | 143.05 | 135.60 | 11.34 | 1.87 | 4.03 | 4.59 | 32.20 | 2.69 | 0.44 | 2.37 | 2.60 |
| 800 | 93.05 | 117.95 | 12.23 | 2.48 | 4.39 | 5.19 | 29.16 | 3.02 | 0.61 | 2.66 | 3.02 |
| 900 | 64.76 | 110.52 | 13.73 | 3.31 | 4.57 | 5.57 | 24.91 | 3.10 | 0.75 | 2.48 | 2.85 |
| 1000 | 34.58 | 90.09 | 15.32 | 4.93 | 3.39 | 4.02 | 21.87 | 3.72 | 1.20 | 1.14 | 1.23 |
| 1100 | 26.20 | 75.23 | 14.70 | 5.35 | 4.24 | 5.48 | 18.23 | 3.56 | 1.30 | 1.99 | 2.35 |
| 1200 | 17.81 | 56.65 | 13.42 | 5.75 | 2.73 | 3.26 | 12.15 | 2.88 | 1.23 | 0.48 | 0.50 |

(b) NEtcone20 <0.05

| Cut | B | SU1 | | | | | SU2 | | | | |
|---|---|---|---|---|---|---|---|---|---|---|---|
| | | S | $S1$ | $S2$ | $S3$ | $S4$ | S | $S1$ | $S2$ | $S3$ | $S4$ |
| 500 | 182.92 | 106.81 | 7.90 | 1.16 | 3.56 | 3.98 | 24.30 | 1.80 | 0.26 | 2.22 | 2.41 |
| 600 | 146.26 | 105.88 | 8.75 | 1.43 | 3.30 | 3.69 | 24.30 | 2.01 | 0.33 | 1.90 | 2.04 |
| 700 | 110.64 | 102.16 | 9.71 | 1.81 | 3.12 | 3.50 | 23.69 | 2.25 | 0.42 | 1.71 | 1.84 |
| 800 | 71.11 | 89.16 | 10.57 | 2.44 | 3.61 | 4.22 | 22.48 | 2.67 | 0.62 | 2.12 | 2.38 |
| 900 | 51.20 | 84.52 | 11.81 | 3.18 | 3.78 | 4.54 | 18.83 | 2.63 | 0.71 | 2.20 | 2.54 |
| 1000 | 30.39 | 70.58 | 12.80 | 4.37 | 2.70 | 3.13 | 17.01 | 3.09 | 1.05 | 1.03 | 1.11 |
| 1100 | 22.01 | 59.44 | 12.67 | 4.97 | 3.76 | 4.85 | 13.37 | 2.85 | 1.12 | 2.01 | 2.45 |
| 1200 | 16.77 | 43.65 | 10.66 | 4.68 | 2.25 | 2.65 | 9.72 | 2.37 | 1.04 | 0.59 | 0.63 |

Table 7.2: Significances as function of cut in Meff. Top table use lepton isolation etcone20 < 10 GeV, while bottom table uses the normalize netcone20 < 0.05. Significances are: $S1$ $S/\sqrt{B}$, $S2 : S/\sqrt{(B + (0.5B)^2)}$, $S3 : (SF - 0F)/\sqrt{(SF + OF)}$ and $S4 : (SF - 0F)/\sqrt{(2 \cdot OF)}$ . Second column of the table reports number of background events (B), while first column of each SUSY sample is number of Signal (S) events.

(a) ETcone20<10 GeV

| Cut | B | SU3 | | | | | SU4 | | | | |
|---|---|---|---|---|---|---|---|---|---|---|---|
| | | S | $S1$ | $S2$ | $S3$ | $S4$ | S | $S1$ | $S2$ | $S3$ | $S4$ |
| 500 | 230.01 | 352.28 | 23.23 | 3.04 | 11.83 | 16.27 | 1258.70 | 82.99 | 10.85 | 14.24 | 17.70 |
| 600 | 188.11 | 348.56 | 25.41 | 3.67 | 11.90 | 16.73 | 1158.17 | 84.44 | 12.18 | 13.45 | 16.67 |
| 700 | 143.05 | 334.62 | 27.98 | 4.61 | 11.93 | 17.30 | 864.84 | 72.31 | 11.93 | 11.26 | 13.83 |
| 800 | 93.05 | 305.81 | 31.70 | 6.44 | 11.95 | 18.37 | 559.12 | 57.96 | 11.77 | 9.62 | 12.01 |
| 900 | 64.76 | 264.91 | 32.92 | 7.94 | 11.30 | 17.88 | 352.55 | 43.81 | 10.57 | 6.93 | 8.41 |
| 1000 | 34.58 | 211.00 | 35.88 | 11.55 | 10.20 | 16.86 | 227.23 | 38.64 | 12.44 | 5.11 | 6.11 |
| 1100 | 26.20 | 164.52 | 32.14 | 11.70 | 9.28 | 15.73 | 141.84 | 27.71 | 10.09 | 3.82 | 4.50 |
| 1200 | 17.81 | 114.33 | 27.09 | 11.60 | 6.54 | 9.75 | 89.51 | 21.21 | 9.08 | 1.70 | 1.85 |

(b) NEtcone20 <0.05

| Cut | B | SU3 | | | | | SU4 | | | | |
|---|---|---|---|---|---|---|---|---|---|---|---|
| | | S | $S1$ | $S2$ | $S3$ | $S4$ | S | $S1$ | $S2$ | $S3$ | $S4$ |
| 500 | 182.92 | 297.44 | 21.99 | 3.22 | 11.02 | 15.34 | 966.75 | 71.48 | 10.46 | 11.91 | 14.61 |
| 600 | 146.26 | 294.65 | 24.36 | 3.98 | 11.07 | 15.78 | 889.63 | 73.56 | 12.00 | 11.25 | 13.77 |
| 700 | 110.64 | 281.64 | 26.78 | 5.00 | 10.99 | 16.10 | 665.16 | 63.24 | 11.81 | 9.15 | 11.03 |
| 800 | 71.11 | 260.26 | 30.86 | 7.12 | 11.12 | 17.35 | 422.78 | 50.14 | 11.57 | 7.92 | 9.73 |
| 900 | 51.20 | 223.08 | 31.18 | 8.39 | 10.64 | 17.30 | 264.41 | 36.95 | 9.95 | 5.47 | 6.50 |
| 1000 | 30.39 | 183.11 | 33.22 | 11.33 | 9.41 | 15.44 | 179.03 | 32.48 | 11.08 | 3.57 | 4.08 |
| 1100 | 22.01 | 144.07 | 30.71 | 12.04 | 8.64 | 14.67 | 110.17 | 23.49 | 9.21 | 2.50 | 2.81 |
| 1200 | 16.77 | 100.39 | 24.52 | 10.76 | 6.15 | 9.17 | 67.48 | 16.48 | 7.23 | 0.74 | 0.77 |

Table 7.3: Significances as function of cut in Meff. Top table use lepton isolation etcone20 < 10 GeV, while bottom table uses the normalize netcone20 < 0.05. Significances are: $S1$ $S/\sqrt{B}$, $S2$ : $S/\sqrt{(B+(0.5B)^2)}$, $S3$ : $(SF-0F)/\sqrt{(SF+OF)}$ and $S4$ : $(SF-0F)/\sqrt{(2\cdot OF)}$. Second column of the table reports number of background events (B), while first column of each SUSY sample is number of Signal (S) events.

(a) ETcone20<10 GeV

| Cut | B | SU6 | | | | | SU8 | | | | |
|---|---|---|---|---|---|---|---|---|---|---|---|
| | | S | $S1$ | $S2$ | $S3$ | $S4$ | S | $S1$ | $S2$ | $S3$ | $S4$ |
| 500 | 230.01 | 87.92 | 5.80 | 0.76 | 3.97 | 4.48 | 54.74 | 3.61 | 0.47 | 3.17 | 3.51 |
| 600 | 188.11 | 87.36 | 6.37 | 0.92 | 3.86 | 4.38 | 54.74 | 3.99 | 0.58 | 2.97 | 3.29 |
| 700 | 143.05 | 83.44 | 6.98 | 1.15 | 3.96 | 4.57 | 50.71 | 4.24 | 0.70 | 2.98 | 3.34 |
| 800 | 93.05 | 78.40 | 8.13 | 1.65 | 4.27 | 5.13 | 49.10 | 5.09 | 1.03 | 3.31 | 3.86 |
| 900 | 64.76 | 67.20 | 8.35 | 2.01 | 3.89 | 4.71 | 43.47 | 5.40 | 1.30 | 3.38 | 4.07 |
| 1000 | 34.58 | 59.36 | 10.09 | 3.25 | 2.94 | 3.48 | 36.22 | 6.16 | 1.98 | 2.35 | 2.76 |
| 1100 | 26.20 | 52.08 | 10.18 | 3.70 | 3.27 | 4.06 | 28.98 | 5.66 | 2.06 | 2.52 | 3.08 |
| 1200 | 17.81 | 43.68 | 10.35 | 4.43 | 1.71 | 1.91 | 20.93 | 4.96 | 2.12 | 0.42 | 0.44 |

(b) NEtcone20 <0.05

| Cut | B | SU6 | | | | | SU8 | | | | |
|---|---|---|---|---|---|---|---|---|---|---|---|
| | | S | $S1$ | $S2$ | $S3$ | $S4$ | S | $S1$ | $S2$ | $S3$ | $S4$ |
| 500 | 182.92 | 62.16 | 4.60 | 0.67 | 3.15 | 3.50 | 40.25 | 2.98 | 0.44 | 2.65 | 2.91 |
| 600 | 146.26 | 62.16 | 5.14 | 0.84 | 2.91 | 3.23 | 40.25 | 3.33 | 0.54 | 2.36 | 2.59 |
| 700 | 110.64 | 58.80 | 5.59 | 1.04 | 2.85 | 3.21 | 37.03 | 3.52 | 0.66 | 2.24 | 2.47 |
| 800 | 71.11 | 54.88 | 6.51 | 1.50 | 3.27 | 3.85 | 35.42 | 4.20 | 0.97 | 2.65 | 3.06 |
| 900 | 51.20 | 48.16 | 6.73 | 1.81 | 3.27 | 3.95 | 30.59 | 4.28 | 1.15 | 3.02 | 3.67 |
| 1000 | 30.39 | 43.68 | 7.92 | 2.70 | 2.36 | 2.75 | 24.95 | 4.53 | 1.54 | 1.92 | 2.23 |
| 1100 | 22.01 | 39.20 | 8.36 | 3.28 | 2.80 | 3.45 | 20.12 | 4.29 | 1.68 | 2.42 | 3.05 |
| 1200 | 16.77 | 32.48 | 7.93 | 3.48 | 1.30 | 1.44 | 14.49 | 3.54 | 1.55 | 0.52 | 0.54 |

The last cut before plotting invariant mass distributions is on Meff. We will use the same cuts on all data samples considered, and will therefore have to make a compromise in order not to affect SUSY points with low cross section too hard, like for example SU2. We therefore set our cut to to 800GeV and proceed with plotting the invariant mass of opposite sign same flavour di-leptons.

Table 7.4: Number of signal events after consequetive cuts. Lepton isolation etcone20<10GeV, $p_T^{lep1,lep2}$> 20,10 GeV. Generator level cuts (Gen Cuts) $\not{E}_{\mathrm{T}}$ >100 GeV, 2 jets $p_T^{1,2}$ >100,50 GeV.

(a) etcone20 < 10 GeV

| Cuts | SU1 | SU2 | SU3 | SU4 | SU6 | SU8 |
|---|---|---|---|---|---|---|
| Crossections | 7430 | 4860 | 18590 | 262000 | 4480 | 6440 |
| Gen Cuts | 631 | 143 | 1374 | 11801 | 435 | 338 |
| >= 2 leptons | 630 | 143 | 1373 | 11799 | 434 | 337 |
| 2 leptons >20,10 GeV | 568 | 132 | 1221 | 9796 | 380 | 287 |
| OS Dileptons | 414 | 91 | 979 | 7005 | 246 | 181 |
| OS leptons, isolated | 219 | 42 | 611 | 3399 | 119 | 76 |
| >= 3 jets | 202 | 41 | 534 | 3112 | 111 | 72 |
| Jet pt | 160 | 39 | 411 | 2143 | 93 | 59 |
| EtMiss>150 GeV | 141 | 33 | 352 | 1266 | 88 | 55 |
| EffMass>800 GeV | 111 | 25 | 265 | 353 | 67 | 43 |

(b) Normalized etcone20 < 0.05

| Cuts | SU1 | SU2 | SU3 | SU4 | SU6 | SU8 |
|---|---|---|---|---|---|---|
| Crossection | 7430 | 4860 | 18590 | 262000 | 4480 | 6440 |
| Gen Cuts | 631 | 143 | 1374 | 11801 | 435 | 338 |
| >= 2 leptons | 630 | 143 | 1373 | 11799 | 434 | 337 |
| 2 leptons >20,10 GeV | 568 | 132 | 1221 | 9796 | 380 | 287 |
| OS Dileptons | 414 | 91 | 979 | 7005 | 246 | 181 |
| OS leptons, isolated | 170 | 30 | 521 | 2634 | 87 | 56 |
| >= 3 jets | 156 | 29 | 454 | 2413 | 81 | 54 |
| Jet pt | 123 | 29 | 345 | 1647 | 67 | 42 |
| EtMiss> 150 GeV | 107 | 24 | 297 | 972 | 62 | 40 |
| EffMass >800 GeV | 85 | 19 | 223 | 264 | 48 | 31 |

Table 7.5: Number of SM background events grouped into categories. Cuts are made consequetive cuts. Lepton isolation etcone20<10GeV, $p_T^{lep1,lep2}$> 20,10 GeV. Generator level cuts (Gen Cuts) $\not{E}_{\mathrm{T}}$ >100 GeV, 2 jets $p_T^{1,2}$ >100,50 GeV.

(a) Etcone20 < 10 GeV

| Cuts | TTbar | W | Z | QCD | VV | Sum B |
|---|---|---|---|---|---|---|
| Crossection | 820505 | 141398 | 97132 | 1608872 | 34400 | 2702307 |
| Gen Cuts | 6093 | 330 | 115 | 5725 | 17 | 12281 |
| >= 2 leptons | 6087 | 327 | 111 | 5700 | 16 | 12241 |
| 2 leptons >20,10 GeV | 5168 | 260 | 97 | 4625 | 15 | 10164 |
| OS Dileptons | 3839 | 165 | 89 | 3569 | 12 | 7674 |
| OS leptons, isolated | 1624 | 8 | 66 | 0 | 6 | 1704 |
| >= 3 jets | 1246 | 4 | 18 | 0 | 2 | 1270 |
| Jet pt | 590 | 2 | 9 | 0 | 0 | 601 |
| EtMiss>150 GeV | 235 | 2 | 5 | 0 | 0 | 241 |
| EffMass >800 GeV | 63 | 1 | 1 | 0 | 0 | 65 |

(b) Normalized etcone20 < 0.05

| Cuts | TTbar | W | Z | QCD | VV | Sum B |
|---|---|---|---|---|---|---|
| Crossection | 820505 | 141398 | 97132 | 1608872 | 34400 | 2702307 |
| Gen Cuts | 6093 | 330 | 115 | 5725 | 17 | 12281 |
| >= 2 leptons | 6087 | 327 | 111 | 5700 | 16 | 12241 |
| 2 leptons >20,10 GeV | 5168 | 260 | 97 | 4625 | 15 | 10164 |
| OS Dileptons | 3839 | 165 | 89 | 3569 | 12 | 7674 |
| OS leptons, isolated | 1281 | 2 | 62 | 0 | 5 | 1350 |
| >= 3 jets | 975 | 1 | 16 | 0 | 1 | 993 |
| Jet pt | 458 | 1 | 8 | 0 | 0 | 467 |
| EtMiss> 150 GeV | 184 | 1 | 5 | 0 | 0 | 190 |
| EffMass >800 GeV | 50 | 0 | 1 | 0 | 0 | 51 |

## 7.2 Invariant mass of the two opposite sign, same flavour leptons

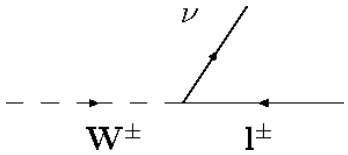


Figure 7.5: Leptonic W-boson decay

Plotting the invariant mass $M_{ll}$ of two opposite sign same flavour leptons will, due to the missing energy from $\widetilde{\chi}_1^0$ give us a continuous distribution with a theoretical end-point as an upper limit from kinematic constraints. An analogous method has been well tested in extraction of the W mass. The neutrino $\nu$ is in this case responsible for the difficulty in mass measurement through W decay. The end point method is also used to measure or set limits on the mass of the electron neutrino through weak nuclear $\beta$-decay.

In the simplest case, when the intermediate slepton in figure 7.1 is off-shell, the invariant mass will have a maximum

$$m(l\bar{l}) \leq m_{\widetilde{\chi}_2^0} - m_{\widetilde{\chi}_1^0} \tag{7.5}$$

However, if the slepton is real we must instead use the relation

$$m(ll)_{max} = m_{\widetilde{\chi}_2^0}\sqrt{(1-\frac{m_{\widetilde{l}}^2}{m_{\widetilde{\chi}_2^0}^2})(1-\frac{m_{\widetilde{\chi}_1^0}}{m_{\widetilde{l}}^2})} \tag{7.6}$$

derived through simple energy and momentum conservation laws. Deriving the mass of $\widetilde{\chi}_2^0$ needs additional end-point measurements, in order to relate to all the unknown masses in the formula. Inverting these formulas then gives us the masses of the sparticles in the chosen decay-chain. A full set of invariant mass formulas can be found in Appendix B as a reference [1].

Since events with two leptons of opposite sign and same flavour are a subset of all events with two opposite sign leptons and any flavour, performing mass measurements is usually dependent on larger integrated luminosity than discovery. By using statistical fit methods one parametrises the invariant mass distribution and extracts the end point. If the integrated luminosity is too low, the fit can be difficult and the precision of the end-point measurement will be low. We will show the invariant mass distribution both for signal points with a large cross section using the Bulk region point SU3 and the Low Mass point SU4, and for the Focus point region SU2 which has a very low cross section. For SU2 the intermediate slepton is off shell, and the relation 7.5 can be used. For SU1 one should in principle see two end points, since both the $\widetilde{l}_R$ and $\widetilde{l}_L$ are kinematically allowed. Due to time-constraints the fit of the invariant mass distributions will not be done, and therefore no calculation of masses. Still, just plotting the distributions will give us a feeling on how accurately the end points are reproduced compared to theory, and therefore how well they may be measured.

Figure 7.6 shows the invariant mass distribution for the SUSY signal sample SU3 after applying consecutive cuts. We see that the SM background vanishes as we apply cuts, even before we have flavour subtracted our events. At an integrated luminosity of $1fb^{-1}$ we are not left with a large amount of signal events, but we can still see a clear fall-off of the distribution at100 GeV. The theoretical end-point measurement is at around 100 GeV.

If we were able to match only truly leptons coming from the decay chain in figure 7.1 the end-point would be absolute, with no smearing at higher values which we can see in all plots in figure

[1] Thanks to Dr. Borge K. Gjelsten

7.6. The distribution would also become more triangular without the shoulder we can see at low values. The end-point measurements are therefore particularly sensitive to our lepton isolation, since we would suppress extra leptons contaminating the distribution.

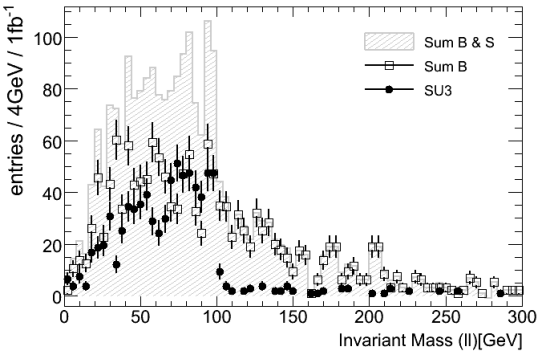


(a) 2 isolated os leptons

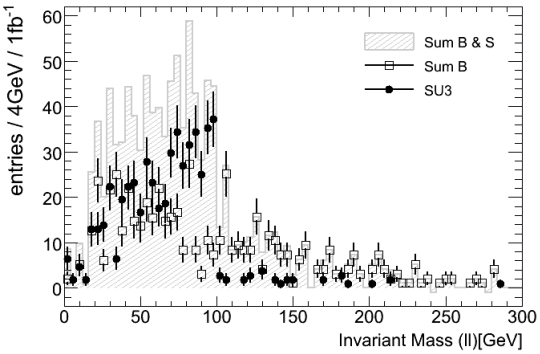


(b) 3 jets with $p_T$ req.

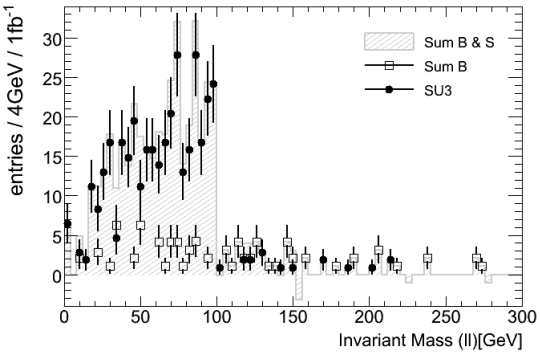


(c) $\not{E}_{\mathrm{T}}$ >150GeV

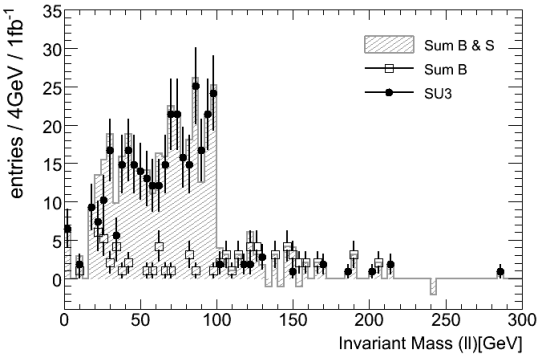


(d) Meff >800GeV

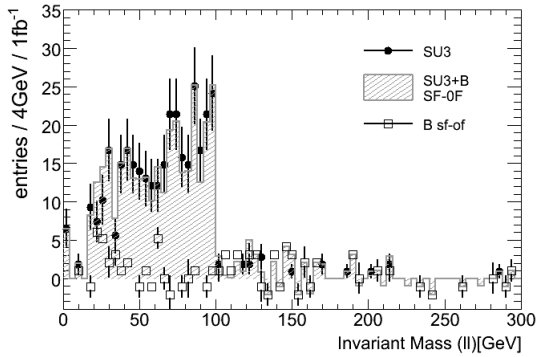


(e) Flavour subtracted

Figure 7.6: Invariant mass of two opposite sign same flavour leptons after consecutive cuts for the SUSY signal sample SU3, and the SM background. Lepton isolation etcone20<10GeV

Figures 7.7 show the invariant mass distribution for 4 of our signal samples both when using the standard etcone20 lepton isolation, and for the normalized etcone20.

In SU1, since $m(\widetilde{\chi}_2^0)$>$m(\widetilde{l}_R), m(\widetilde{l}_L)$ we would expect two end points, one around 55 GeV and the other around 100 GeV, which we can calculate through the theoretical formula 7.6. Even though the luminosity is too low to see a smooth distribution there is a clear SF-OF excess. A higher luminosity would be needed to make a proper fit.

Figure 7.7(c) b) shows that any end-point measurement for SU2 is impossible at $1 fb^{-1}$. As well as all the signal is lost, and fluctuations are large. The theoretical end-point can be calculated using relation 7.5 since the $\widetilde{\chi}_2^0$ must decay through a virtual slepton. End-points would then be $m(\widetilde{\chi}_3^0) - m(\widetilde{\chi}_1^0)$ and $m(\widetilde{\chi}_2^0) - m(\widetilde{\chi}_1^0)$ which gives us 76 GeV and 57 GeV respectively. Again, higher luminosity would be needed, and possibly more optimal cuts than used in this analysis, in order not to suppress the signal.

In SU4 the decay of $\widetilde{\chi}_2^0$ must, as for SU2 go through a virtual slepton in a 3-body decay $\widetilde{\chi}_2^0 \rightarrow l^{\pm}\, l^{\mp} \widetilde{\chi}_1^0$. The end point would then simply be the difference $m(\widetilde{\chi}_2^0) - m(\widetilde{\chi}_1^0)$ which is about 53 GeV. Already from figure 7.7(g) we have a clear SF-OF excess and could attempt a fit.

It must be noted that we cannot see any effect on the shape of the invariant mass distribution after flavour subtraction. This is due to the low statistics, and an imporved shape closer to the theoretical predition would be obtained with larger statistics.

The effect of the alternative isolation does not make any significant change on our invariant mass distribution, see figure 7.7. As the distributions stay fairly the same, it is not clear that our proposed better isolation requirement actually improves the invariant mass distribution. Naturally, we would have to make proper fits to make any conclusion at all, but at least by eye there is no real improvement. Neither is there a significant worsening of the distributions. Since we did see in chapter 5 that the normalized etcone isolation does perform better in selecting primary leptons, it could still be a method to consider when precise measurements are needed. This would then have to be with larger integrated luminosities.

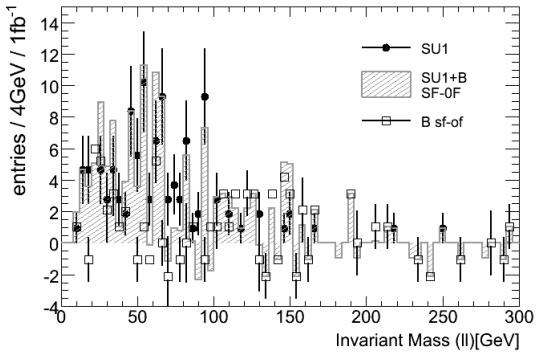


(a) SU1, etcone20<10 GeV

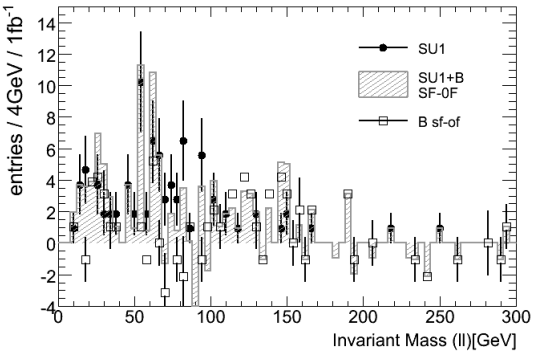


(b) SU1, netcone20<0.05

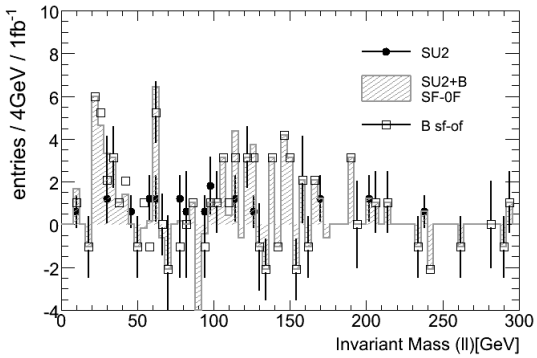


(c) SU2, etcone20<10 GeV

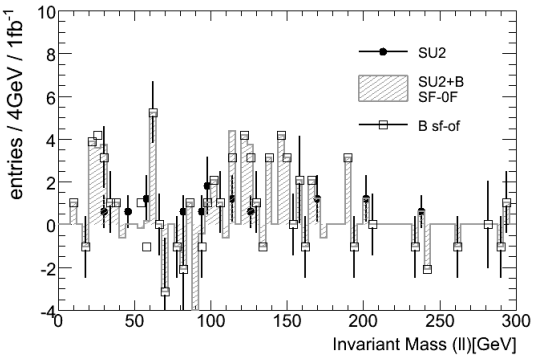


(d) SU2, netcone20<0.05

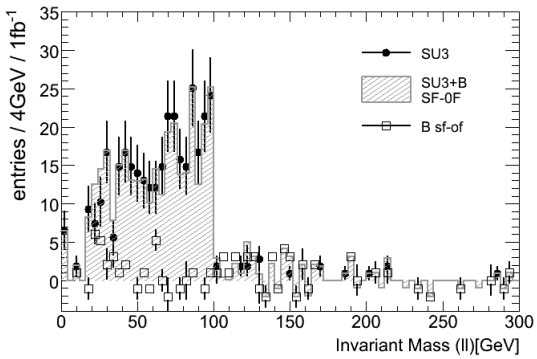


(e) SU3, etcone20<10 GeV

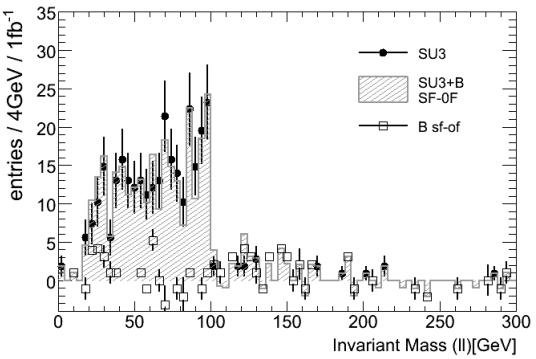


(f) SU3, netcone20<0.05

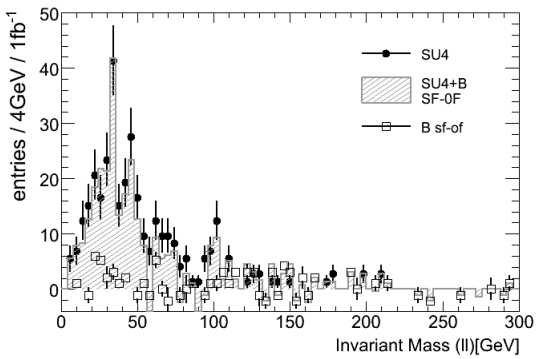


(g) SU4

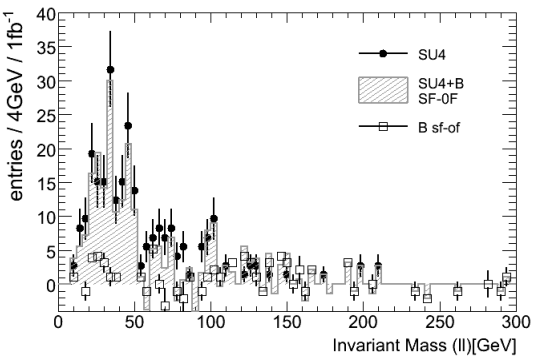


(h) SU4, netcone20<0.05

Figure 7.7: Invariant mass of two leptons of opposite sign and opposite flavour after all cuts and flavour subtraction. Plots to the left have applied the standard etcone20 < 10 GeV isolation requirement, while the plots to the right have used the normalized lepton isolation etcone20 <0.05

## 7.3 Conclusions

We have studied lepton isolation and event selection cuts for the opposite sign dilepton SUSY channel. In chapter 5 we found an alternative way of isolating leptons which seemed to be more effective in suppressing extra leptons. We saw, however that our significances got worse when applying this alternative lepton isolation for low values of Meff cut. This suggests harder cuts needed and new optimization on the cuts. Even though our sample was cleaner, meaning containing relatively more primary leptons than extra leptons compared to the standard etcone isolation, we could not really appreciate any positive effect, neither when considering significances, nor any obvious effect on the lepton invariant mass edge. This conclusion is however premature, since more detailed study, and in particular extraction and calculation of masses is needed to see if the end-point precision is improved with the alternative lepton isolation. Unfortunately this is beyond the scope of this analysis, but should be considered before making a final conclusion.

Should Supersymmetry prove to exist, and manifest itself in one of the benchmark points considered here, it could be possible to discover. Especially the Bulk Region point SU3, the Low Mass point SU4, SU1 and with more luminosity SU6, look promising. The Focus Region point SU2 and SU8, however are considerably more challenging to discover, and for a possible discovery one would need higher luminosities and a more optimized search.

# Appendix A

# CERN Summer School 2007 - CMS experience

As a summer student at CERN, summer 2007, experience with another of the main detectors at LHC was aquired. During the Global Runs of CMS, the detector, the trigger and the data-acquisition system were tested in a single coherent experiment. Cosmic muons traversing the detector were detected, triggered on and reconstructed, and analysis of the data from these runs were part of the commissioning. The summer-student project consisted of analyzing data from the Level 1 (L1) Trigger system and correlations between its various subsystems taken during 3 Global Runs over summer.

### A.0.1 Analysis Tools

The analysis was done using the CMS Software (CMSSW) and ROOT. The analysis code was written in C++. Raw data from the runs were unpacked, NTuples constructed and finally analyzed with a custom-made analysis.

### A.0.2 Level 1 Trigger System of CMS

The L1 Trigger system is hardware based and consists of 3 subsystem (figure A.1): the L1 muon trigger, the L1 calorimeter trigger and the L1 global trigger (GT). The Muon System is again divided into 4 subsystems: The Drift Tube Triggers: Drift Tube Track Finders (DTTF), the Cathode Strip Chamber (CSC) trigger, the Resistive Plate Chamber (RPC) trigger and finally the Global Muon Trigger (GMT) to combine and sort muons. The Calorimeter Trigger is divided into the Forward Hadronic Calorimeter (HF) trigger systems, the Electromagnetic Calorimeter (ECAL) trigger, the Hadronic Calorimeter (HCAL) trigger and the Global Calorimeter Trigger (GCT). For this study the relevant triggers have been the Muon Trigger and the Global Trigger.

#### GT and trigger decision

The GT makes the trigger decision. It bases its decision on muons passed on from the calorimeter-trigger and the muon-trigger. Via the Timing and Trigger Control System (TTC) it sends the Level 1 accept (L1A) back to the detector electronics and the trigger-subsystems. The event-data from the detector and the trigger-readout are waiting in pipelines and read out if the TTC transmits a

L1A. For the relevant trigger subsystems, 3 sets of data are then read out: the event data itself together with the data from the preceding and following bunch.

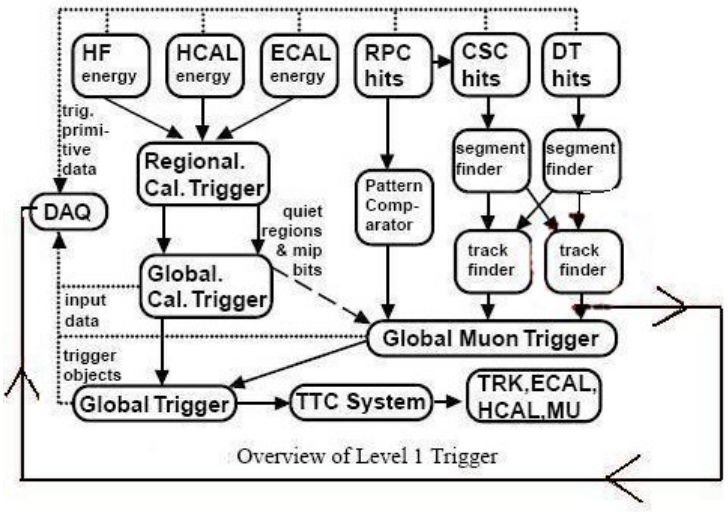


Figure A.1: The Level 1 Trigger of CMS. 3 Subsystems: Muon Trigger, Calorimeter Trigger and Global Trigger.

## A.0.3 Global Runs

### Setup of Detector and Trigger Components

Each Global Run (GR) was performed with one sector of the Drift Tube (DT) system active at a time. For all three, June, July and August GRs the DT readout (DTDDU) was included, but neither the CSCs nor the RPCs. In the June GR only the Muon Trigger system was included, the Calorimeter components were not in place. For July and August GRs, the Global Calorimeter Trigger (GCT) was included in the readout only.

Simple trigger requirements were used: Any muon passed on from the DT, which required muon segments in 2 or more stations of the DT, would trigger. Trigger rules in the GT should only have inhibited a trigger if 2 consecutive event-candidates were too close in time. The exact time-limits can be found in the CMS L1 Trigger Technical Design Report, but go as:

- No more than 1 Level 1 Accept per 75 ns - minimum 2 bunch crossings (bx) separation
- No more than 2 Level 1 Accepts per 625 ns - 25 bx separation
- and so on

Strictly speaking, the GR do not operate with bunch crossings since it uses cosmic muons and not a beam. However, the global LHC clock runs according to bunch-crossings and orbits, and the detector follows this clock also in the Global Runs.

### June GR

The available data for analysis were limited due to problems in the synchronization of the readout of parts of the system. The Drift Tube Track Finder (DTTF) was included in the trigger and timed in. For some runs the GT was included, but unfortunately not timed in properly. This resulted in the Timing and Trigger Control System (TCCS) pointing to empty bunches and no data was

recorded from the GT. Some runs had the full event-data from the Drift Tube readouts (DTDDU) available.

We studied 4 runs: Run 12411, 12153, 12436 and 12443. Of these only 12411 had DTDDU information. Runs 12411 and 12153 did not include the GT and used a Local Trigger Controller (LTC) as "dummy" readout giving us timing-information. The other two runs had GT readout but had no data due to the synchronization problems.

The data available allowed us to focus our study on bunch assignment. The TTC should mark the triggered event as bunch 0, the bunch before as bunch -1 and the bunch after as bunch 1. We studied if this was actually done, we found discrepancies and we investigated if this was due to detector noise that was registered.

### Results

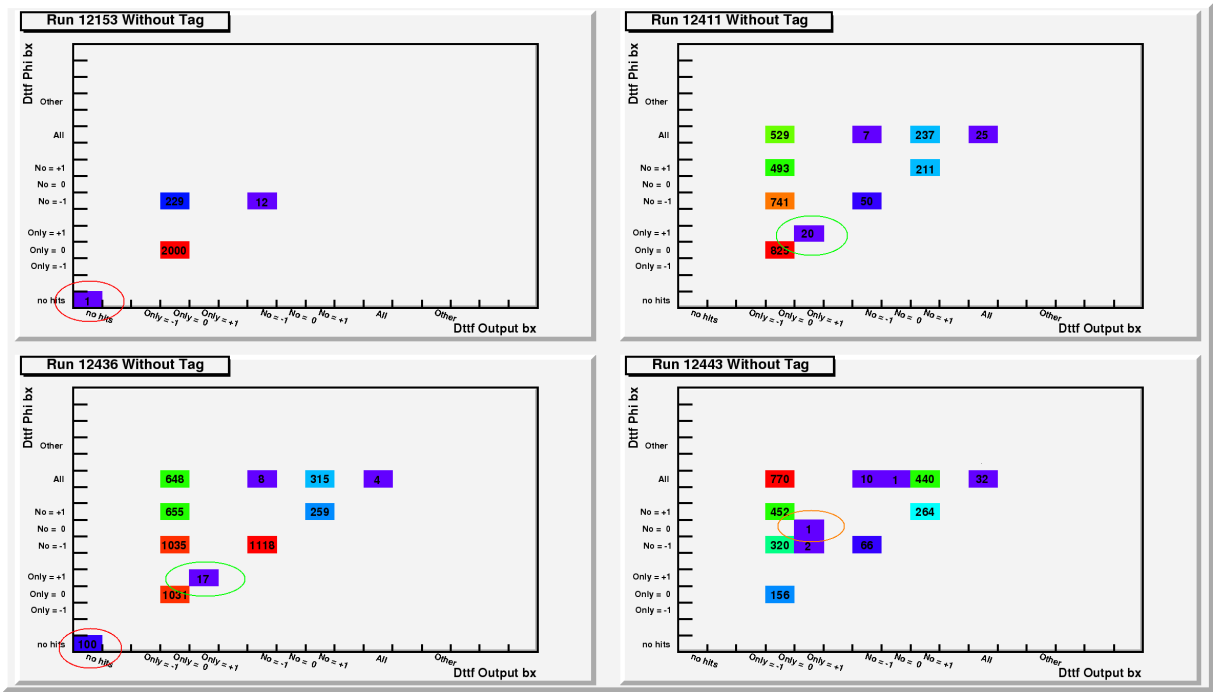


Figure A.2: Figures show the 4 studied runs. Y-axis has the DTTF input in phi direction, while the x-axis shows the DTTF output. Each event is coded according to which of the 3 recorded bunches had muons. Red circle: Events without data. Green Circle: Events without data in bunch 0. Orange circle: Events with data in bunch -1 and 1, but not bunch 0. Also notice events where there was data in both bunch -1 and bunch 0.

From figure A.2 we notice the following:

1. There were events with no data.
2. There were events where bunch 1 had muons, but not bunch 0.
3. There were events where bunch -1 and 0 had muons.
4. There was one event where bunch -1 and 1 had muons, and not bunch 0.

### POINT 1: No data events

Plotting bunch encoding over event number (time) showed that these cases occurred either in the very beginning or the very end of these two runs. The 100 such events in run 12436 came all together in one sequence indicating a sudden change in the configuration, possibly due to a switch

to random trigger in the GT. This has not been verified, and is only one possible explanation. No further studies were possible for these cases due to lack of data from other systems.

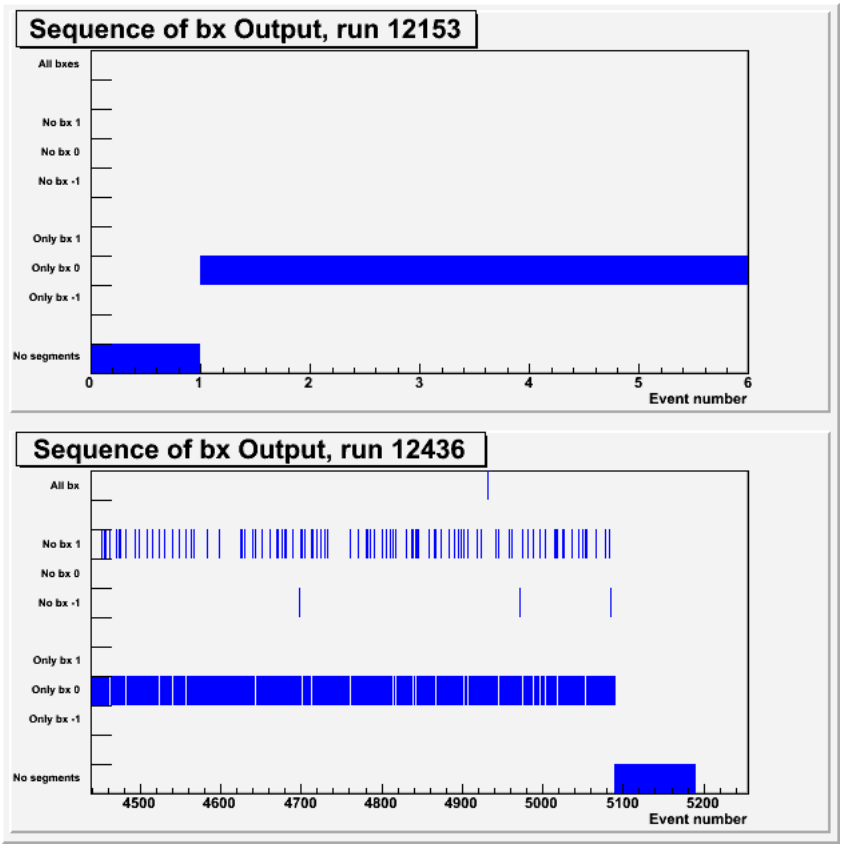


Figure A.3: The events where there was no data occurred for one of the runs as the very first event, and for the other run as the very last events.

**POINT 2: Events where only bunch 1 contains muons.**

The same type of plot as above revealed a sudden change of the bunch-assignment close to the start of the runs. All the events where only bunch 1 was filled came in one sequence and in the beginning of the runs. These events had obviously triggered since they were recorded, and indeed, further study showed that more than 2 stations had segments, this being the only requirement for a muon being passed on to the GT and triggering. It turned out that there had been manual interventions with the DT readout boards, switching from sector 4 to sector 0. This gave us uncorrelated data in the start-up of the runs before the switch was made. When studying the time of shift between sectors we saw that the event numbers coincided with the switch of bunch-numbers.

**POINT 3: Events with muons in both bunch -1 and bunch 0.**

These events were of special interest since they could have revealed faults in the trigger. Studies showed that the muons in bunch -1 did fulfill the trigger requirements, and should have triggered (thus being placed in bunch 0 ) unless trigger rules inhibited this. This was looked into for the July and August runs in detail.

**POINT 4: 1 single event where only bunch -1 and 1 are filled.**

This event was not studied closely. It occurred in the middle of the run so it could not be explained by the switch of sector readout boards.

The analysis done on the June data regarding the correlation between bunch assignment and noise-events did not give any conclusive results.

#### July GR

In the July GR the DTTF, GT, HCAL and ECAL were included in the readout. Only the GT was properly timed in, and therefore there was no available data from the DTTF input. However, the GMT data contains the DTTF Output (being the GMT input) and this was used for correlation studies. Real time (orbit + bunch information) was not recorded in July Runs, but we could extract the bunch identification within one orbit.

#### Results

GMT Output did not show incidents of points 1, 2 and 4 observed in the June GR. We did however see events where both bunch -1 and bunch 0 had muons, and also where all bunches had muons (Point 3 in list above). The events were checked for relation to noise which could explain that trigger-rules had inhibited the trigger of the bunch -1 muons, but allowing the following bunch to trigger. Obvious noise in our case were events with very many DT hits, resulting from external noise in the cavern such as welding.

From figure A.4 we can see a correlation between noise-events and events with bunch -1 filled. 2107 out of 2551 events with muons in bunch -1 had muons in all three bunches, and out of these, about 1700 events were noise-events. One of the interesting and unexplained points of these plots is the smaller distribution with hits below 100, so-called “normal” events of the bottom plots. If these events were not related to noise they could point to an unstable trigger latency.

When studying the time between triggers measured the in $\Delta$bx, i.e. number of bunches between two triggers, for the various categories of events and with special emphasis on the bunch -1 events, we see from figure A.5 that there is a correlation between noise-events and the bunch -1 events, however, it is not fully conclusive. There were still plenty of events with larger $\Delta$bx, that both had a low number of hits in the DT and came with large spacing between the triggers.

#### August GR

For the August GR, the DTTF, GT and DTDDU readouts were included and timed-in in one and the same run. Having all this data could have allowed extensive study of the Point 3) cases for the August runs. Because of limited time available for the analysis we were only able to confirm what we already had seen for July, that for events with muons in bunch -1 and 0 there were cases where the time between triggers was large, see figure A.6. This indicated that the trigger rules could not fully explain the fact that there were muons reported in bunch -1 that did not trigger. Further studies were regrettably not possible due to the time restrictions.

### A.0.4 Conclusion

June Global Run showed irregularities in bunch assignment. A closer study of the reasons for these irregularities showed that some of these could be explained by problems in the start-up of the runs and did not reflect the performance of the trigger. The unanswered question after the June study was related to Point 3) in the discussion above (events with muons in bunch -1 and 0). This study continued for July and August. July data showed correlation with noise for events with muons bunch -1 and 1 when we separated the noise-events from the “normal” events. For

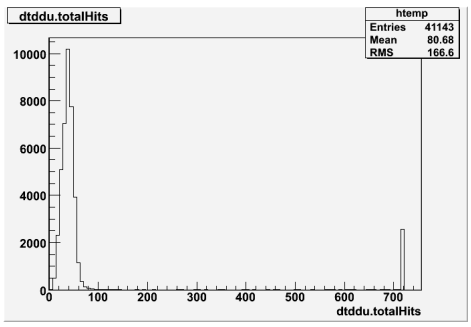


(a) DT Total Hits

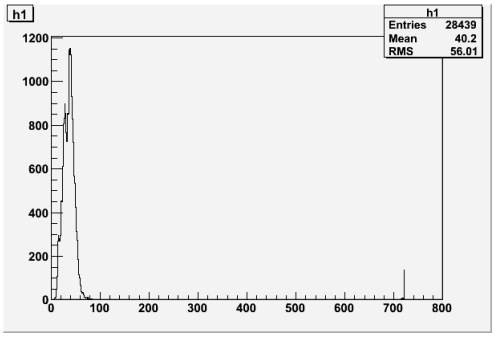


(b) DT Hits only in bunch 0

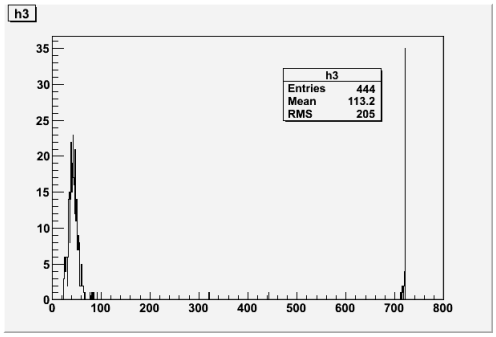


(c) DT Hits Events with muons in bunches -1 and 0

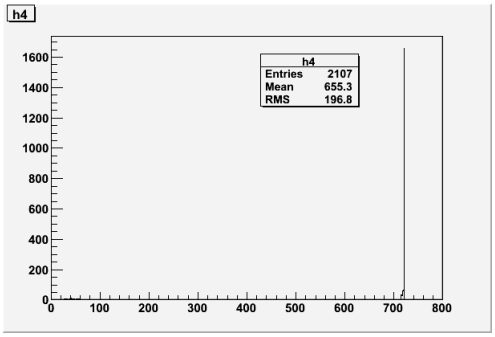


(d) DT Hits Bunches -1 and 0 and 1 all with muons

Figure A.4: Plots a-d show number of hits in the DT for the various classifications of events from July Run 14851. a) shows DT hits for all events. b) where only bunch 0 had events, notice the small number of noise-events with hits around 700. c) For events where there were muons in bunches -1 and 0 in the same event there was a large fraction of noise-events. It is still interesting that there were quite a number of events that were not obviously noise. d) shows DT hits for events that had muons in all bunches. The number of events that were not noise is vanishingly small.

the noise events the majority of the events followed the trigger rules, showing that the noise came in bursts. There were, however, some events with muons in bunch -1, for which the time between two triggers was large. This was also seen in August for the events that did not have noise. These events were not understood, and would need further investigation.

The June GR results were presented at the Trigger Technical Coordination meeting the 14. August and the CMG Group meeting the 20. August. For the CMG meeting, also some preliminary results from July were shown. As one immediate consequence of this study a one-dimensional version of the bunch encoding plot in figure A.2 was integrated in the on-line data-quality monitoring.

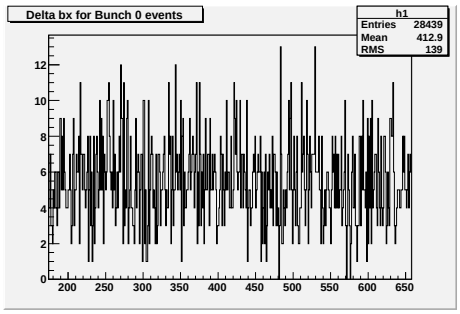


(a) Events with muons only in bunch 0. Flat distribution

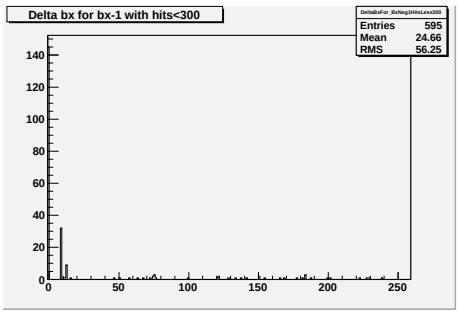


(b) Events with muons in bunch -1. "Normal" number of hits in DT. Small peak at small $\Delta$bx, but also plenty of events with large $\Delta$bx.

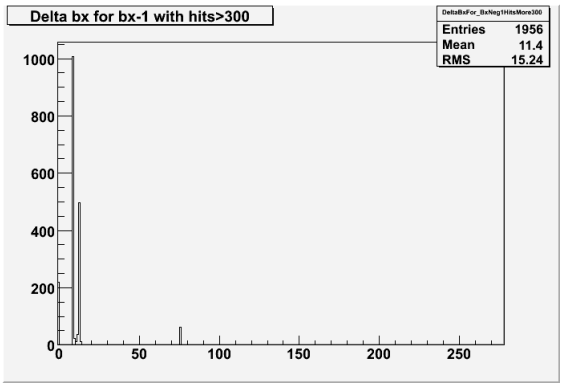


(c) Events with muons in bunch -1 with high rate of DT Hits. Clear peak at small $\Delta$bx

Figure A.5: Plot a) shows the flat distribution of events with only muons in bunch 0, this is as expected for normal events. Plot b) shows events with muons in bunch -1. There is a small peak at small $\Delta$bx indicating noise but mostly the events are spread out over all values of $\Delta$bx. For the bunch -1 events with large number of DT hits there is a much clearer peak at small $\Delta$bxes. The double-peak structure observed in the $Delta$bx plots is explained by the trigger rules. All 3 plots are from Run 14851.

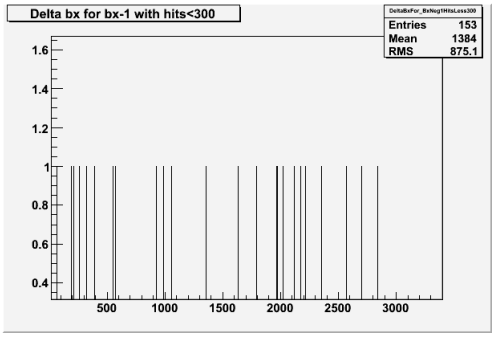


(a) Flat distribution

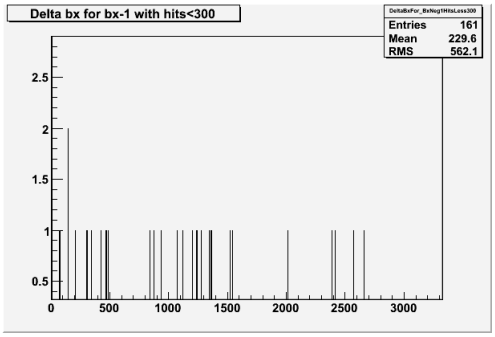


(b)

Figure A.6: Plot a) from Run 17153. This run had only a few events with a very high number of hits. Almost noise-free. The Plot shows $\Delta$bx for the bunch -1 cases. There is an even distribution over the whole scale. Plot b) is from Run 17166. This run had no events that could be classified as noise from hits in the DT. Also here an even distribution of $\Delta$bx.

# Appendix B

# End point formulas

$$\left(m_{ll}^{\max}\right)^2 = \left(m_{\tilde{\chi}_2^0}^2 - m_{\tilde{l}_R}^2\right)\left(m_{\tilde{l}_R}^2 - m_{\tilde{\chi}_1^0}^2\right)/m_{\tilde{l}_R}^2 \tag{B.1}$$

$$\left(m_{qll}^{\max}\right)^2 = \left\{ \begin{array}{lll} \frac{\left(m_{\tilde{q}_L}^2 - m_{\tilde{\chi}_2^0}^2\right)\left(m_{\tilde{\chi}_2^0}^2 - m_{\tilde{\chi}_1^0}^2\right)}{m_{\tilde{\chi}_2^0}^2} & \text{for} \quad \frac{m_{\tilde{q}_L}}{m_{\tilde{\chi}_2^0}} > \frac{m_{\tilde{\chi}_2^0}}{m_{\tilde{l}_R}}\frac{m_{\tilde{l}_R}}{m_{\tilde{\chi}_1^0}} & (1) \\ \frac{\left(m_{\tilde{q}_L}^2 m_{\tilde{l}_R}^2 - m_{\tilde{\chi}_2^0}^2 m_{\tilde{\chi}_1^0}^2\right)\left(m_{\tilde{\chi}_2^0}^2 - m_{\tilde{l}_R}^2\right)}{m_{\tilde{\chi}_2^0}^2 m_{\tilde{l}_R}^2} & \text{for} \quad \frac{m_{\tilde{\chi}_2^0}}{m_{\tilde{l}_R}} > \frac{m_{\tilde{l}_R}}{m_{\tilde{\chi}_1^0}}\frac{m_{\tilde{q}_L}}{m_{\tilde{\chi}_2^0}} & (2) \\ \frac{\left(m_{\tilde{q}_L}^2 - m_{\tilde{l}_R}^2\right)\left(m_{\tilde{l}_R}^2 - m_{\tilde{\chi}_1^0}^2\right)}{m_{\tilde{l}_R}^2} & \text{for} \quad \frac{m_{\tilde{l}_R}}{m_{\tilde{\chi}_1^0}} > \frac{m_{\tilde{q}_L}}{m_{\tilde{\chi}_2^0}}\frac{m_{\tilde{\chi}_2^0}}{m_{\tilde{l}_R}} & (3) \\ \left(m_{\tilde{q}_L} - m_{\tilde{\chi}_1^0}\right)^2 & \text{otherwise} & (4) \end{array} \right\} \tag{B.2}$$

$$\left(m_{ql(\text{low})}^{\max}, m_{ql(\text{high})}^{\max}\right) = \left\{ \begin{array}{lll} \left(m_{ql_{\text{n}}}^{\max}, m_{ql_{\text{f}}}^{\max}\right) & \text{for} \quad 2m_{\tilde{l}_R}^2 > m_{\tilde{\chi}_1^0}^2 + m_{\tilde{\chi}_2^0}^2 > 2m_{\tilde{\chi}_1^0} m_{\tilde{\chi}_2^0} & (1) \\ \left(m_{ql(\text{eq})}^{\max}, m_{ql_{\text{f}}}^{\max}\right) & \text{for} \quad m_{\tilde{\chi}_1^0}^2 + m_{\tilde{\chi}_2^0}^2 > 2m_{\tilde{l}_R}^2 > 2m_{\tilde{\chi}_1^0} m_{\tilde{\chi}_2^0} & (2) \\ \left(m_{ql(\text{eq})}^{\max}, m_{ql_{\text{n}}}^{\max}\right) & \text{for} \quad m_{\tilde{\chi}_1^0}^2 + m_{\tilde{\chi}_2^0}^2 > 2m_{\tilde{\chi}_1^0} m_{\tilde{\chi}_2^0} > 2m_{\tilde{l}_R}^2 & (3) \end{array} \right\} \tag{B.3}$$

$$\left(m_{ql_{\text{n}}}^{\max}\right)^2 = \left(m_{\tilde{q}_L}^2 - m_{\tilde{\chi}_2^0}^2\right)\left(m_{\tilde{\chi}_2^0}^2 - m_{\tilde{l}_R}^2\right)/m_{\tilde{\chi}_2^0}^2 \tag{B.4}$$

$$\left(m_{ql_{\text{f}}}^{\max}\right)^2 = \left(m_{\tilde{q}_L}^2 - m_{\tilde{\chi}_2^0}^2\right)\left(m_{\tilde{l}_R}^2 - m_{\tilde{\chi}_1^0}^2\right)/m_{\tilde{l}_R}^2 \tag{B.5}$$

$$\left(m_{ql(\text{eq})}^{\max}\right)^2 = \left(m_{\tilde{q}_L}^2 - m_{\tilde{\chi}_2^0}^2\right)\left(m_{\tilde{l}_R}^2 - m_{\tilde{\chi}_1^0}^2\right)/\left(2m_{\tilde{l}_R}^2 - m_{\tilde{\chi}_1^0}^2\right) \tag{B.6}$$

$$\begin{aligned} \left(m_{qll(\theta>\frac{\pi}{2})}^{\min}\right)^2 = & \Big[\left(m_{\tilde{q}_L}^2 + m_{\tilde{\chi}_2^0}^2\right)\left(m_{\tilde{\chi}_2^0}^2 - m_{\tilde{l}_R}^2\right)\left(m_{\tilde{l}_R}^2 - m_{\tilde{\chi}_1^0}^2\right) \\ & -\left(m_{\tilde{q}_L}^2 - m_{\tilde{\chi}_2^0}^2\right)\sqrt{\left(m_{\tilde{\chi}_2^0}^2 + m_{\tilde{l}_R}^2\right)^2\left(m_{\tilde{l}_R}^2 + m_{\tilde{\chi}_1^0}^2\right)^2 - 16m_{\tilde{\chi}_2^0}^2 m_{\tilde{l}_R}^4 m_{\tilde{\chi}_1^0}^2} \\ & +2m_{\tilde{l}_R}^2\left(m_{\tilde{q}_L}^2 - m_{\tilde{\chi}_2^0}^2\right)\left(m_{\tilde{\chi}_2^0}^2 - m_{\tilde{\chi}_1^0}^2\right)\Big]/\left(4m_{\tilde{l}_R}^2 m_{\tilde{\chi}_2^0}^2\right) \end{aligned} \tag{B.7}$$

where 'low' and 'high' on the left-hand side in Eq. (B.3) refer to minimising and maximising with respect to the choice of lepton. Furthermore 'min' in Eq. (B.7) refers to the threshold in the subset of the $m_{qll}$ distribution for which the angle between the two lepton momenta (in the slepton rest frame) exceeds $\pi/2$.

Notice that the different cases listed in Eq. (B.2) are distinguished by *mass ratios* of neighbouring particles in the hierarchy, $m_{\tilde{q}_L}/m_{\tilde{\chi}_2^0}$, $m_{\tilde{\chi}_2^0}/m_{\tilde{l}_R}$ and $m_{\tilde{l}_R}/m_{\tilde{\chi}_1^0}$. Since each decay in the chain involves two massive particles and one massless one, the boosts from one rest frame to another are conveniently expressed in terms of such mass ratios.

# Appendix C

# Single Background Sample CutFlow Tables

## C.1 Standard etcone20 isolation

| Cuts | T1 | TTbar | Z$ee$ | Z$\mu\mu$ | Z$\tau\tau$ | Z$\nu\nu$ | W$e\nu$ | W$\mu\nu$ | W$\tau\nu$ |
|---|---|---|---|---|---|---|---|---|---|
| Crossection | 449820 | 370685 | 46200 | 9604 | 5000 | 41328 | 49049 | 28640 | 55909 |
| Gen Cuts | 6057 | 36 | 21 | 19 | 66 | 10 | 110 | 158 | 62 |
| >= 2 leptons | 6056 | 31 | 21 | 17 | 65 | 8 | 109 | 158 | 61 |
| 2 leptons >20,10 GeV | 5147 | 21 | 21 | 15 | 56 | 5 | 93 | 122 | 44 |
| OS Dileptons | 3829 | 10 | 21 | 15 | 51 | 2 | 57 | 80 | 28 |
| OS leptons, isolated | 1624 | 0 | 21 | 15 | 30 | 0 | 5 | 2 | 1 |
| >= 3 jets | 1246 | 0 | 0 | 8 | 11 | 0 | 3 | 1 | 0 |
| Jet pt | 590 | 0 | 0 | 2 | 7 | 0 | 1 | 1 | 0 |
| EtMiss>150 GeV | 235 | 0 | 0 | 2 | 3 | 0 | 1 | 1 | 0 |
| EffMass > 800 GeV | 63 | 0 | 0 | 0 | 1 | 0 | 1 | 0 | 0 |

Table C.1: Number of SM background events after consequetive cuts for each individual background sample. Lepton isolation etcone20<10GeV, $p_T^{lep1,lep2}$> 20,10 GeV. Generator level cuts (Gen Cuts) / $\mathrm{E_T}$ >100 GeV, 2 jets $p_T^{1,2}$ >100,50 GeV.

| Cuts | J4 | J5 | J6 | J7 | J8 | WW | ZZ | WZ |
|---|---|---|---|---|---|---|---|---|
| Crossection | 916400 | 655000 | 32150 | 5300 | 22 | 24500 | 2100 | 7800 |
| Gen Cuts | 3330 | 2118 | 254 | 23 | 0 | 10 | 2 | 5 |
| >= 2 leptons | 3317 | 2110 | 252 | 21 | 0 | 10 | 2 | 5 |
| 2 leptons >20,10 GeV | 2512 | 1884 | 216 | 14 | 0 | 9 | 1 | 5 |
| OS Dileptons | 1887 | 1516 | 157 | 8 | 0 | 8 | 1 | 3 |
| OS leptons, isolated | 0 | 0 | 0 | 0 | 0 | 3 | 1 | 2 |
| >= 3 jets | 0 | 0 | 0 | 0 | 0 | 0 | 0 | 1 |
| Jet pt | 0 | 0 | 0 | 0 | 0 | 0 | 0 | 0 |
| EtMiss>150 GeV | 0 | 0 | 0 | 0 | 0 | 0 | 0 | 0 |
|  | 0 | 0 | 0 | 0 | 0 | 0 | 0 | 0 |
| EffMass | 0 | 0 | 0 | 0 | 0 | 0 | 0 | 0 |

Table C.2: Number of SM background events after consequetive cuts for each individual background sample. Lepton isolation etcone20<10GeV, $p_T^{lep1,lep2}$> 20,10 GeV. Generator level cuts (Gen Cuts) / $\mathrm{E_T}$ >100 GeV, 2 jets $p_T^{1,2}$ >100,50 GeV.

## C.2 Normalized etcone isolation

| Cuts | T1 | TTbar | Zee | Zmumu | Ztautau | Znunu | Wenu | Wmunu | Wtaunu |
|---|---|---|---|---|---|---|---|---|---|
| Crossection | 449820 | 370685 | 46200 | 9604 | 4500 | 41328 | 49049 | 28640 | 55909 |
| Gen Cuts | 6057 | 36 | 21 | 19 | 66 | 10 | 110 | 158 | 62 |
| >= 2 leptons | 6056 | 31 | 21 | 17 | 65 | 8 | 109 | 158 | 61 |
| 2 leptons >20,10 GeV | 5147 | 21 | 21 | 15 | 56 | 5 | 93 | 122 | 44 |
| OS Dileptons | 3829 | 10 | 21 | 15 | 51 | 2 | 57 | 80 | 28 |
| OS leptons, isolated | 1281 | 0 | 21 | 15 | 26 | 0 | 1 | 1 | 0 |
| >= 3 jets | 975 | 0 | 0 | 8 | 8 | 0 | 0 | 1 | 0 |
| Jet pt | 458 | 0 | 0 | 2 | 6 | 0 | 0 | 1 | 0 |
| EtMiss> 150 GeV | 184 | 0 | 0 | 2 | 3 | 0 | 0 | 1 | 0 |
| EffMass >800 GeV | 50 | 0 | 0 | 0 | 1 | 0 | 0 | 0 | 0 |

Table C.3: Number of SM background events after consequetive cuts for each individual background sample. Normalized lepton isolation netcone20<0.05, $p_T^{lep1,lep2}$> 20,10 GeV. Generator level cuts (Gen Cuts) $\not{E}_{\mathrm{T}}$ >100 GeV, 2 jets $p_T^{1,2}$ >100,50 GeV.

| Cuts | J4 | J5 | J6 | J7 | J8 | WW | ZZ | WZ |
|---|---|---|---|---|---|---|---|---|
| Crossection | 916400 | 655000 | 32150 | 5300 | 22 | 24500 | 2100 | 7800 |
| Gen Cuts | 3330 | 2118 | 254 | 23 | 0 | 10 | 2 | 5 |
| >= 2 leptons | 3317 | 2110 | 252 | 21 | 0 | 10 | 2 | 5 |
| 2 leptons >20,10 GeV | 2512 | 1884 | 216 | 14 | 0 | 9 | 1 | 5 |
| OS Dileptons | 1887 | 1516 | 157 | 8 | 0 | 8 | 1 | 3 |
| OS leptons, isolated | 0 | 0 | 0 | 0 | 0 | 3 | 1 | 2 |
| >= 3 jets | 0 | 0 | 0 | 0 | 0 | 0 | 0 | 1 |
| Jet pt | 0 | 0 | 0 | 0 | 0 | 0 | 0 | 0 |
| EtMiss> 150 GeV | 0 | 0 | 0 | 0 | 0 | 0 | 0 | 0 |
| EffMass >800 GeV | 0 | 0 | 0 | 0 | 0 | 0 | 0 | 0 |

Table C.4: Number of SM background events after consequetive cuts for each individual background sample. Normalized lepton isolation netcone20<0.05, $p_T^{lep1,lep2}$> 20,10 GeV. Generator level cuts (Gen Cuts) $\not{E}_{\mathrm{T}}$ >100 GeV, 2 jets $p_T^{1,2}$ >100,50 GeV.

# References


[1] H. Baer, F.E. Paige, S.D. Protopopescu, and X. Tata. http://www.hep.fsu.edu/~isajet/.

[2] Howard Baer and Xerxes Tata. *Weak Scale Supersymmetry*. Cambridge University Press, 2006.

[3] R. Brun and F. Rademakers. http://root.cern.ch/.

[4] C. Burgess and G. Moore. *The Standard Model, A Primer*. Cambridge University Press, 2007.

[5] ATLAS Collaboration. https://twiki.cern.ch/twiki/bin/view/Atlas/SusyView.

[6] ATLAS Collaboration. *ATLAS MissingET Overall Performance CSC $\not\!\!E_{\mathrm{T}}$ Note*.

[7] ATLAS Collaboration. *SUSY CSC5 Note*.

[8] ATLAS Collaboration. *The ATLAS Experiment at the CERN Large Hadron Collider*, 2007.

[9] Geant4 Collaboration. Nuclear instruments and methods in physics research a 506 (2003) 250-303. http://geant4.web.cern.ch/geant4/index.shtml.

[10] ATLAS Collarboration. Atlas detector and physics performance, technical design report. Technical report, ATLAS Collaboration, 1999.

[11] G. Corcella, I.G. Knowles, G. Marchesini, S. Moretti, K. Odagiri, P. Richardson, M.H. Seymour, and B.R. Webber. Herwig 6.5. http://hepwww.rl.ac.uk/theory/seymour/herwig/.

[12] A Doxiadis and M Kayl. Estimating the isolated lepton rate in multi-jet events. Technical report, Nikhef National Institute for Subatomic Physics, Amsterdam, The Netherlands, 2008.

[13] ATLAS eGamma work group. https://twiki.cern.ch/twiki/bin/view/Atlas/ElectronReconstruction#Electron_identification.

[14] ATLAS Susy Work Group. https://twiki.cern.ch/twiki/bin/view/Atlas/SusyEventFilesInfo.

[15] S.P. Martin. A supersymmetry primer. Technical Report hep-ph/9709356v4, Department of Physics, Northern Illinois University, 2006.

[16] Luc Pape and Daniel Treille. *Supersymmetry facing experiment: much ado (already) about nothing (yet)*, 2006.

[17] T. SjÃűstrand, S. Mrenna, and P. Skands, 2006. http://home.thep.lu.se/~torbjorn/Pythia.html.

[18] ATLAS Muon work group. https://twiki.cern.ch/twiki/bin/view/Atlas/MuonPerformance.